ISSN 0915-6364

NATIONAL INSTITUTE FOR FUSION SCIENCE

Charge Exchange Recombination Spectroscopy of Li III Ions for Fusion Plasma Diagnostics

S. Zou, T. Kato, I. Murakami

(Received - Sep. 14, 2001)

NIFS-DATA-69 Oct. 2001

RESEARCH REPORT
NIFS-DATA Series

TOKI, JAPAN

NIFS
Atomic and Molecular Database
http://dbshino.nifs.ac.jp

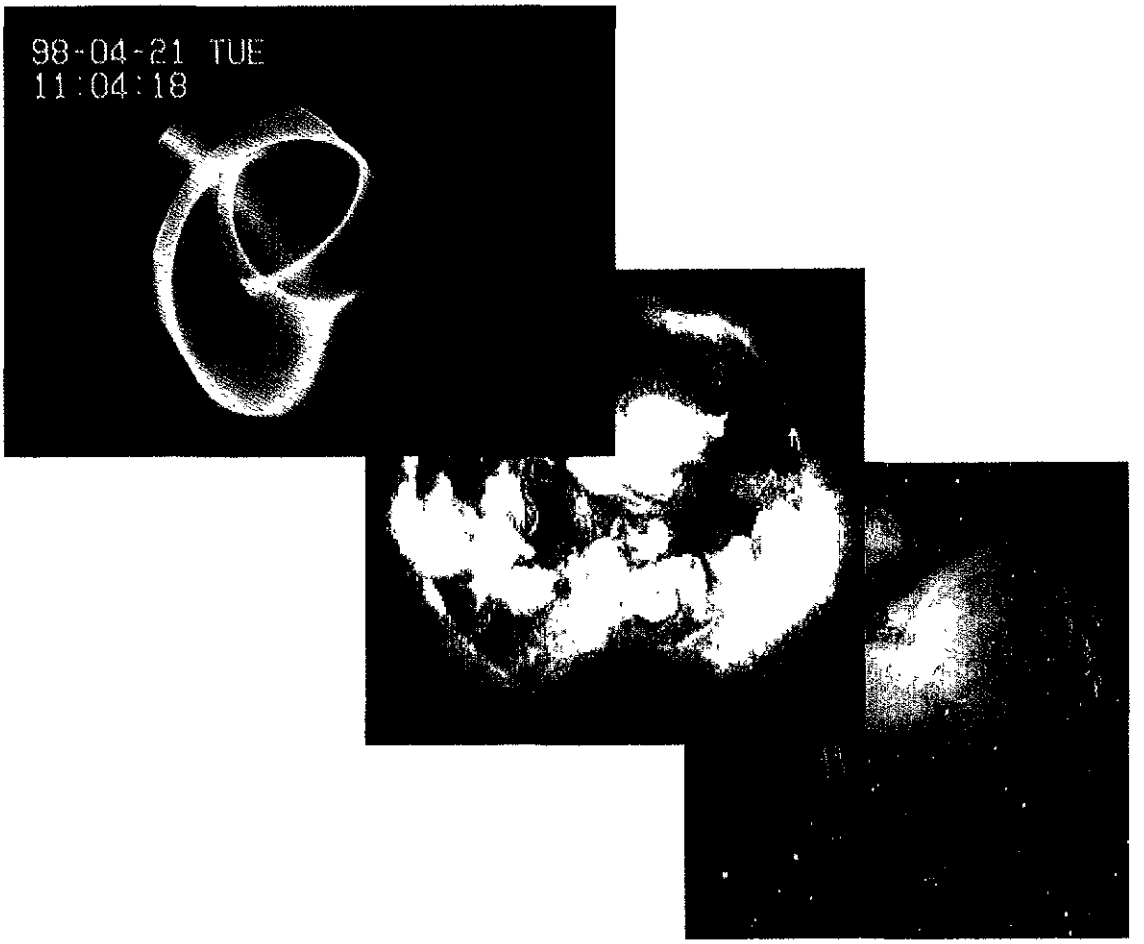

Data and Planning Center
National Institute for Fusion Science

Atomic and Molecular Data for Fusion Science and Related Fields

- We compile atomic and molecular data for atomic processes in a plasma for fusion science and related fields. Users can retrieve the data by elements or other attributes and display them in a tabular and in a graphical form.

- Bibliographic databases also are available. They are used independently or in connection with the numerical databases.

- The databases are available through Web at **URL=http://dbshino.nifs.ac.jp/** and free of charge for research purpose for registered users. It is possible to register at the same URL address.

DATABASES

Numerical Databases

- **AMDIS** ... Cross sections for ionization, excitation, recombination and dissociation of atoms, ions, and molecules by electron impact. Rate coefficients also are compiled for recombination processes.
- **CHART** ... Cross sections for charge transfer and ionization of atoms, ions, and molecules by ion collisions.
- **SPUTY** ... Sputtering yields for monatomic solids by ions.
- **BACKS** ... Particle- and energy-backscattering coefficients of light ions from solids. Distribution of energy and angle of scattered particles also are included.

Bibliographic Databases

- **FUSION** ... bibliography for fusion sciences and plasma physics, extracted from INSPEC.
- **AM** ... bibliography for atomic and molecular physics, extracted from INSPEC.
- **ORNL** ... bibliography for atomic collisions, compiled by Oak Ridge National Laboratory (ORNL).

Examples of the display

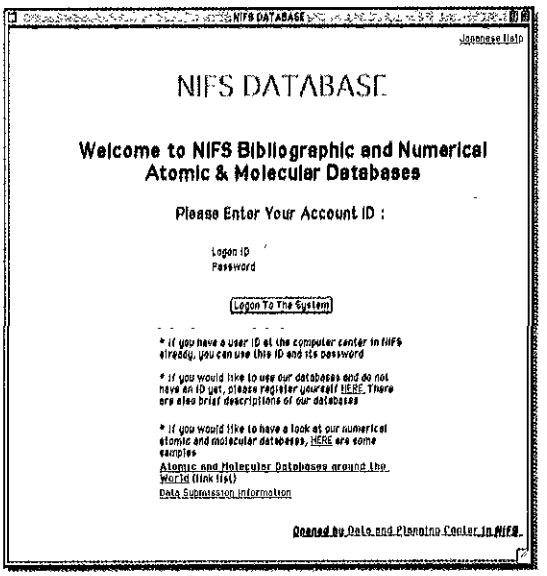

Homepage entrance

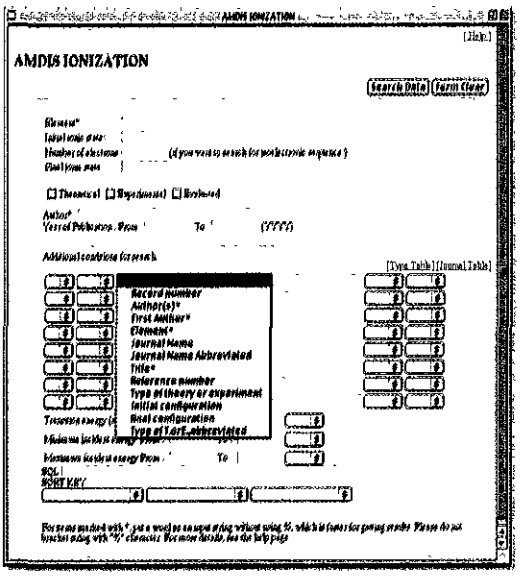

Page for search of ionization cross section data from AMDIS

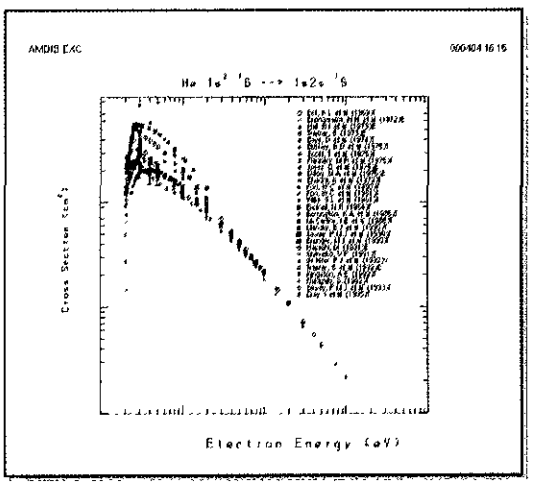

Graphic output of numerical data of excitation cross section from AMDIS

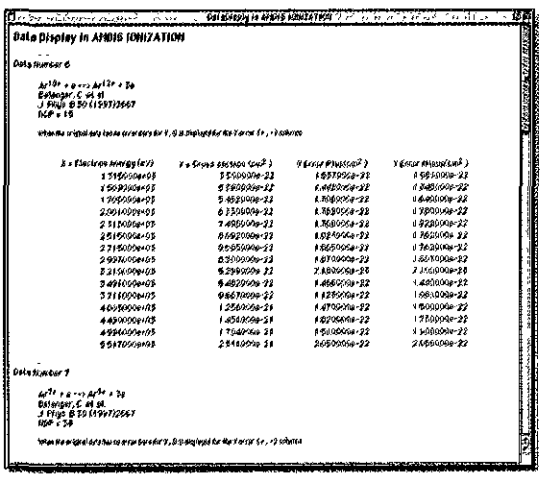

Output of numerical data table of ionization cross section from AMDIS

Our database is widely used

Since the beginning of website operation in 1997, more than 500 users have registered.

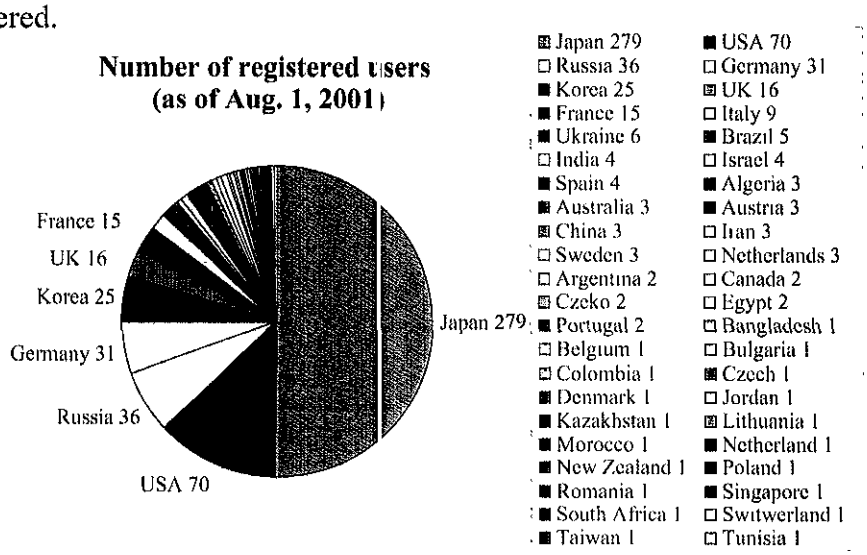

The numerical databases are accessed more than 200 times per month. The bibliographic databases are also used frequently.

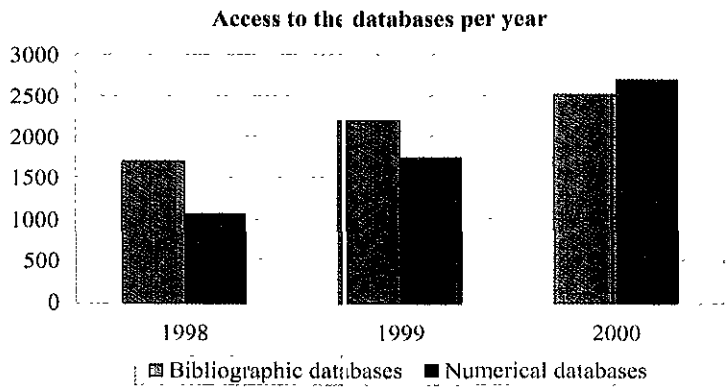

Any questions or requests should be sent via email to dbmaster@dbshino.nifs.ac.jp

NIFS

Data and Planning Center
National Institute for Fusion Science
Oroshi-cho, Toki, Gifu 509-5292, Japan
URL=http://www.nifs.ac.jp
URL= http://dbshino.nifs.ac.jp
email: dbmaster@dbshino.nifs.ac.jp

Charge exchange recombination spectroscopy of Li III ions for fusion plasma diagnostics

S. Zou

Graduated University for Advanced Studies, Japan

T. Kato, I.Murakami

National Institute for Fusion Science, Oroshi, Toki 509-5292, Japan

Abstract

A detailed calculation is presented of the line emission of Li^{2+} ions in a plasma where a neutral hydrogen beam is injected. A collisional-radiative model including charge exchange process has been developed, in which nl subshell resolved populations are treated up to $n \sim 20$. The population densities are discussed for three components: excitation, recombination and charge exchange processes. The Zeeman effect for fine structure component and apparent broadening for line profiles have been examined by detailed numerical calculations of spectra profiles for the emission lines of Li III ions from $n = 5$ to $n = 4$ transitions with a magnetic field B=2 Tesla. The perturbation of Zeeman broadening on ion temperature measurements is also estimated. At high magnetic field and low ion temperature, Zeeman broadening must be included for reliable interpretation of the measured spectra. Our calculation can be applied to measure the magnetic field in plasmas.

Keywords: Charge exchange (CX), Spectroscopy, Neutral beam (NB), Li III, Zeeman effect

I. INTRODUCTION

Recently, Li pellet injection has been proposed for investigating particle transport in plasmas of the Heliotron E [1], CHS [2] and LHD. The injected Li pellet is ablated in the central region of plasma and Li impurities are fully ionized by electrons and ions in a short period. The tracer ions Li^{3+} can be observed by a charge exchange spectroscopy which is based on the atomic process:

$$Li^{q+} + H^0 \rightarrow Li^{(q-1)+}(nl) + H^+ \tag{1a}$$

$$Li^{(q-1)+}(nl) \rightarrow Li^{(q-1)+}(n'l') + h\nu \tag{1b}$$

where a fully stripped Li^{3+} ion captures an electron from hydrogen atoms in a neutral heating beam, and then results in a Li^{2+} ion in an excited state (n, l). The subsequent photon emission provide the density and velocity distributions of Li^{3+} ions. The technique has been used to diagnose the particle transport as well as plasma parameters. Most of the measurements have been done with the visible lines of Li^{2+} ions from $n = 5$ to $n = 4$ transitions using an optical fiber to obtain multi-point simultaneous measurements.

Change exchange (CX) lines (Li III $\Delta n = 5 - 4$) are perturbed by several atomic physics and environmental effects [3]. Environmental influences include (i) the background line emission produced by electron impact excitation from hydrogen-like Li ions in the cool plasma periphery, (ii) Zeeman and motional Stark line broadening which arise from the interactions of ions with the strong magnetic fields in the system, and (iii) the presence of secondary low-energy neutrals in the vicinity of the neutral beam in the plasma, and apparent broadening arising from a recombined ion plume which drifts into the line of sight. Atomic properties and processes which can change the observed line shapes include the presence of non-negligible atomic fine structure in these highly excited states and basic energy dependence of the charge exchange cross section.

In this paper, a collisional-radiative (CR) model including charge exchange process is developed, in which separated nl subshell populations are treated up to $n \sim 20$. Using our

CR model, we calculated the line emissions of Li^{2+} ions produced by charge exchange, electron impact excitation and recombination. The basic atomic processes to produce emission lines (especially charge exchange recombination, excitation from the low levels and radiative recombination) have been studied separately to see how these process populate the excited states.

We also make a computer code to diagonalize the Hamiltonian including the perturbation of magnetic field, and calculate the wavelength and transition probability for a doublet line in arbitrary magnetic field. The basic idea is presented by Bethe and Salpeter [4]. With our code, we calculated the Zeeman splitting lines of Li III $\Delta n = 5 - 4$ transitions with no field and with a magnetic field B=2 Tesla. The two issues of fine structure broadening and Zeeman splitting are discussed in detail.

A brief description of the CR model and atomic data which we used for the calculation is given in Secs. II and III, respectively. The detailed calculation results for population densities, line intensities and line profiles are shown in Sec. IV. The conclusions are given in Sec. V. We shown the spectra produced by CX, excitation and recombination in magnetic field. The apparent broadening introduced by Zeeman effect can change the spectral profiles significantly and must be included for reliable interpretation of the measured spectra.

II. COLLISIONAL-RADIATIVE MODEL

We consider a thermal plasma composed of electrons and protons, together with minority impurity species of lower abundance. The excited-state populations of hydrogen-like lithium ions are determined primarily by collisions with electrons and protons, by spontaneous radiative decay and by interaction with beam atoms. The rate equation of Li^{2+} in the i-th state is given by

$$\frac{dn(i)}{dt} = \{\sum_{j \neq i} n_e C_{ji} n(j) + \sum_{j>i} A_{ji} n(j)\} - \{\sum_{j \neq i} n_e C_{ij} n(i) + \sum_{j<i} A_{ij} n(i)\} + \{n_e \alpha_i n_+ + n_h \beta_i n_+\} - \{n_e S_i n(i)\} \quad (2)$$

where n_e is the electron density, n_+ is the density of fully stripped Li^{3+} ions, n_h is the density of neutral hydrogen in beam. C_{ji} is the collisional excitation/deexcitation rate coefficient and A_{ji} is the radiative transition probability from j-th state to i-th state. S_i is the rate coefficient for direct collisional ionization from the i-th state. α_i is the composite electron-ion recombination rate coefficient, where three-body recombination and radiative recombination processes are included. β_i is the charge exchange recombination rate coefficient, for which a bare nucleus Li^{3+} captures an electron from neutral hydrogen and then forms a hydrogen-like Li ion in i-th state. The heavy particle (proton) collisions are included in the model for angular momentum mixing.

In a collisional radiative viewpoint, the populations of excited states may be separated into three independent components; excitation from the ground state, free-electron recombination and charge exchange capture from neutral hydrogen [5–7], respectively. Then the population densities can be described, in the quasi-steady-state picture, by

$$n(i) = n_e E_i n(1) + n_e R_i n_+ + n_h G_i n_+ \qquad i \geq 2 \tag{3}$$

where E_i, R_i and G_i are called the effective population coefficients, and represent the effective contribution from the ground state via excitation and from fully stripped ion via electron-ion recombination and charge exchange reaction, respectively. Substituting eq.(3) to eq. (2), the following three sets of equations for E_i, R_i, G_i are obtained,

$$E_i = \frac{C_{1i} + \sum'_{j\neq i} n_e C_{ji} E_j + \sum_{j>i} A_{ji} E_j}{n_e S_i + \sum_{i\neq j} n_e C_{ij} + \sum_{i>j} A_{ij}} \tag{4a}$$

$$R_i = \frac{\alpha_i + \sum'_{j\neq i} n_e C_{ji} R_j + \sum_{j>i} A_{ji} R_j}{n_e S_i + \sum_{i\neq j} n_e C_{ij} + \sum_{i>j} A_{ij}} \tag{4b}$$

$$G_i = \frac{\beta_i + \sum'_{j\neq i} n_e C_{ji} G_j + \sum_{j>i} A_{ji} G_j}{n_e S_i + \sum_{i\neq j} n_e C_{ij} + \sum_{i>j} A_{ij}} \tag{4c}$$

The primed sums extend only over excited states. Solving the three sets of equations with $i \geq 2$, one obtains the populations of excited states, and then the rate equation, eq. (2), for the ground state can be rewritten in terms of E_i, R_i and G_i, viz.

$$\frac{dn(1)}{dt} = -n_e S_{eff} n(1) + n_e \alpha_{eff} n_+ + n_h \beta_{eff} n_+$$

$$= -n_e S_{cr} n(1) + n_e \alpha_{cr} n_+ \tag{5}$$

with

$$S_{eff} = S_1 + \sum_{j=2} C_{1j} - \sum_{j=2} [E_j (n_e C_{j1} + A_{j1})] \tag{6a}$$

$$\alpha_{eff} = \alpha_1 + \sum_{j=2} [R_j (n_e C_{j1} + A_{j1})] \tag{6b}$$

$$\beta_{eff} = \beta_1 + \sum_{j=2} [G_j (n_e C_{j1} + A_{j1})] \tag{6c}$$

and

$$S_{cr} = S_{eff} \tag{7a}$$

$$\alpha_{cr} = \alpha_{eff} + \frac{n_h}{n_e} \beta_{eff} \tag{7b}$$

Here, S_{cr} and α_{cr} are called collisional-radiative ionization and recombination rate coefficients, respectively, and represent the effective rate coefficients for ionization and recombination of the plasma. When $n_e S_{cr} n(1) = n_e \alpha_{cr} n_+$, ionization and recombination are balanced.

III. ATOMIC DATA

In order to analyze the visible spectral lines we need the atomic data involving highly excited states such as $n = 5$. In our collisional radiative model in eq. (3) we included the $n - l$ resolved states up to $n = 20$. We need a complete set of data up to $n = 20$ for our CR calculation. The data for excitation by electron impact for highly excited states are not available in the literature for H-like Li ions. In this paper, the electron-impact excitation data are calculated by Coulomb-Born -Exchange (CBE) approximation for transitions between the low levels with $1s \leq nl \leq 5g$, by n^{-3} scaling law for $n_i l_i \rightarrow n_f l_f$ with $1s \leq n_i l_i \leq 4f$ and $6s \leq n_f l_f$, and by Mewe's semi-empirical formula [8] for transitions between high-lying states with $6s \leq nl$. The CBE calculation is carried out with the use of the ATOM code [9]. We have compared the results for $z^2\Omega$, where z is the nuclear charge of ions and Ω is collision strength, by CBE and other methods distorted wave (DW) approximation by

HULLAC code [10], DW by Clark *et al.* [11] and pesudo-state R-matrix (RMPS) [12]. Some of the comparisons are shown in Figs. 1, 2 and 3 as examples. We can see the results by CBE and by DW [10] are in good agreement with each other better than 10% even near the threshold region, the z^2 scaling works well for the incident energy above twice the threshold. For the weak transitions (non-dipole transitions) $1s-2s$ and $1s-5s$, we also compared our results with pseudo-state R-matrix (RMPS) calculation by Badnell *et al.* [12] in Fig. 1. The data by CBE lie above the results by RMPS [12] by about 30%. For the collision energy just above threshold, the collision strength by RMPS are much larger than those of CBE due to resonance effects. For the transition between two highly excited states (such as $4s-5s$), the CBE and DW [10] results are two or three times larger than those of RMPS in the low energy region as shown in Fig. 3 . In the high energy region, these calculations are in a good agreement with each other. Fortunately, the electron temperature is much higher than the threshold of $4s-5s$ for the case of our interest. RMPS data (which should be best) are incomplete and disagree with other data. High-accurate and complete calculations are needed for H-like Li ions excitation process.

The $l-mixing$ collisions by electrons and ions are important to determine the populations of excited states, and the corresponding rate coefficients are estimated by the Jacobs' formula [13]. The ionization rate coefficients from the ground state and all the excited states are are estimated by Lotz's empirical formula [14]. The collisional de-excitation and three-body recombination rate coefficients are derived by detailed balance from the excitation and ionization rate coefficients. The spontaneous radiative processes for all allowed transitions and one forbidden transition, $2s(^2S)-1s(^2S)$, are included. Radiative recombination rate coefficients are obtained by detailed balance principle from the photo-ionization cross sections [15].

The direct charge exchange recombination rate coefficient to a state i is estimated as

$$\beta_i = v\sigma_i$$

where v is the particle velocity of the beam and σ_i is the state selected charge exchange

cross sections. Data for state selected cross sections are taken from various sources in the recent literature [16,17], which are found in NIFS database CHART [18]. Fig. 4 shows the energy dependence of total CX cross sections for Li^{3+} with H(1s) [16] and H(2s) [17]. The numerical data are taken from the NIFS database CHART. We also plot in Fig. 4 the estimated values by empirical formula [19] to see the asymptotic behavior of CX cross sections. Figs. 5 and 6 show the n-dependence and l-dependence of charge exchange cross sections at different kinetic energies. For extending the data to high n excited states, we assume a n^{-3} dependence with n higher than $n = 5$. This dependence is appropriate at high collision energies($E_h > 25$ keV/amu), although at low collision energies, a steeper decrease is expected.

IV. RESULTS

A. Population densities

In our calculation, the population densities of excited states are expressed with the populations of Li^{2+} in the ground state and the bare nucleus Li^{3+} as described in eq. (2). In order to get the populations of $n(1)$ and n_+, we need to solve the time dependent rate equation, eq. (4), for Li^{2+}(1s) and Li^{3+}. When the time variation of plasma parameters is much slower than the ionization ($\sim 1/(n_e \cdot S_{cr})$) and recombination ($\sim 1/(n_e \cdot \alpha_{cr})$) time scales, the plasma is in a steady state. In our calculation, we assumed $n(1)/n_+ = \alpha_{cr}/S_{cr}$ to calculate the spectra. We have adopted fixed kinetic energies for beam particles at $E_h = 25$ keV/amu and $E_h = 100$ keV/amu. As shown in Fig. 4, the CX cross section from excited state of neutral hydrogen decreases rapidly with increasing collision energy. So the contribution from excited-state neutral hydrogen can be neglected.

In Fig. 7, we plot the n-dependence calculated of population coefficients (E_i: excitation, R_i: recombination and G_i: charge exchange) for the np and nd states. We assume the electron temperature and density are $T_e = 1000$ eV and $n_e = 10^{13}$ cm^{-3}. The neutral

hydrogen density is assumed to be $n_h = 10^{-5} n_e$. We scaled the CX cross sections for higher than $n = 5$ by n^{-3} dependence until $n = 8$. We did not include CX cross sections for $n > 9$. Therefore the population coefficients G_i drop sharply for $n \geq 9$.

The temperature dependence of the three population coefficients (E_i, R_i and G_i divided by statistical weights) for $5l$-state are shown in Fig. 8. The excitation population coefficients E_i/g_i increase rapidly with electron temperature in the low temperature region and get the maximum values at hundred electron-volts (the threshold of excitation). After maximum values, E_i/g_i slightly decrease with the increase of electron temperature. The recombination population coefficients (R_i/g_i) drop rapidly with electron temperature, and the charge exchange population coefficients (G_i/g_i) are almost temperature independent in the whole temperature region. The reason why the population density of $5s$ is always larger than other $5l$ is the smallest radiative decay from the $5s$ state.

Fig. 9 shows the density dependence of the three population coefficients (E_i, R_i, G_i divided by statistical weights). The excitation population coefficients E_i/g_i show different density dependence for states with different angular quantum number l. In the low density region ($n_e \leq 10^{10}$ cm^{-3}), E_i/g_i are density independent. In the intermediate density region (10^{11} cm$^{-3} \leq n_e \leq 10^{16}$ cm^{-3}), the excitation population coefficients E_i/g_i for high l states such as $5g$ increase with electron density. The populations of $5g$ (or $5f$) state significantly increases due to the excitation from the excited states when the electron density larger than 10^{11} cm^{-3}. In the high density region ($n_e \geq 10^{17}$ cm^{-3}), since the populations of excited states tend to the complete saturation phase, the excitation population coefficients E_i/g_i are proportional to n_e^{-1}. The recombination population coefficients R_i/g_i of $5s$ state is about two order of magnitude larger than others in the low density region because of the larger radiative recombination cross section to $5s$ and smaller radiative transition probability from $5s$. In the high density region, the collisional processes become dominant and then R_i/g_i tend to be a constant. The charge exchange population coefficients G_i/g_i show similar density dependence with E_i/g_i in the low and high density region. However, in the intermediate density region the changes of G_i/g_i for $5g$ and $5f$are small. In Figs. 8 and 9, the ratio of

density of neutral hydrogen n_h to electron density n_e is taken to be $n_h/n_e = 10^{-5}$.

In Fig. 10, we plot the collisional-radiative ionization and recombination rate coefficients as a function of the electron temperature with different ratios of n_h/n_e, where the density of electron is taken to be $n_e = 10^{13}$ cm^{-3}. It can be seen that for a hot plasma ($T_e \geq 30$ eV), the collisional-radiative ionization rate coefficients are much larger than the collsional-radiative recombination rate coefficients. Therefore in the ionization equilibrium or near-equilibrium region, $n_+ \gg n(1)$ because $n_+/n(1) = S_{CR}/\alpha_{CR}$. It also can be seen, the collisional-radiative recombination rate coefficients increase with the neutral hydrogen density, and the increase is almost temperature independent. As the recombination process, the contribution of the charge exchange recombination is large than that of electron-ion recombination (radiative recombination) under the condition which we are considering($n_e = 10^{13}$ cm^{-3}, $T_e = 1000$ eV, $n_h/n_e = 10^{-5}$). Here, charge exchange reaction acts as an additional recombination process shifting the local ionization balance to lower charge states comparing to the ionization equilibrium by electron collision only.

Fig. 11 shows the population densities of excited states assuming the ionization equilibrium, $n_+/n(1) = S_{CR}/\alpha_{CR}$. With the principal quantum number n increasing, the population density $n(i)$ converges to a constant. The effects of charge exchange are important even for highly excite state because charge exchange reactions shift the ionization balance. In the case without NBI, the specially high population of $3d$ should be due to excitation from $2s$ state. The relative electron flow and population density for nd are shown in Fig. 12(a). The excitation rate coefficients from $1s - 3d$, $4d$, $5d$ and $2s - 3d$, $4d$, $5d$ are shown in Fig. 12(b).

B. Line Intensity

From eq. (3), the populations of excited states are separated into three independent components dependent on the excitation from the ground state, free-electron capture and charge-exchange capture from neutral hydrogen. Thus, the line intensity from j-th state to

i-th state may be expressed as,

$$I_{ji} = q^{ex}_{eff}(i \to j) n_e n(1) + q^{rec}_{eff}(i \to j) n_e n_+ + q^{cx}_{eff}(i \to j) n_e n_+ \tag{8}$$

where

$$q^{ex}_{eff}(i \to j) = E_i A_{ji} \tag{9a}$$

$$q^{rec}_{eff}(i \to j) = R_i A_{ji} \tag{9b}$$

$$q^{cx}_{eff}(i \to j) = G_i A_{ji} \frac{n_h}{n_e} \tag{9c}$$

Here q^{ex}_{eff}, q^{rec}_{eff} and q^{cx}_{eff} are the so-called local effective emission rate coefficients, and they represent the emission originated from excitation, recombination and charge-exchange, respectively. From these effective emission rate coefficients (calculated for fixed electron and proton temperatures, density, and neutral beam particle energies), the spectra can be determined for arbitrary beam particle flux densities n_h and arbitrary deviations from the ionization equilibrium. We assumed the proton temperature equal to the electron temperature.

In Figs. 13(a), (b) and (c), we show the line intensity of Li III at $T_e = 1000eV$ and $n_e = 10^{13}$ cm^{-3}, in which the upper levels are populated by excitation, recombination and charge exchange, respectively. In each case, the emission $\Delta n = 1$ is the strongest one in its series which locate at longer wavelength side. To understand the emission mechanism, we plot the line intensity ratios of $I(\Delta n = 1)/I(2-1)$ and Lyman series $I(n-1)/I(2-1)$, in Fig.14 and 15, respectively. In these figures, we plot the line intensity ratios for excitation, recombination and charge exchange components separately, and for the emissions including three components in ionization equilibrium with $n_h = 10^{-5} n_e$. It should be noted that the charge exchange reaction plays two roles in the problem: (1)directly populating the excited levels, then introducing CX lines; and (2)shifting the ionization balance to the lower charge stage by producing Li^{2+} ions, then increasing excitation components from $Li^{2+}(1s)$. From Fig. 14, one can see the ratios $I(\Delta n = 1)/I(2-1)$ of excitation component decrease sharply with principal quantum number n. In Fig. 15, the ratios of excitation lines decrease

slower than those in Fig. 14. Although the excitation from the ground state populates np states more than other states, the line intensities for $\Delta n = 1$ are mainly emitted from the states with larger angular momentum. For example, the intensity for $n = 5 - 4$ is dominated by $5f - 4d$ and/or $5g - 4f$, although $5p - 1s$ is the only possible transition for $n = 5 - 1$ in Lyman series. The ratio of charge exchange components decreases more slowly than that of excitation component, because the nl distribution of charge exchange cross section over principal quantum number n and angular quantum number l are broader than that of excitation from the ground state for the collision energy $E_h = 100$ keV/amu as we have shown in Figs. 5 and 6. From Figs. 14 and 15, we can see the line intensity ratios $I(n-1)/I(2-1)$ including three components in ionization equilibrium with $n_h/n_e = 10^{-5}$ are almost the same as the charge exchange component. In Fig. 16 , we plot the percentage contribution of excitation, recombination and charge exchange for Li III $\Delta n = 5-4$ emission. Under typical conditions of fusion plasmas ($T_e = 1000$ eV, $n_e = 10^{13}$ cm^{-3}, $n_h = 10^{-5} n_e$, $E_h = 100$ keV/amu), the line emission of Li III $\Delta n = 5-4$ is mainly due to charge exchange recombination.

C. Line Profile

The emission lines from $n = 5$ to $n = 4$ transitions are in the visible range and they are often measured in fine resolved spectra which can resolve the fine structure lines. Before the detailed discussion of spectral profiles of Li III $\Delta n = 5 - 4$, we would like to show the population densities of $5l$ states in Fig. 19, where these upper levels are populated by excitation (E_i), recombination (R_i) and charge exchange (G_i) under different conditions as shown in the figure.

In Fig. 17, we show the spectral distribution of fine structure lines for $5l - 4l'$ transitions in the case of no magnetic field. The transition probabilities are plotted as a function of wavelength. In magnetically confined plasma, the spectral profiles are perturbed by the Zeeman effect which arises from the interactions of ions with the strong magnetic field existed

in the system. We have made a computer code which can be used to calculate Zeeman effect on energy level and transitions probabilities for arbitrary magnetic field strength [4]. We estimated the influence of the magnetic field on the visible spectral line Li III $\Delta n = 5 - 4$ under field strength B=2 Tesla. Fig. 18 (a)-(f) show the transition probabilities of the Zeeman splitting lines for each separate transitions: $5s - 4p$, $5p - 4s$, $5d - 4p$, $5d - 4f$, $5f - 4d$, $5g - 4f$. Fig. 18 (g) is the sum of all the splitting lines.

In order to estimate the spectral line profiles emitted from ions in plasma, we need to know the population densities of the resolved magnetic sublevels, energy levels and transition probabilities of ions in magnetic field. In a magnetic confined plasma which are heated by neutral beam, there are two special direction defined by magnetic field and neutral heating beam respectively. At the moment, we take the quantization axis along the magnetic field and consider the spectral lines are emitted from thermal plasma where the velocities of plasma particles are isotropic distribution. We also assume the unbalance population distribution over magnetic sublevels are relaxed by the collisions with plasma particles (electrons and ions) rapid enough, and thus the population densities are equal over the magnetic sublevels. In the paper, we consider that the sight line is perpendicular to the magnetic field. Fig. 20 (a) shows the line profiles produced by electron-impact excitation for the line of Li III $\Delta n = 5 - 4$ transitions. The solid line indicate the spectra for B=2T and the dashed line for the case without magnetic field. The electron temperature $T_e = 1000$ eV and the ion temperature $T_i = 1$ eV to decide the width of the line are assumed in the calculation. The contribution of different nl transitions is shown in Fig. 20(b) without magnetic field and in Fig. 20(c) for B=2T. The lines through from $5p - 4s$ and $5s - 4p$ are the strong peaks at shorter wavelength (4498.3 Å) and at longer wavelength (4499.35 Å). When the ion temperature is high $T_i = 200$ eV, the difference between B=0.0 and B=2.0 T can not be distinguished as shown in Fig. 20(d). When the line broadening is dominated by the thermal motion of ions, the spectral profiles is given as follows,

$$J_{ji}(\lambda) = I_{ji}\frac{2}{\Gamma}\sqrt{\frac{\ln 2}{\pi}}Exp\left[-4\ln 2\frac{(\lambda - \lambda_0)^2}{\Gamma^2}\right] \tag{10}$$

where λ_0 is the photon wavelength from j-th state to i-th state, and Γ is the full width half maximum value.

$$\Gamma = 7.7 \times 10^{-5} \lambda_0 \sqrt{T_i / A_i}$$

where T_i is the ion temperature measured in eV, A_i is the atomic mass of ions.

Next we see the spectra produced by charge exchange recombination with collision energy $E_h = 100$ keV/amu or $E_h = 25$ keV/amu. The calculated CX spectra for B=0 and B=2.0 T are shown in Figs. 21(a) and 22(a), respectively. Peak of these CX lines are near 4499Åwhich are produced from the $5f - 4d$ transition as shown in Figs. 21 (b)-(c) and 22 (b)-(c). However, in case of $E_h = 25$ keV/amu, the line emission from $5g - 4f$ transition contributes more than that of $E_h = 100$ keV/amu. Due to the broader l-distribution of the CX cross sections at $E_h = 25$ keV/amu. Fig. 21(d) and 22(d) show the line profiles for $T_i = 200$ eV. Fig. 23(a) shows the spectra produced by radiative recombination at electron temperature $T_e = 10$ eV with B=0.0 T and B=2.0 T. According to the calculated spectra, peak of the line locates at around 4499.1Åwhich is produced from the transition $5g - 4f$. For the radiative recombination spectra, the line of $5g - 4f$ dominates others as shown in Fig. 23(b) and (c).

In order to compare the spectra produced by different mechanism, we plot the charge exchange spectra with $E_h = 100$ keV/amu (dotted line) and $E_h = 25$ keV/amu (dashed line) in Fig.24(a), and excitation spectra and radiative recombination spectra in Fig. 24(b). We also plot in Fig. 24(a) the statistical equilibrium spectra. From Fig. 24(a), we can see that, with the increase of the collision kinetic energy E_h increase, the intensity of CX lines decrease because of CX cross sections decrease with E_h. The peak of statistical equilibrium spectra is at the longer wavelength (4499.1Å) than those of CX spectra. Comparing Fig. 24(a) with Fig. 24(b), the peak of recombination spectra is close to the peak of statistical equilibrium spectra and the apparent width of excitation spectra is broader than those of charge exchange, recombination and statistical equilibrium spectra. The broader excitation spectra is due to the larger intensity from p states.

To estimate the perturbation of Zeeman broadening on ion temperature measurements,

we plot the statistical equilibrium spectra with B=0.0 (solid line), 2.0 (dashed line), 5.0 (dotted line), 10.0 (dot-dashed line) Tesla with real ion temperature $T_i = 10$ eV in Fig. 25. From these spectral profiles, we can deduced the apparent ion temperatures to be 10.8, 28.6 and 110.3 eV for B=0.0, 2.0 and 5.0 Tesla, respectively. The error introduced by Zeeman broadening are factor of 2.65 or 10.2 with B=2.0 or 5.0 T compared with no magnetic field. At very high magnetic fields (on the order of 10 T), the line splitting by normal Zeeman effect has been studied well. When ion temperature is high, the difference between B=0.0 and B=2.0 T can not be distinguished as shown in Figs. 20(d), 21(d), 22(d) and 23(d). Generally the Zeeman effect is neglected for a charged ion because of the Doppler broadening through ion motion. However for a low ion temperature below 50 eV, the Zeeman effect is not negligible for a spectral broadening in magnetic confined plasma with 2 Tesla.

V. CONCLUSION

We have made a $n - l$ resolved collisional radiative model up to $n = 20$ for H-like Li ions including the charge exchange processes. The excitation data used in our model are calculated by the ATOM code [9] which are in a good agreement with DW results [10,11] and disagree with RMPS calculation [12]. RMPS data (which should be best) are incomplete and disagree with other data. Better R-matrix (or other close-coupling) calculations are needed for H-like ions excitation process. In our model, the emissions of Li^{2+} ions are separated into three independent components originating from electron impact excitation, electron-ion recombination and charge exchange. In the case of neutral beam injection, the charge exchange component is dominant.

The spectral profiles emitted from ions in plasma are influenced by several atomic physics and environmental effects. In this paper, we examined the perturbations of atomic fine structure and Zeeman effect which arises from the interactions of ions with the strong magnetic field in the system. At high magnetic field and low ion temperatures, the apparent broadening introduced by Zeeman effect must be included for reliable interpretation of the

measured spectra. We have shown the contribution of the different nl-$n'l'$ transitions in the fine structure Zeeman spectra. When the ion temperature is high enough to swear out the fine structure components and Zeeman effect, the peak position of line profiles produced by charge exchange and by excitation are different by $0.2\mathring{A}$ towards the shorter wavelength than those by recombination and statistical distribution.

ACKNOWLEDGMENTS

We are grateful to acknowledge useful discussions and suggestions during course of this work from Professor R. More, T. Fujimoto, K. Kondo, K. Ida. One of us (S. Zou) would like to thank the Japan Society of Plasma Science and Nuclear Fusion Research for the award of an scholarship to support his study in Japan. We also acknowledge the NIFS database CHART for finding numerical data for charge exchange cross sections.

REFERENCES

[1] K. Kondo, K. Ida *et al.*, J. Nucl. Mater **241-243**, 956(1997).

[2] K. Khlopenkov, Impurity Transport Study by means of Tracer-Encapsulated Pellet Injection. Dissertation for the PhD. Department of Fusion Science, The Graduate University for Advanced Studies, NIFS, Japan (1998).

[3] R. J. Fonck, Rev. Sci. Instrum. **56**, 885(1985).

[4] H. A. Bethe and E. E. Salpeter, Quantum Mechanics of One and Two Electron Atoms, Springer-Verlag (1957).

[5] H. P. Summers, Mon. Not. R. Astron. Soc. **178**, 101(1977).

[6] J. Spence and H. P. Summers, J. Phys. B **19**, 3749(1986).

[7] T. Fujimoto, J. Phys. Soc. Jpn. **47** 265(1979), **47** 272(1979), **49** 1561(1980), **29** 1569(1980), **54**, 2905(1985); J. Quant. Spectrosc. Radiat. Transfer **21**, 439(1979).

[8] R. Mewe, Astron. Astrophys. **20**, 215(1972).

[9] V.P. Shevelko and L.A. Vainshtein, Atomic physics for hot plasmas, Institute of Physics Pub. , 1993

[10] The relativistic multiconfinguration Hebrew University Lawrence Livermore atomic code (HULLAC).

[11] E. H. Clark and J. Abdallah, Jr, Phys. Scr. **T62** 7(1996).

[12] N. R. Badnell and T. W. Gorczyca. J. Phys. B. **30**, 2011(1997).

[13] V. L. Jacobs, J. Davis, Phys. Rev. A. **18**, 697(1978).

[14] W. Lotz, Physik **216**, 1679(1968).

[15] A. Burgess, Mem. R. Astron. Soc. **69**, 1(1964).

[16] N. Toshima, H. Tawara, NIFS-DATA **26**, 1(1995).

[17] R. K. Janev et al. INDC(NDS) 393(1999).

[18] http://dbshino.nifs.ac.jp

[19] R. K. Janev, Atomic and molecular processes in fusion edge plasmas, Plenum Press (1995)

FIGURES

FIG. 1. Electron-impact excitation collision strength for the $1s-2s$ (a) and $1s-5s$ (b) transitions in hydrogen-like ions. The solid quadrangles with line denote the results by the ATOM code; the solid circles, Hullac code; the upward and downward triangles, Clark *et al.* (1996); the open circles, Badnell *et al.* (1997)

FIG. 2. Electron-impact excitation collision strength for the $1s-2p$ (a) and $1s-5p$ (b) transitions in hydrogen-like ions. The solid quadrangles with line denote the results of the ATOM code; the solid circles, Hullac code; the upward and downward triangles, Clark *et al.* (1996)

FIG. 3. Electron-impact excitation collision strength for the $4s-5s$ transition in hydrogen-like Li^{2+} ions. The solid quadrangles with line denote the results of the ATOM code; the solid circles, Hullac code; the open circles, Badnell *et al.* (1997)

FIG. 4. The energy dependence of charge exchange cross section. The solid quadrangles denote the results of Toshima *et al.* (1995)for Li^{3+}+H(1s); the open circles, Janev *et al.* (1999) for Li^{3+}+H(2s). The solid and dash lines are the estimated values for Li^{3+}+H(1s) and Li^{3+}+H(2s) systems by empirical formula, respectively.

FIG. 5. The n-dependence of charge exchange cross section σ_n at collision energies $E_h = 25$ keV/amu and $E_h = 100$ keV/amu for $Li^{3+} + H(1s)$. The open quadrangles are for $E_h = 25$ keV/amu and solid circles for 100 keV/amu.

FIG. 6. The l-dependence of charge exchange cross section σ_{nl} at collision energy $E_h = 25$ keV/amu and $E_h = 100$ keV/amu, where the principal quantum number n equals to 5. The open quadrangles are for $E_h = 25$ keV/amu and solid circles for 100 keV/amu.

FIG. 7. The population coefficients (E_i, R_i and G_i) of np-states (a) and nd-states (b) divided by statistical weights as functions of principal quantum number n at $T_e = 1000$ eV, $n_e = 10^{13}$ cm^{-3}, $E_h = 100$ keV/amu and $n_h = 10^{-5} n_e$.

FIG. 8. The temperature dependence of population coefficients (E_i, R_i, G_i) for $5l$ divided by statistical weights at $E_h = 100$ keV/amu and $n_h = 10^{-5} n_e$. The solid quadrangles are for $5s$; the circles, $5p$; the upward triangles, $5d$; the downward triangles, $5f$; the open circles, $5g$. E_i/g_i, R_i/g_i and G_i/g_i are shown in (a), (b) and (c) respectively.

FIG. 9. The density dependence of population coefficients (E_i, R_i, G_i) for $5l$ divided by statistical weights at $E_h = 100$ keV/amu and $n_h = 10^{-5} n_e$. The solid quadrangles are for $5s$; the circles, $5p$; the upward triangles, $5d$; the downward triangles, $5f$; the open circles, $5g$. E_i/g_i, R_i/g_i and G_i/g_i are shown in (a), (b) and (c) respectively.

FIG. 10. The effective ionization and recombination rate coefficients (S_{cr}, α_{cr}) as functions of electron temperature T_e with no neutral beam injection and with neutral beam density at $n_h = 10^{-4} n_e$, $10^{-5} n_e$ and $10^{-6} n_e$, respectively. In the figure, $E_h = 100$ keV/amu and $n_e = 10^{13}$ cm^{-3}.

FIG. 11. The population densities ($n(i)$) of np and nd states as functions of principal quantum number n with $n_h = 10^{-5} n_e$ and 0, respectively. In the figure, $T_e = 1000$ eV, $E_h = 100$ keV/amu and $n_e = 10^{13}$ cm^{-3}.

FIG. 12. Electron-impact excitation rate coefficients for $1s - nd$ and $2s - nd$ transitions as function of principal quantum number n at $T_e = 1000$ eV and $n_e = 10^{13}$ cm^{-3}.

FIG. 13. Line intensities ($I_{ji}/n_e/n(1s)$ or $I_{jl}/n_e/n_+$) originated from excitation (a), recombination (b) and charge exchange (c) in the wavelength range 10 nm to 500 nm, at $n_h = n_e 10^{-5}$, $E_h = 100$ keV/amu, $T_e = 1000$ eV and $n_e = 10^{13}$ cm^{-3}.

FIG. 14. Line intensity ratios for $I(\Delta n = 1)/I(\Delta n = 2 - 1)$) originated from excitation (a), recombination (b) and charge exchange (c) at $n_h = n_e 10^{-5}$, $E_h = 100$ keV/amu, $T_e = 1000$ eV and $n_e = 10^{13}$ cm^{-3}.

FIG. 15. Line intensity ratios for $I(\Delta n = n' - 1)/I(\Delta n = 2 - 1))$ originated from excitation (a), recombination (b) and charge exchange (c) at $n_h = n_e 10^{-5}$, $E_h = 100$ keV/amu, $T_e = 1000$ eV and $n_e = 10^{13}$ cm^{-3}.

FIG. 16. Percentage contributions to the line intensity of Li III $\Delta n = 5 - 4$ from various processes excitation (a), recombination (b) and charge exchange (c) at $n_h = n_e 10^{-5}$, $E_h = 100$ keV/amu, $T_e = 1000$ eV and $n_e = 10^{13}$ cm^{-3}.

FIG. 17. The spectral distribution of fine structure lines for $5l - 4l'$ transitions for Li III ions in the case of no magnetic field.

FIG. 18. The transition probabilities of the Zeeman splitting lines for separated transitions; $5s - 4p$, $5p - 4s$, $5d - 4p$, $5d - 4f$, $5f - 4d$ and $5g - 4f$. The sum of all the splitting lines is shown in (g). In these figures, the magnetic field strength B is taken as 2T.

FIG. 19. The l-dependence of population coefficients with principal quantum number $n = 5$. The circles denote charge exchange population coefficients G_i/g_i; the quadrangles for excitation population coefficients E_i/g_i; the triangles for recombination population coefficients R_i/g_i.

FIG. 20. The line profiles of Li III ($\Delta n = 5 - 4$) produced by electron-impact excitation. In figures (a) and (d), the solid line indicate the spectra for B=2T and the dash line for the case with no magnetic field. Figures (b) and (c) show the contributions from different transitions with no field and with a magnetic field B=2T. In these figure, the electron temperature and density are taken as $T_e = 10^3$ eV and $n_e = 10^{13}$ cm^{-3}. The ion temperatures are assumed as $T_i = 1$ eV in (a),(b),(c) and as $T_i = 200$ eV in (d).

FIG. 21. The line profiles of Li III ($\Delta n = 5 - 4$) produced by charge exchange with neutral hydrogen. In figures (a) and (d), the solid line indicate the spectra for B=2T and the dash line for the case with no magnetic field. Figures (b) and (c) show the contributions from different transitions with no field and with a magnetic field B=2T. The kinetic energy of neutral hydrogen atoms is taken as $E_h = 100$ keV/amu. The ion temperature is assumed as $T_i = 1$ eV in (a),(b),(c) and as $T_i = 200$ eV in (d).

FIG. 22. The line profiles of Li III ($\Delta n = 5 - 4$) produced by charge exchange with neutral hydrogen. In figure (a), the solid line indicate the spectra for B=2T and the dash line for the case with no magnetic field. Figures (b) and (c) show the contributions from different transitions with no field and with a magnetic field B=2T. The kinetic energy of neutral hydrogen atoms is taken as $E_h = 25$ keV/amu. The ion temperature is assumed as $T_i = 1$ eV in (a),(b),(c) and as $T_i = 200$ eV in (d).

FIG. 23. The line profiles of Li III ($\Delta n = 5 - 4$) produced by electron-ion recombination. In figure (a), the solid line indicate the spectra for B=2T and the dash line for the case with no magnetic field. Figures (b) and (c) show the contributions from different transitions with no field and with a magnetic field B=2T. The electron temperature and density are taken as $T_e = 10$ eV and $n_e = 10^{13}$ cm^{-3}. The ion temperature is assumed as $T_i = 1$ eV in (a),(b),(c) and as $T_i = 200$ eV in (d).

FIG. 24. (a) The line profiles of Li III ($\Delta n = 5-4$) of statistical equilibrium spectra and charge exchange spectra. The solid line indicate the spectra statistical equilibrium; the dashed line, charge exchange spectra with $E_h = 25$ keV/amu; the dotted line, charge exchange spectra with $E_h = 100$ keV/amu. (b)The line profiles of Li III ($\Delta n = 5 - 4$) produced by electron-impact excitation and electron-ion recombination. The dashed line, electron-impact excitation spectra with $T_e = 1000$ eV; the dotted line, electron-ion recombination spectra with $T_e = 10$ eV. The ion temperature is assumed as $T_i = 10$ eV with a magnetic field B=2T.

FIG. 25. The statistical equilibrium spectra of Li III ($\Delta n = 5 - 4$) with B=0.0, 2.0, 5.0, 10.0 Tesla The solid line indicate the spectra for B=0.0 T; the dash line for B=2.0 T; the dot line for B=5.0 T; the dash dot dot line for B=10.0 T. The ion temperature is assumed as $T_i = 10$ eV

Fig. 1(a)

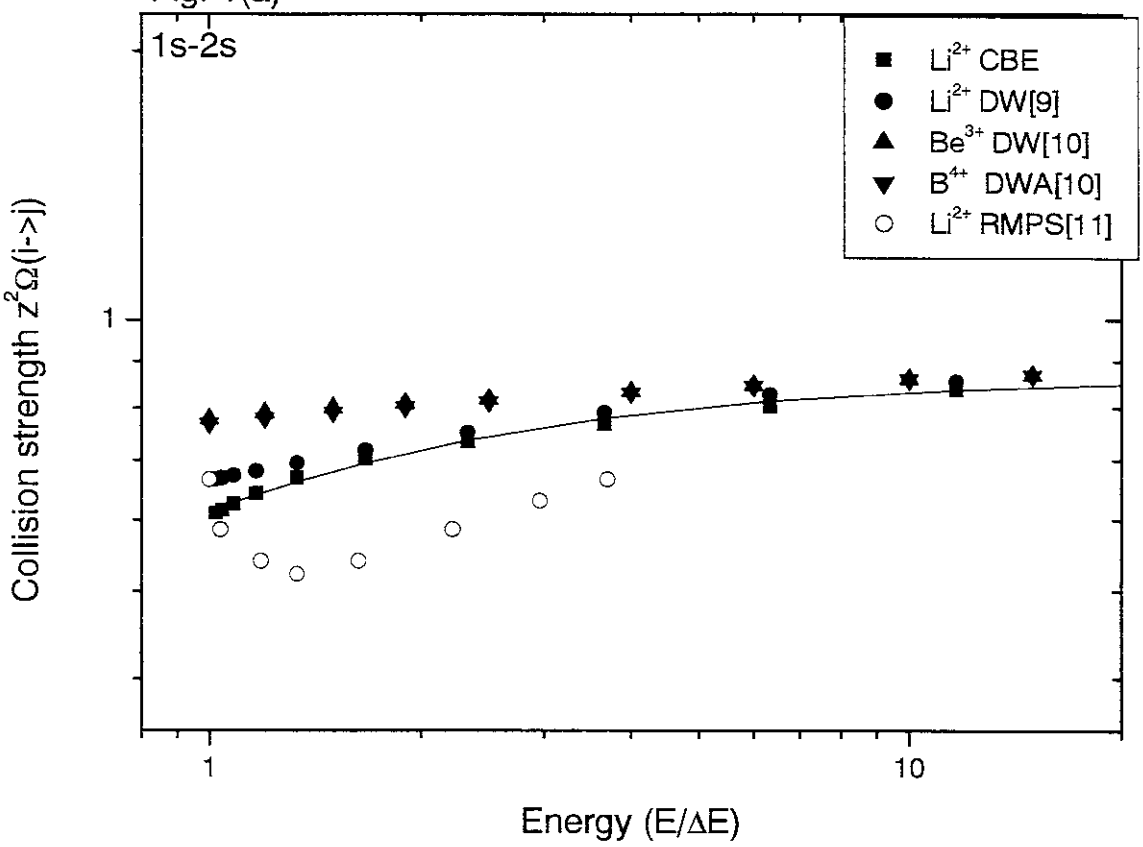
1s-2s
Li2+ CBE
Li2+ DW[9]
Be3+ DW[10]
B4+ DWA[10]
Li2+ RMPS[11]
Collision strength z2Ω(i->j)
1
1
10
Energy (E/ΔE)

Fig. 1(b)

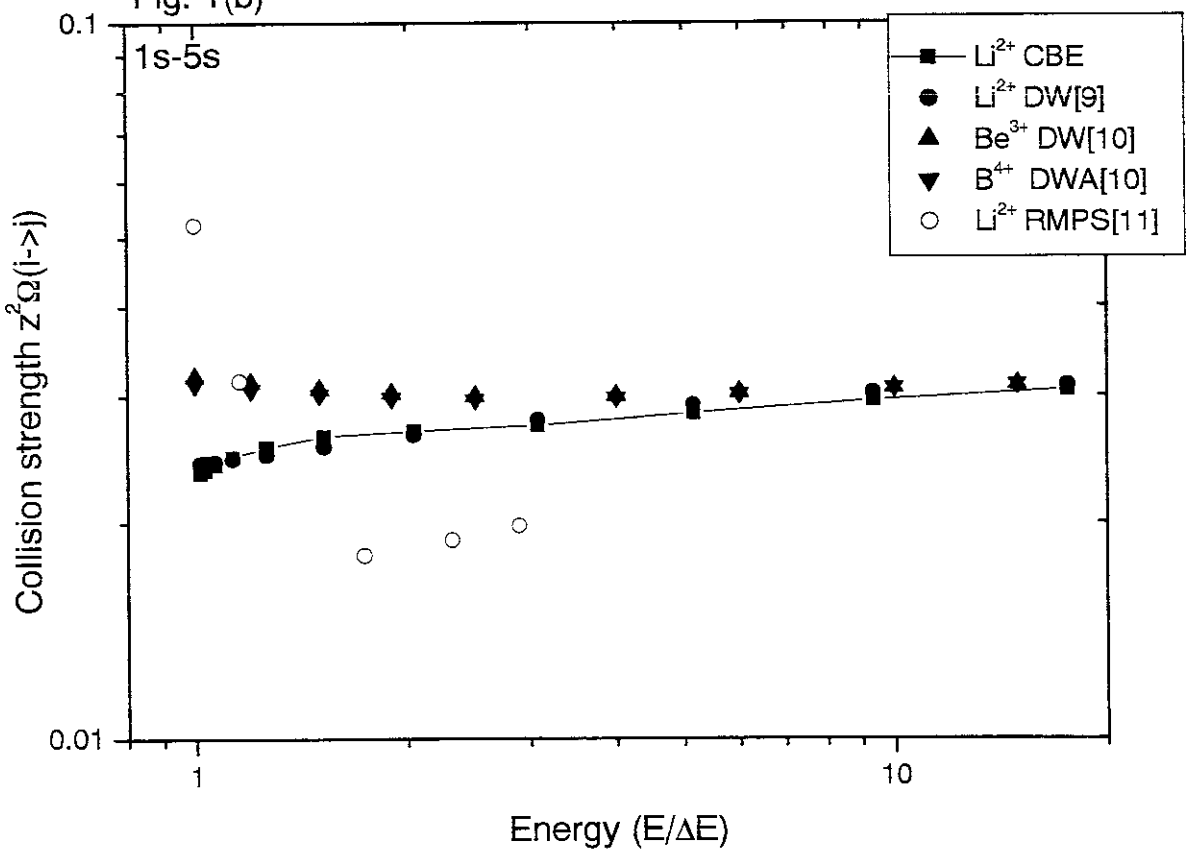
1s-5s
Li2+ CBE
Li2+ DW[9]
Be3+ DW[10]
B4+ DWA[10]
Li2+ RMPS[11]
Collision strength z2Ω(i->j)
0.1
0.01
1
10
Energy (E/ΔE)

Fig. 2(a)

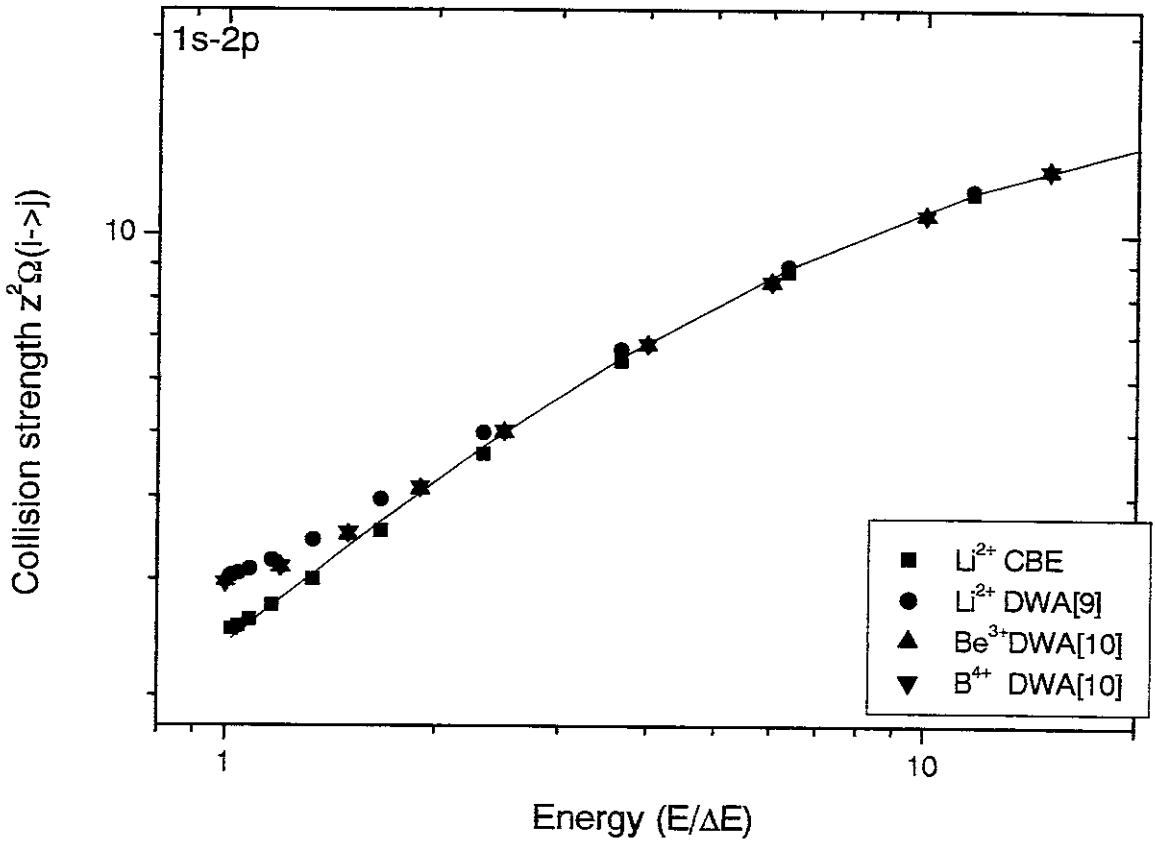
1s-2p
Collision strength $z^2\Omega(i->j)$
10
1
10
Energy (E/ΔE)
Li^{2+} CBE
Li^{2+} DWA[9]
Be^{3+}DWA[10]
B^{4+} DWA[10]

Fig. 2(b)

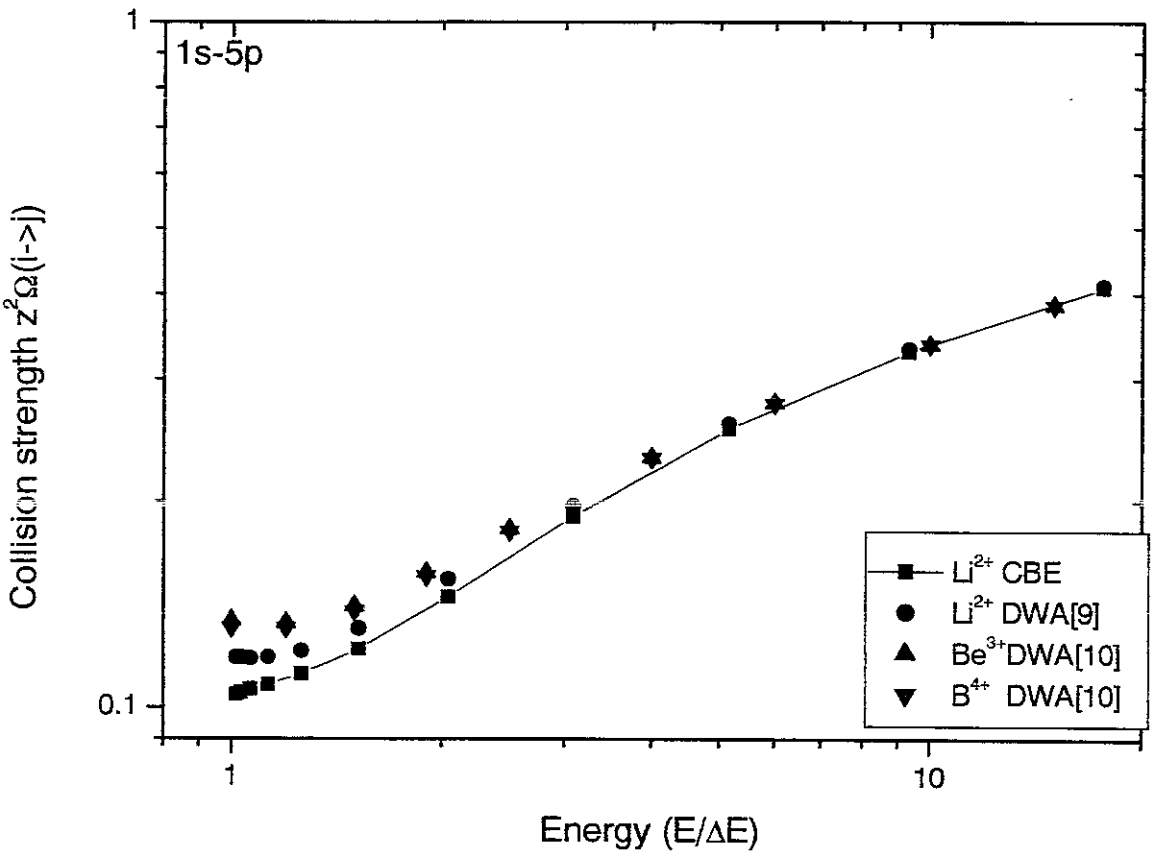
1s-5p
Collision strength $z^2\Omega(i->j)$
1
0.1
1
10
Energy (E/ΔE)
Li^{2+} CBE
Li^{2+} DWA[9]
Be^{3+}DWA[10]
B^{4+} DWA[10]

Fig. 3

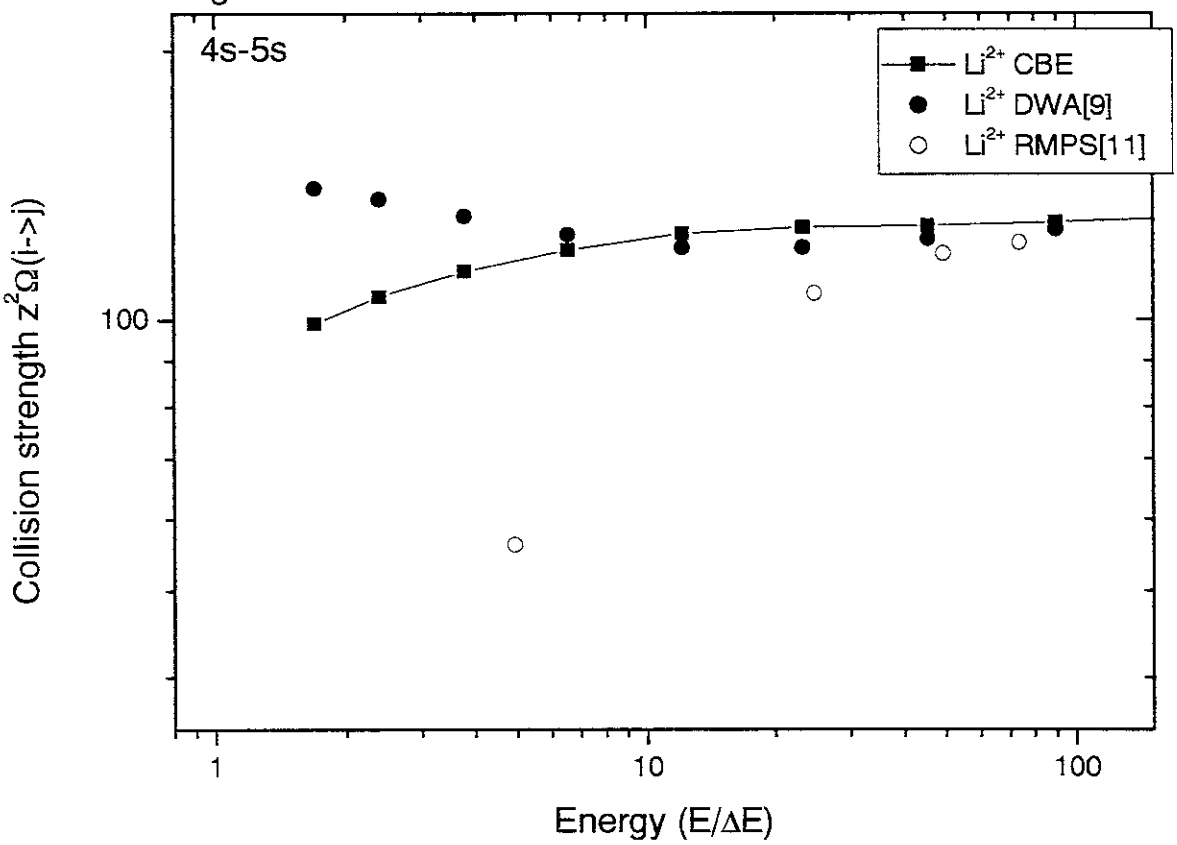
4s-5s
Li2+ CBE
Li2+ DWA[9]
Li2+ RMPS[11]
Collision strength z2Ω(i->j)
100
1
10
100
Energy (E/ΔE)

Fig. 4

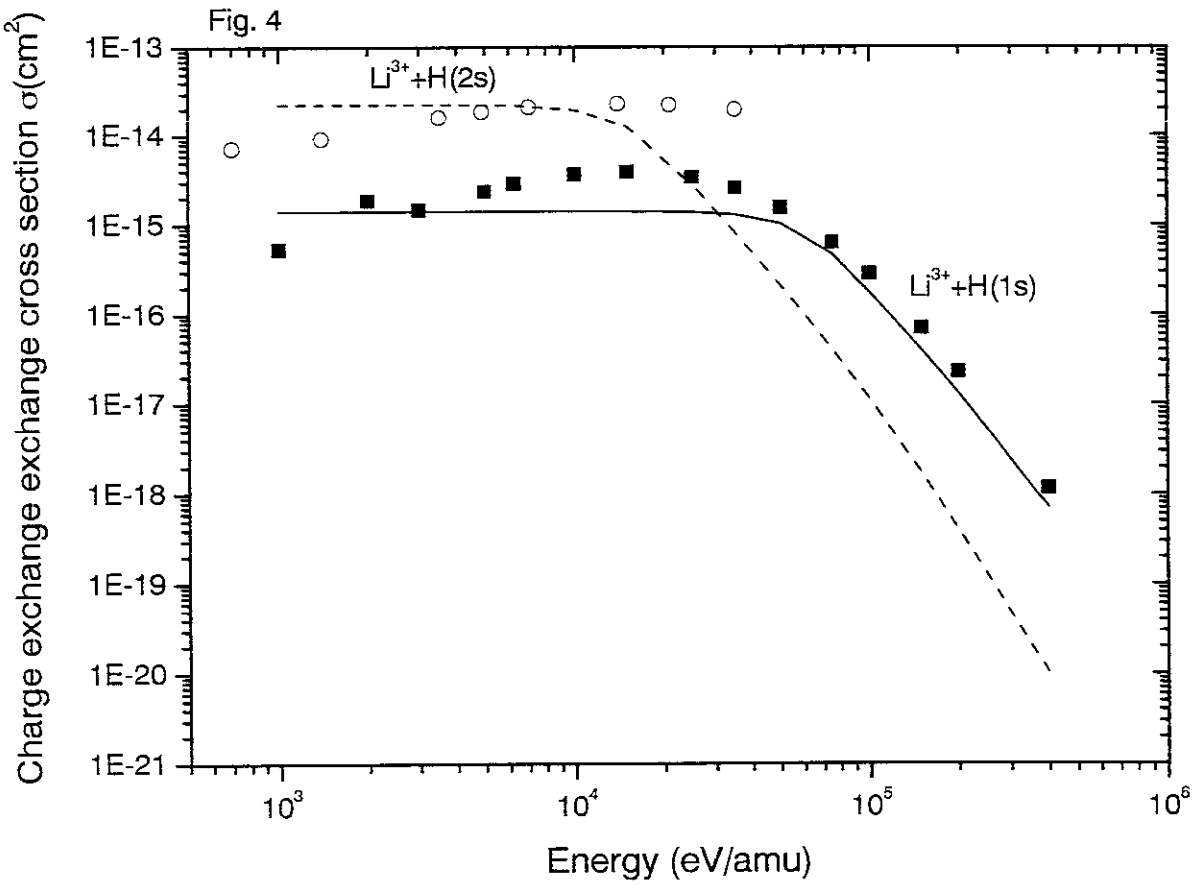
Li3+ +H(2s)
Li3+ +H(1s)
Charge exchange exchange cross section σ(cm2)
1E-13
1E-14
1E-15
1E-16
1E-17
1E-18
1E-19
1E-20
1E-21
10^3
10^4
10^5
10^6
Energy (eV/amu)

Fig. 5

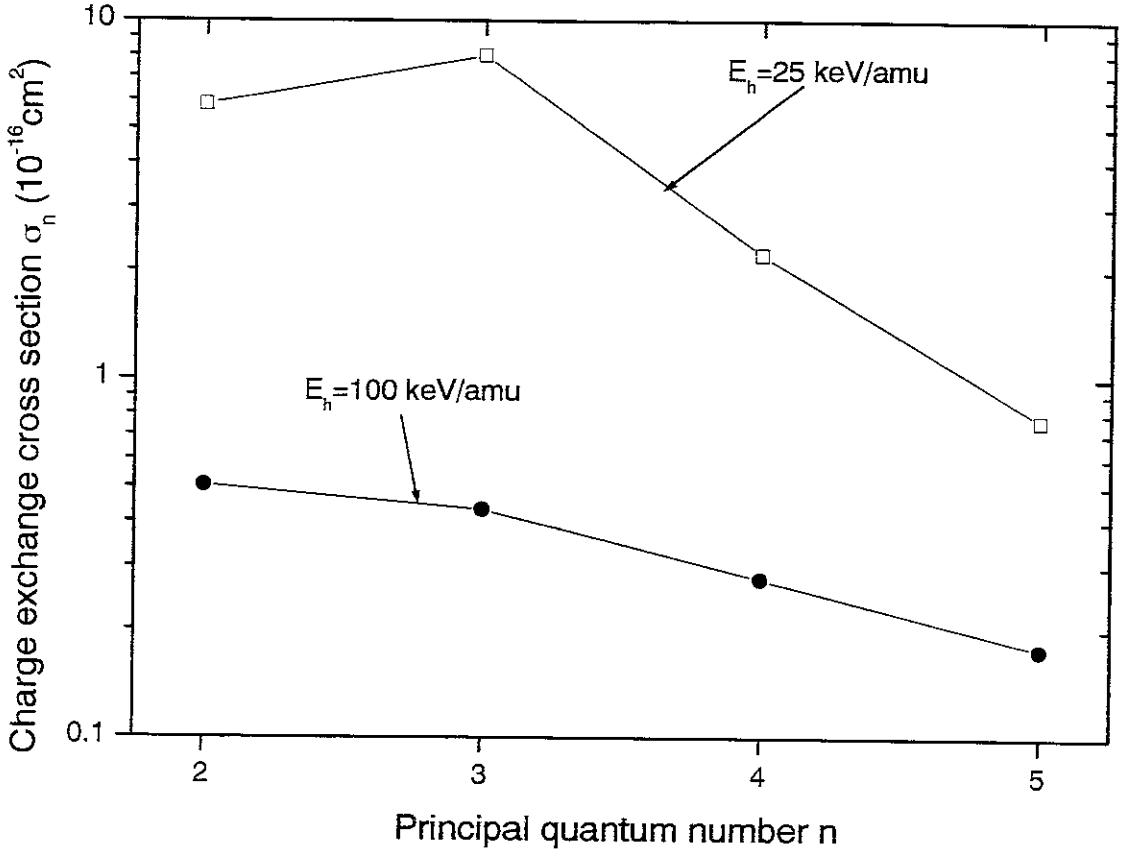
10
1
0.1
2
3
4
5
E_h=25 keV/amu
E_h=100 keV/amu
Charge exchange cross section σ_n (10^{-16}cm^2)
Principal quantum number n

Fig. 6

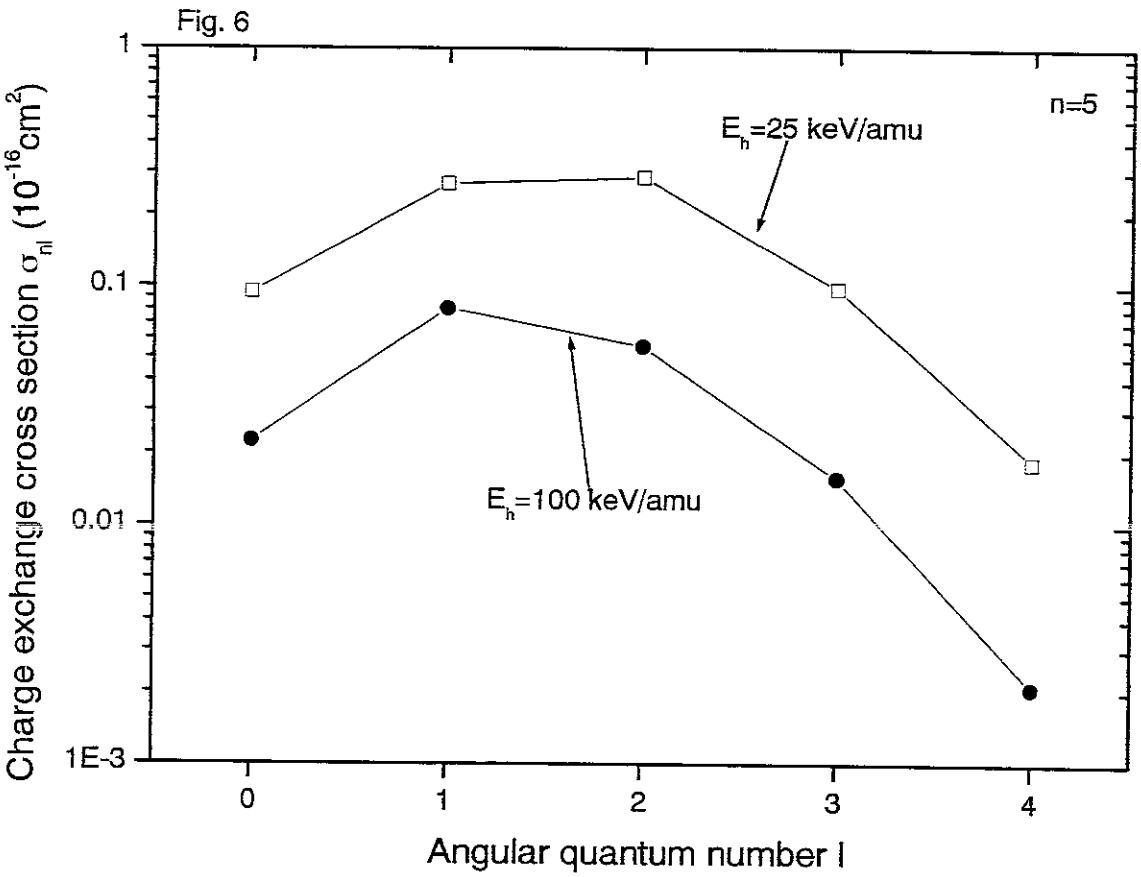
1
0.1
0.01
1E-3
0
1
2
3
4
n=5
E_h=25 keV/amu
E_h=100 keV/amu
Charge exchange cross section σ_{nl} (10^{-16}cm^2)
Angular quantum number l

Fig. 7(a)

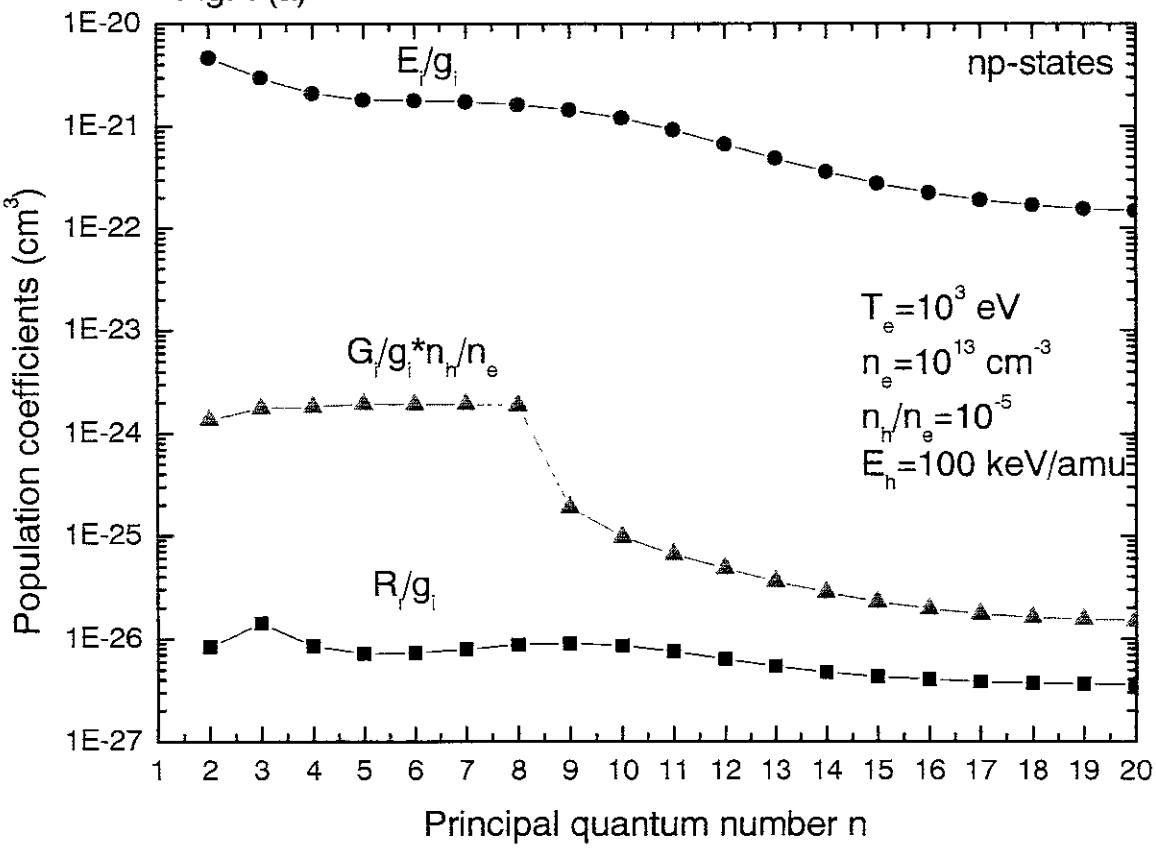
E_f/g_i
np-states
G_f/g_i*n_h/n_e
R_f/g_i
T_e=10^3 eV
n_e=10^13 cm^-3
n_h/n_e=10^-5
E_h=100 keV/amu
Population coefficients (cm^3)
Principal quantum number n

Fig. 7(b)

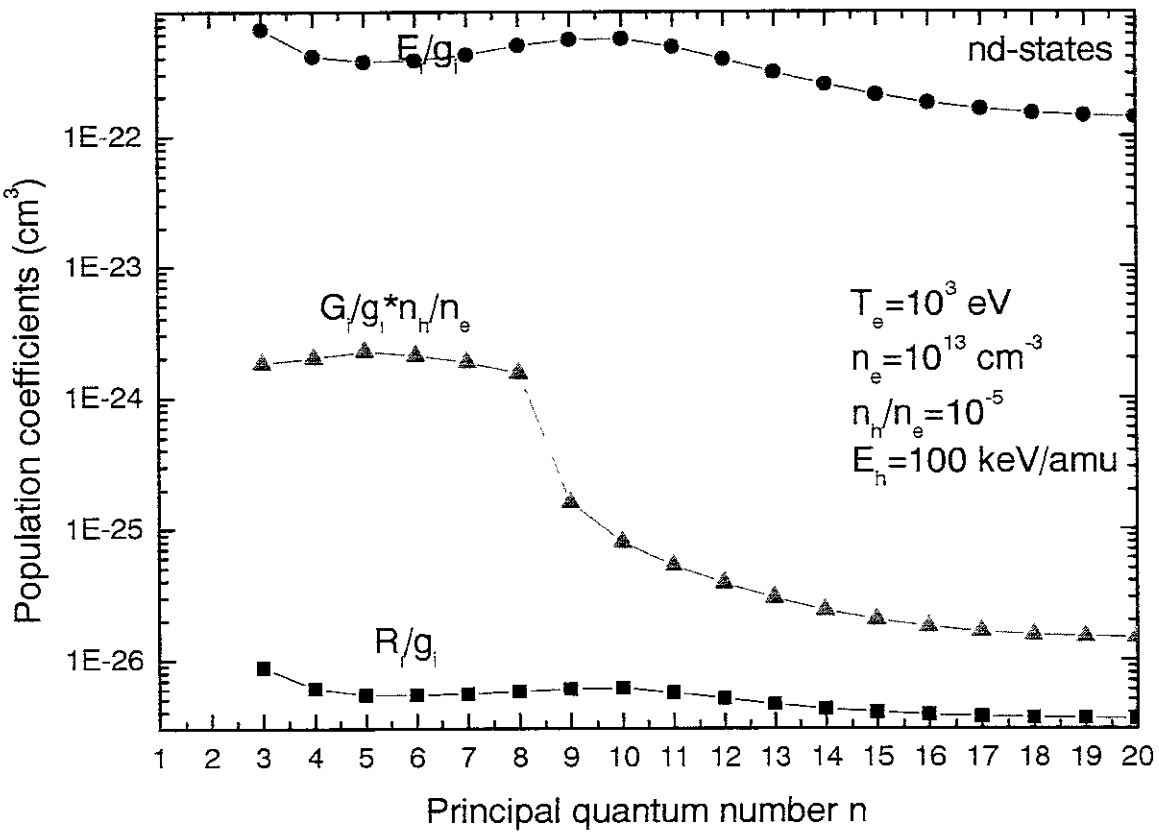
E_f/g_i
nd-states
G_f/g_i*n_h/n_e
R_f/g_i
T_e=10^3 eV
n_e=10^13 cm^-3
n_h/n_e=10^-5
E_h=100 keV/amu
Population coefficients (cm^3)
Principal quantum number n

Fig. 8(a)

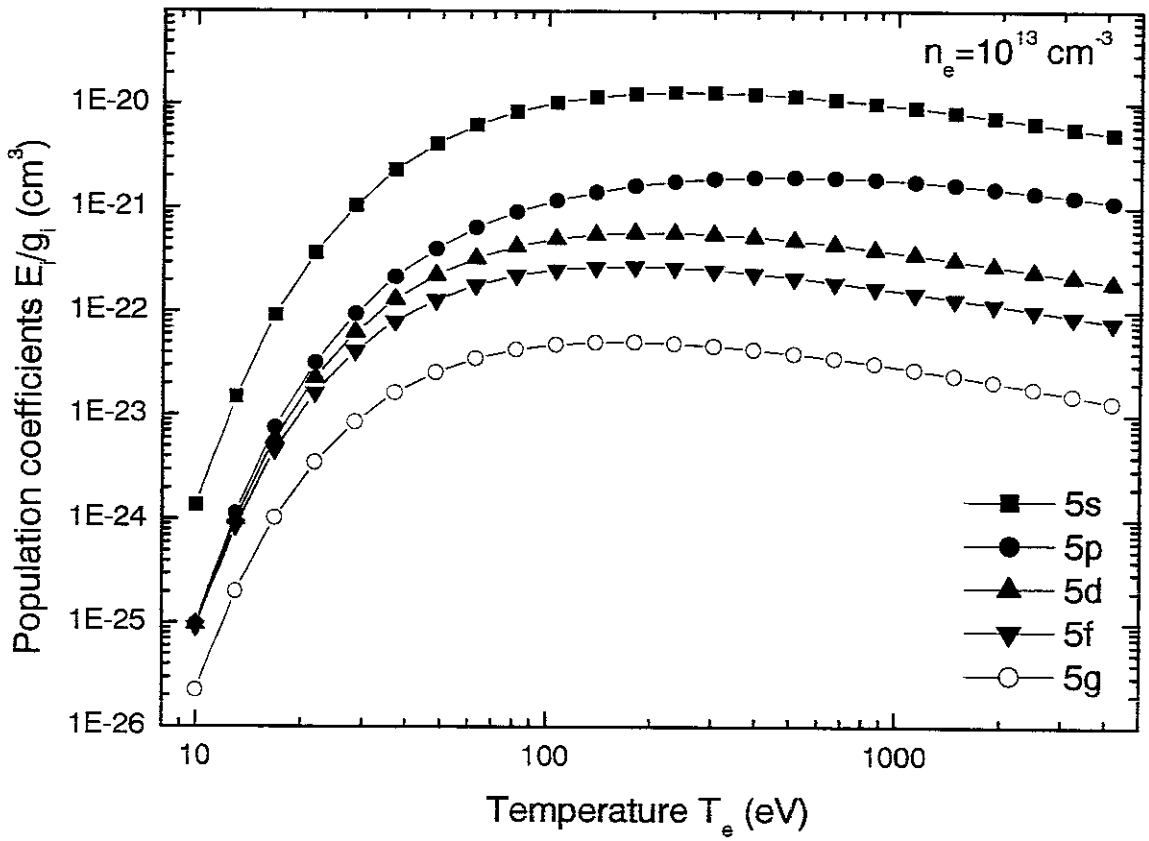
$n_e=10^{13}$ cm^{-3}
Population coefficients E_i/g_i (cm^3)
1E-20
1E-21
1E-22
1E-23
1E-24
1E-25
1E-26
10
100
1000
Temperature T_e (eV)
5s
5p
5d
5f
5g

Fig. 8(b)

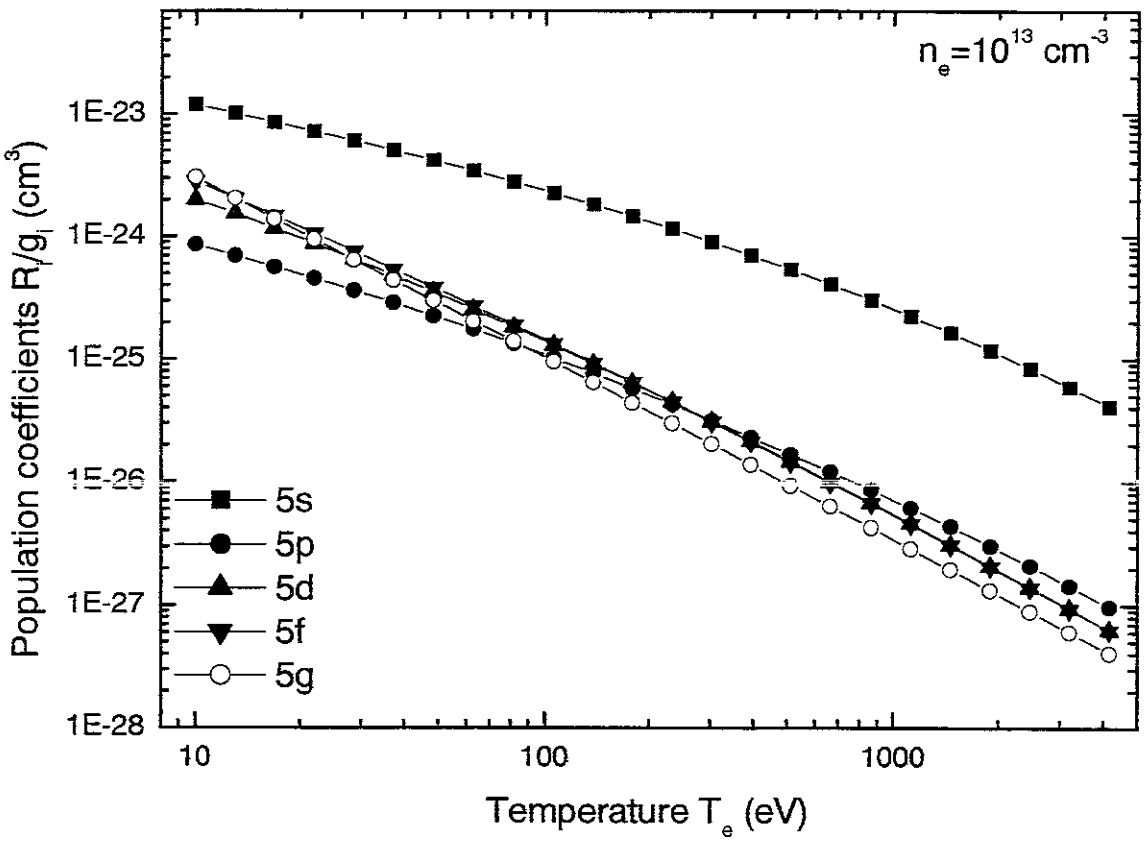
$n_e=10^{13}$ cm^{-3}
Population coefficients R_i/g_i (cm^3)
1E-23
1E-24
1E-25
1E-26
1E-27
1E-28
10
100
1000
Temperature T_e (eV)
5s
5p
5d
5f
5g

Fig. 8(c)

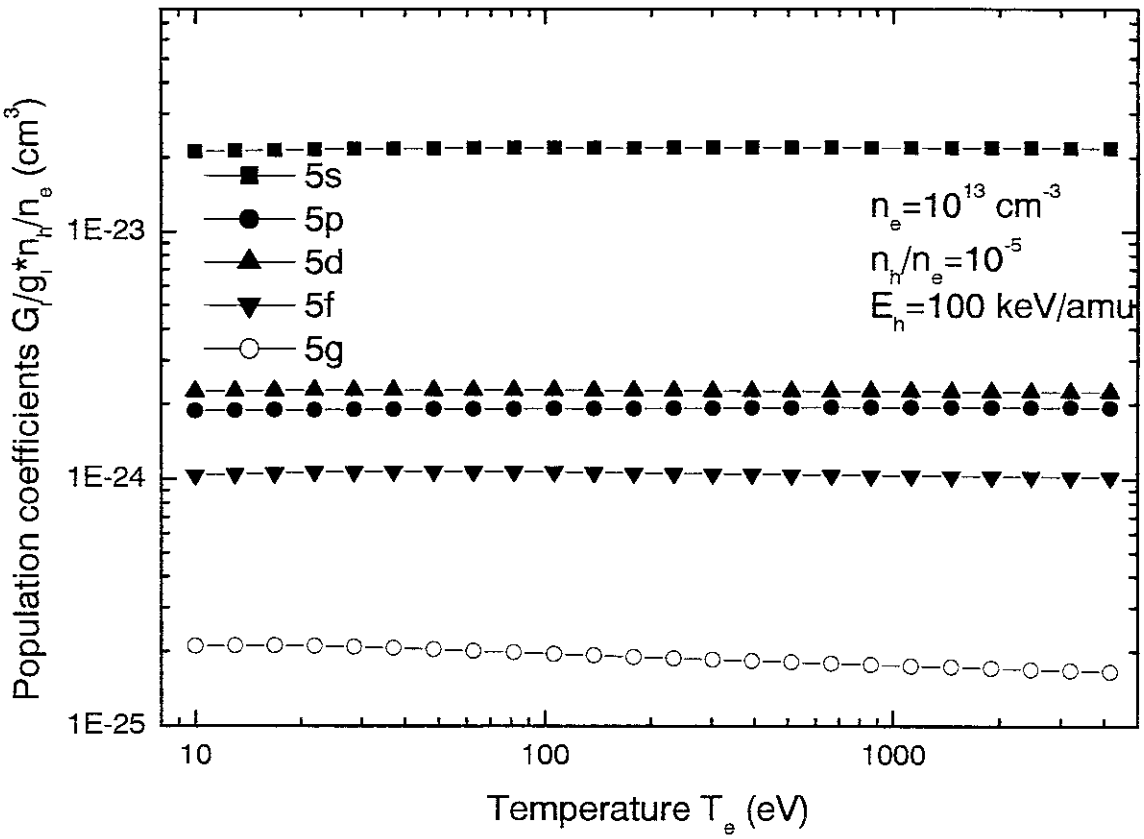
Population coefficients G/g_l*n_h/n_e (cm^3)
1E-23
1E-24
1E-25
10
100
1000
Temperature T_e (eV)
5s
5p
5d
5f
5g
n_e=10^13 cm^-3
n_h/n_e=10^-5
E_h=100 keV/amu

Fig. 9(a)

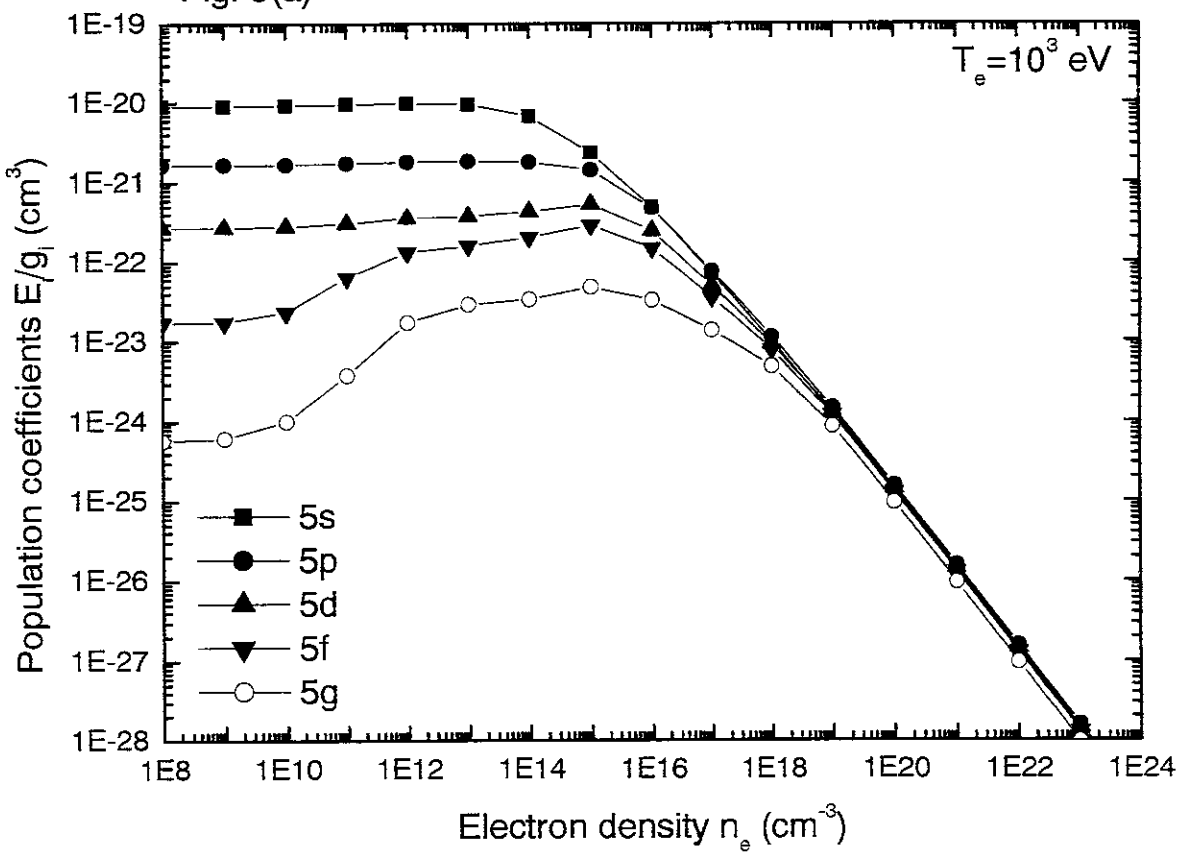
Population coefficients E/g_l (cm^3)
1E-19
1E-20
1E-21
1E-22
1E-23
1E-24
1E-25
1E-26
1E-27
1E-28
1E8
1E10
1E12
1E14
1E16
1E18
1E20
1E22
1E24
Electron density n_e (cm^-3)
T_e=10^3 eV
5s
5p
5d
5f
5g

Fig. 9(b)

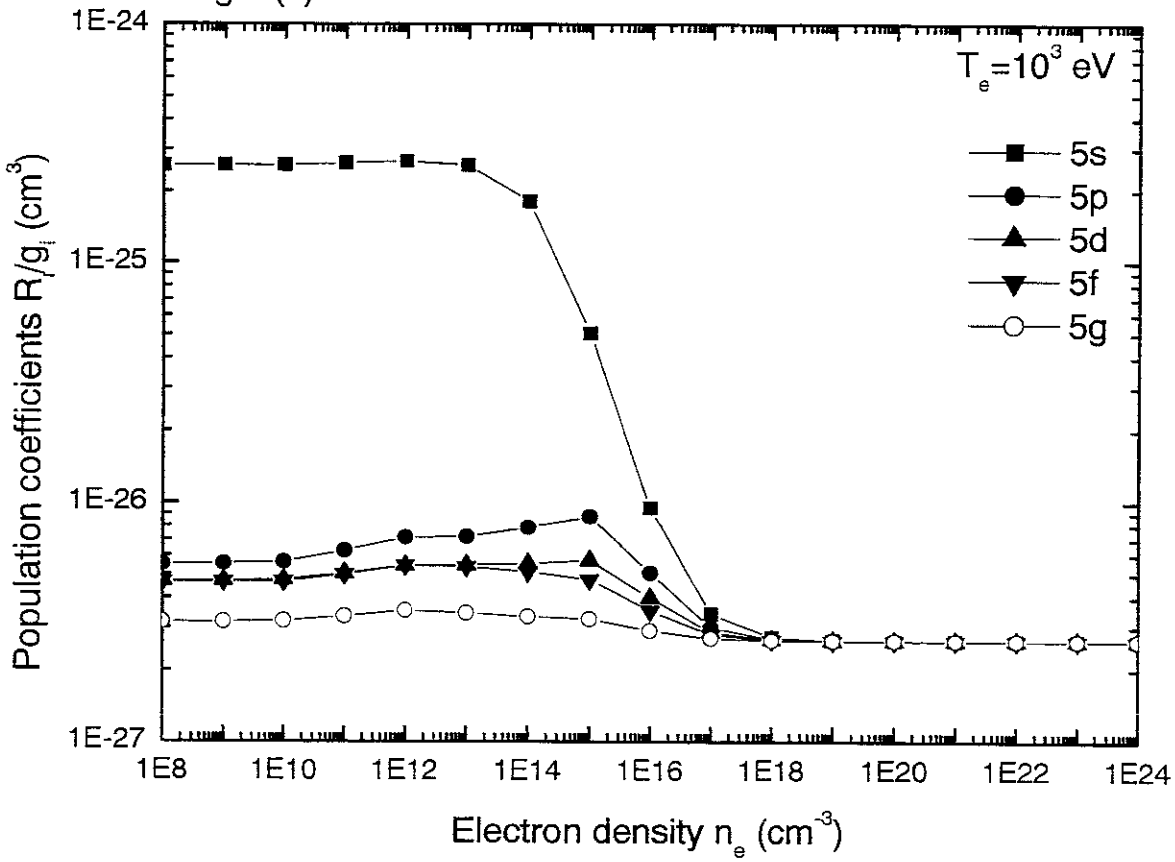
1E-24
1E-25
1E-26
1E-27
Population coefficients R/g (cm3)
T=10 eV
5s
5p
5d
5f
5g
1E8
1E10
1E12
1E14
1E16
1E18
1E20
1E22
1E24
Electron density n (cm-3)

Fig. 9(c)

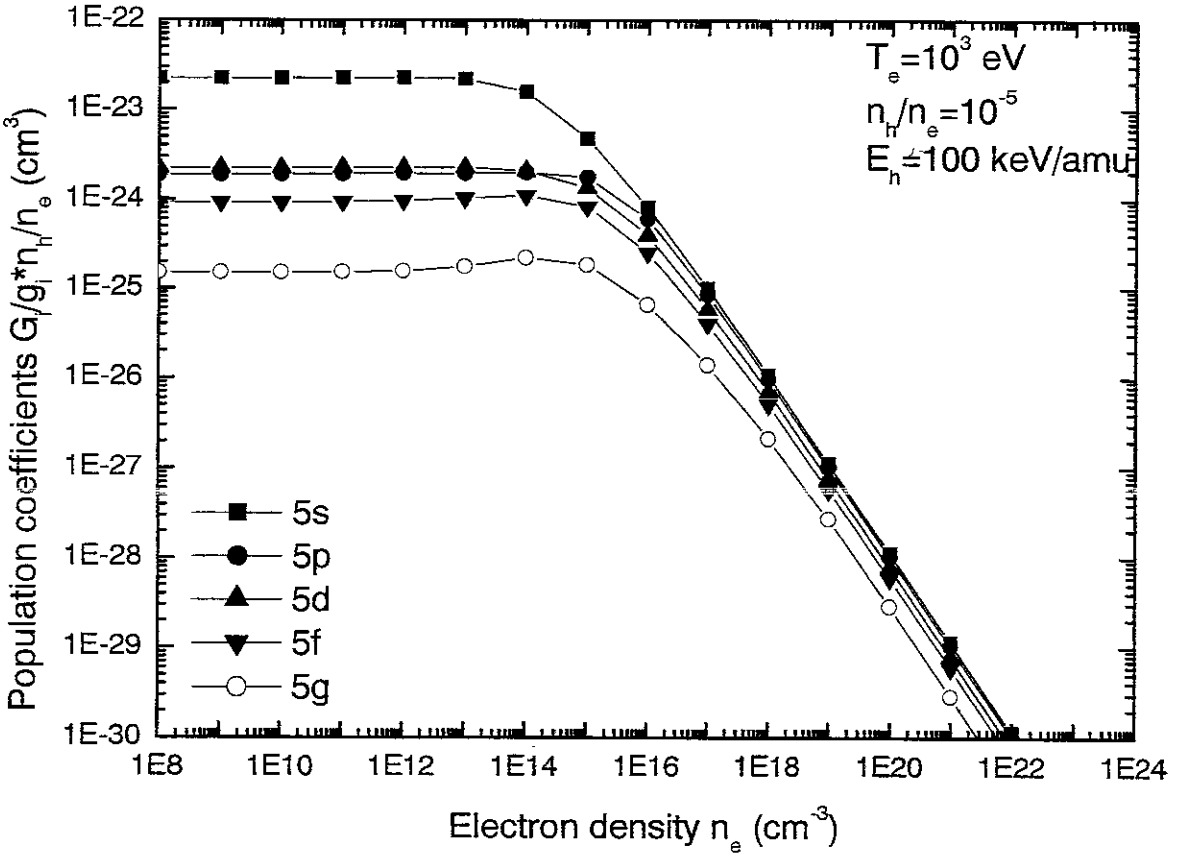
1E-22
1E-23
1E-24
1E-25
1E-26
1E-27
1E-28
1E-29
1E-30
Population coefficients G/g*n/n (cm3)
T=10 eV
n/n=10-5
E=100 keV/amu
5s
5p
5d
5f
5g
1E8
1E10
1E12
1E14
1E16
1E18
1E20
1E22
1E24
Electron density n (cm-3)

Fig. 10

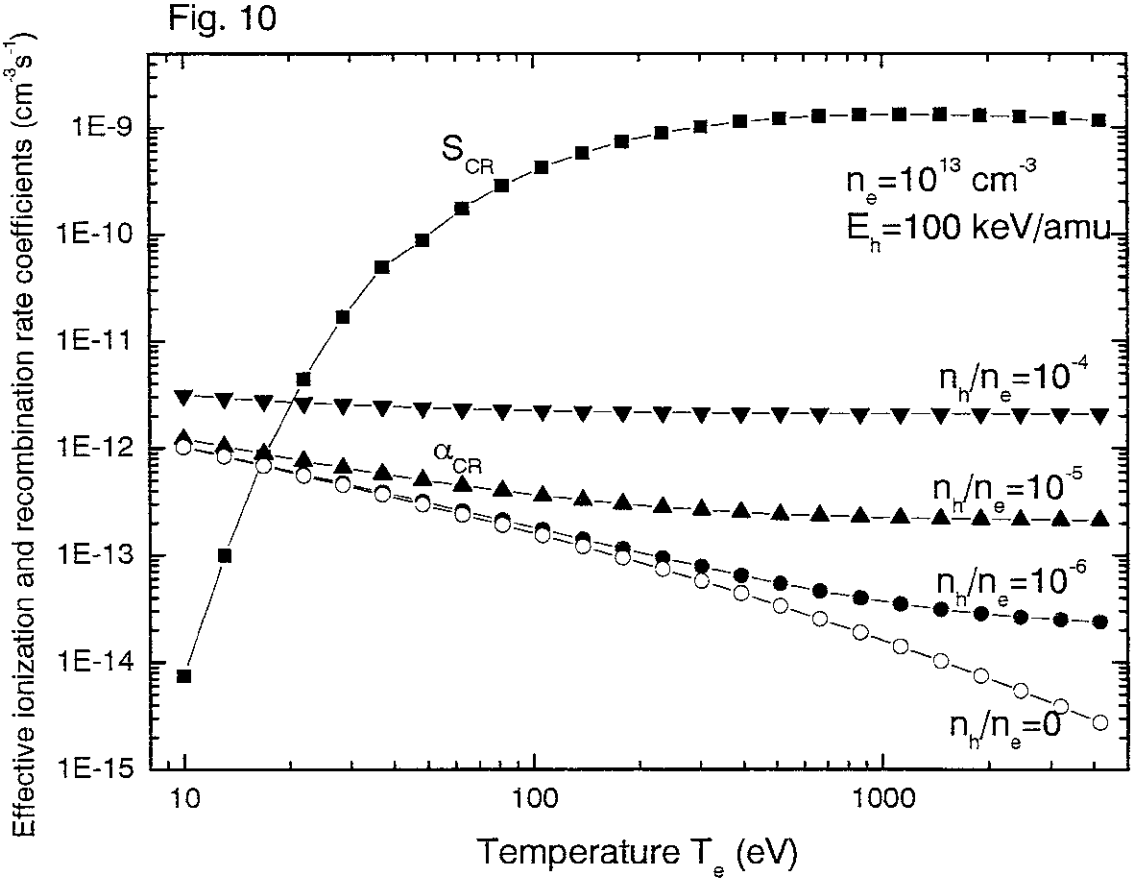
Effective ionization and recombination rate coefficients (cm^{-3}s^{-1})
1E-9
1E-10
1E-11
1E-12
1E-13
1E-14
1E-15
10
100
1000
Temperature T_e (eV)
S_{CR}
α_{CR}
$n_e=10^{13}$ cm^{-3}
E_h=100 keV/amu
$n_h/n_e=10^{-4}$
$n_h/n_e=10^{-5}$
$n_h/n_e=10^{-6}$
$n_h/n_e=0$

Fig. 11

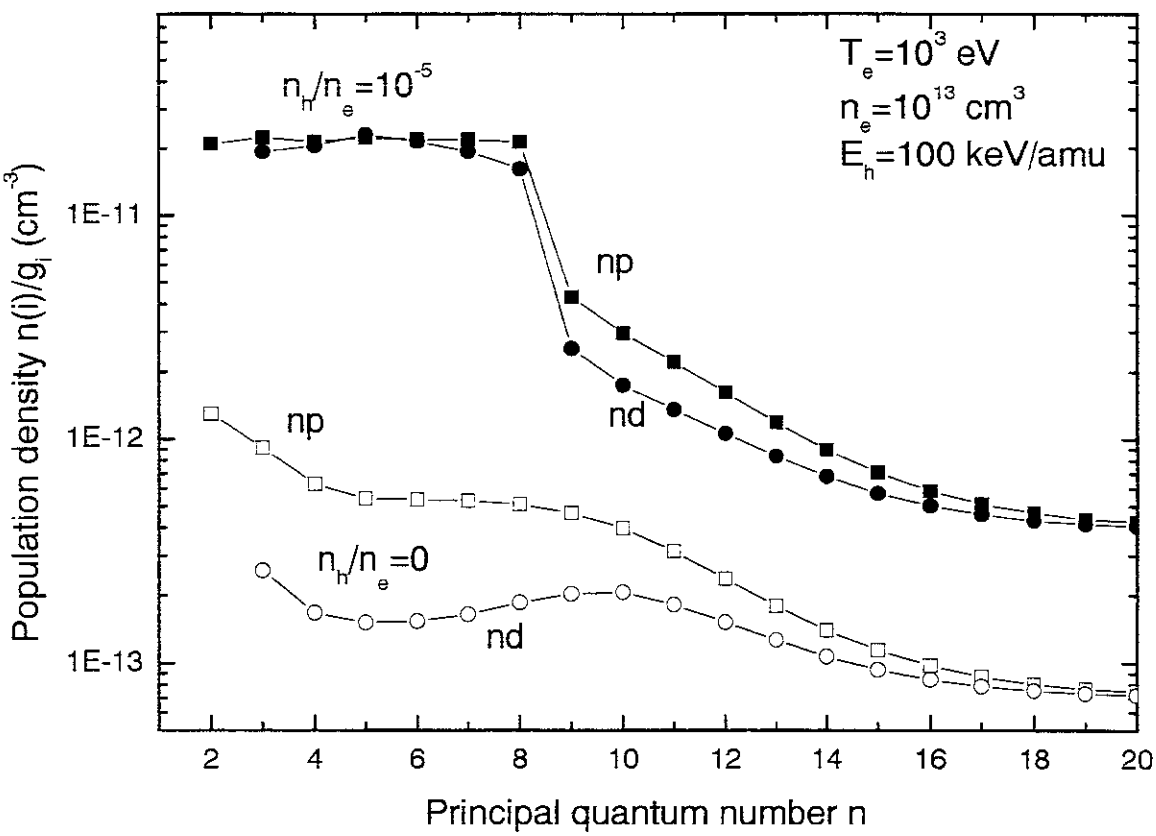
Population density n(i)/g_i (cm^{-3})
1E-11
1E-12
1E-13
2
4
6
8
10
12
14
16
18
20
Principal quantum number n
$T_e=10^3$ eV
$n_e=10^{13}$ cm^3
E_h=100 keV/amu
$n_h/n_e=10^{-5}$
np
nd
np
$n_h/n_e=0$
nd

Fig. 12

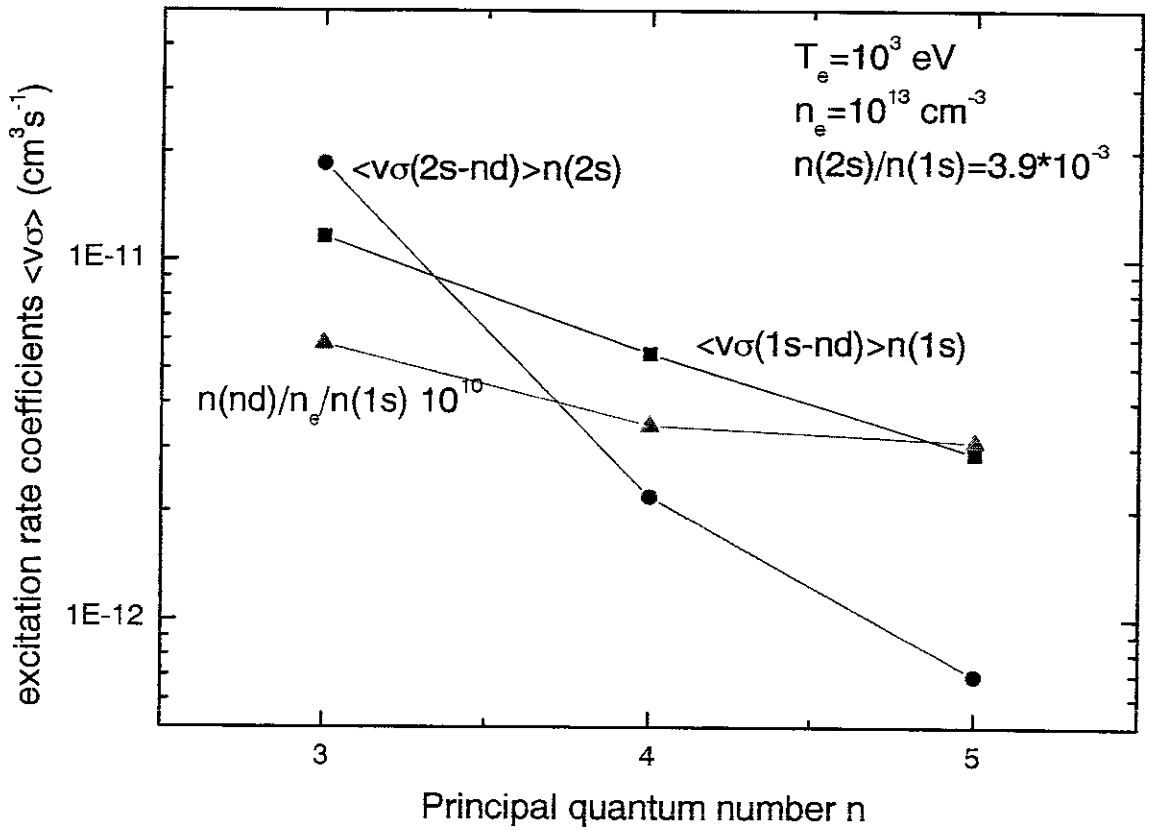

Fig. 13(a)

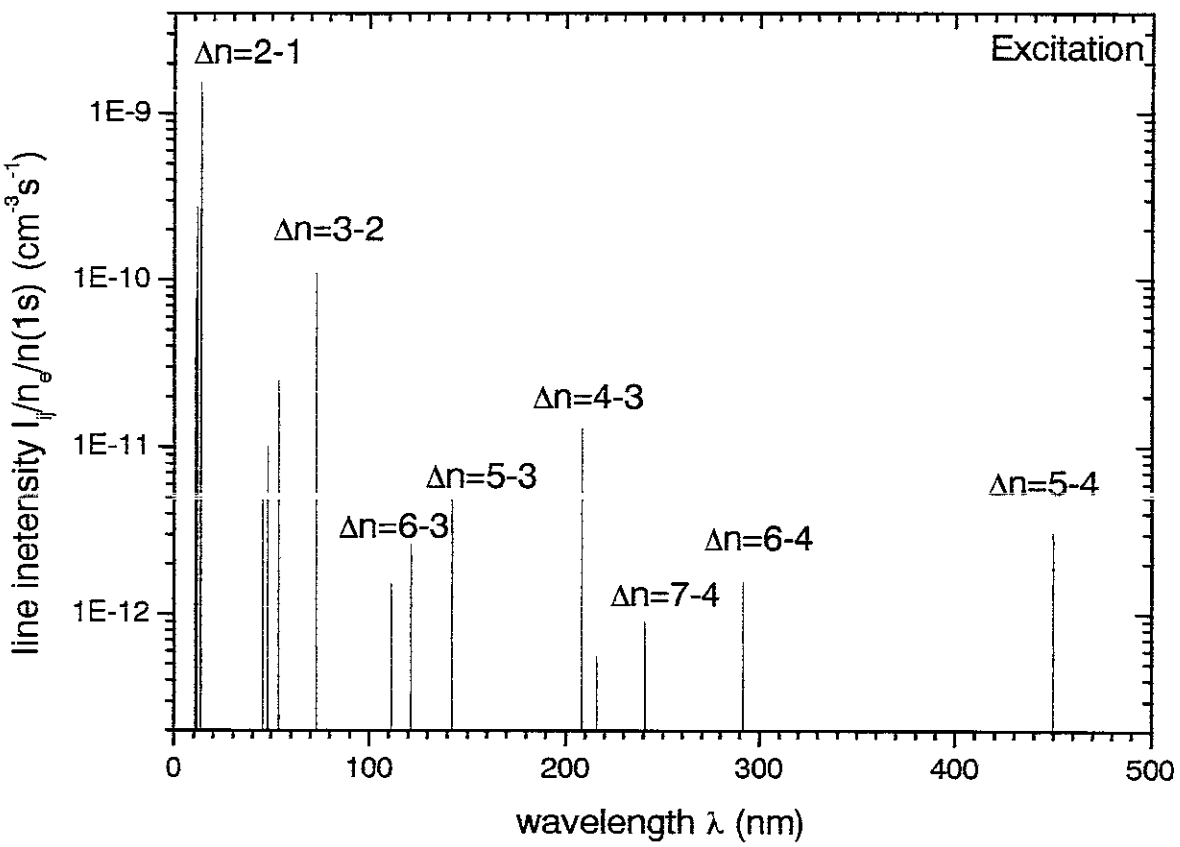

Fig. 13(b)

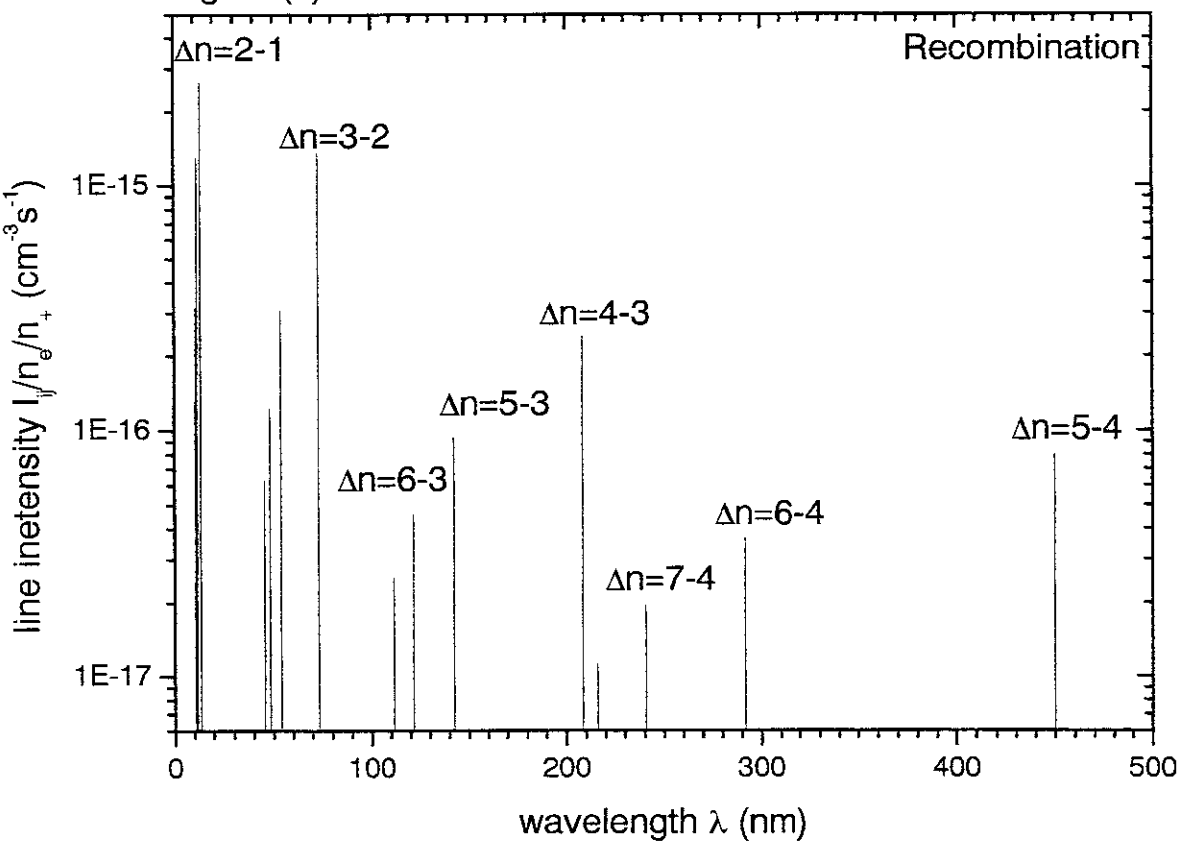

Fig. 13(c)

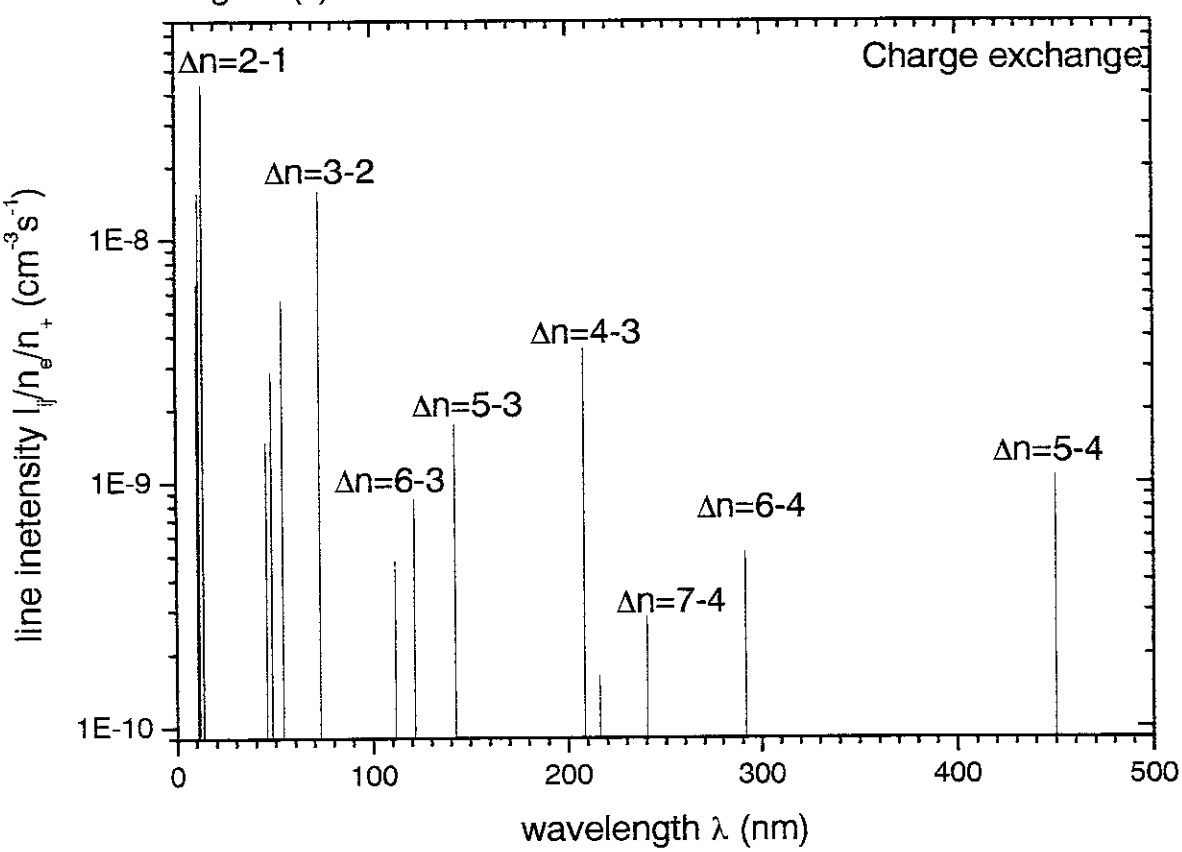

Fig. 14

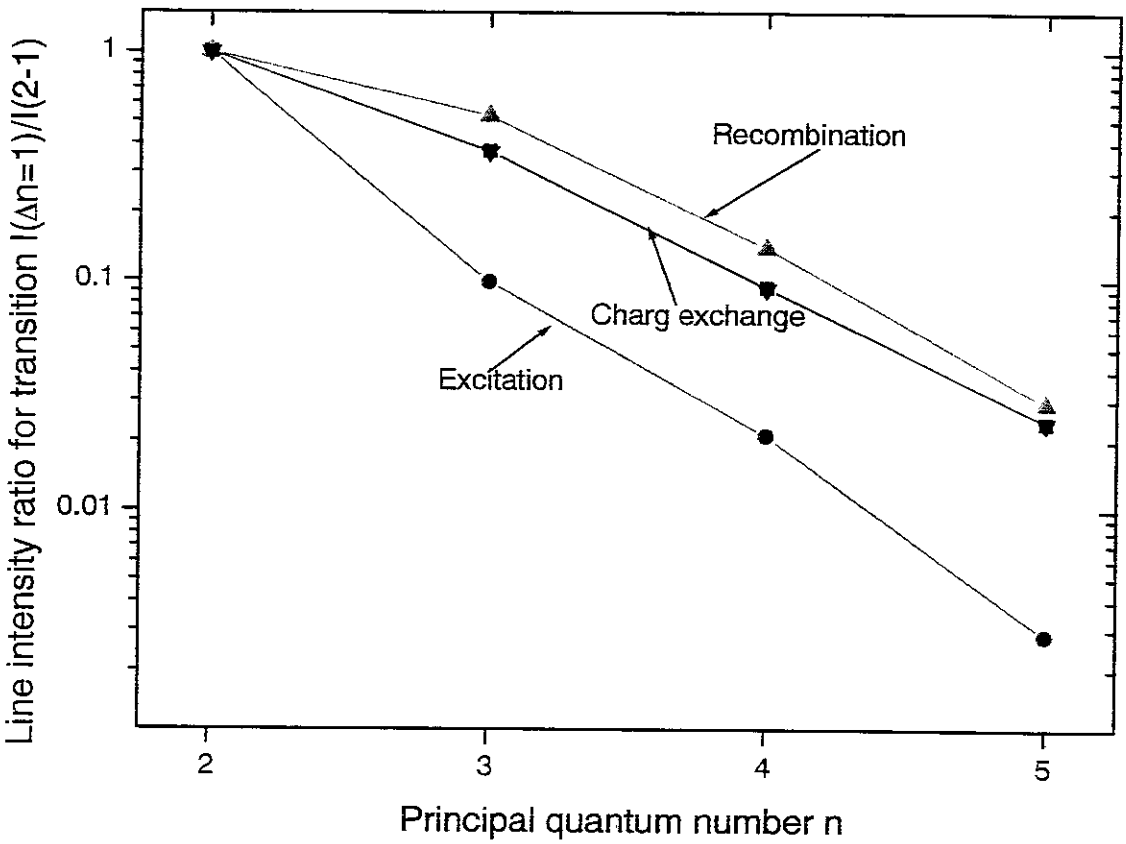
Line intensity ratio for transition I(Δn=1)/I(2-1)
1
0.1
0.01
Recombination
Charg exchange
Excitation
2
3
4
5
Principal quantum number n

Fig. 15

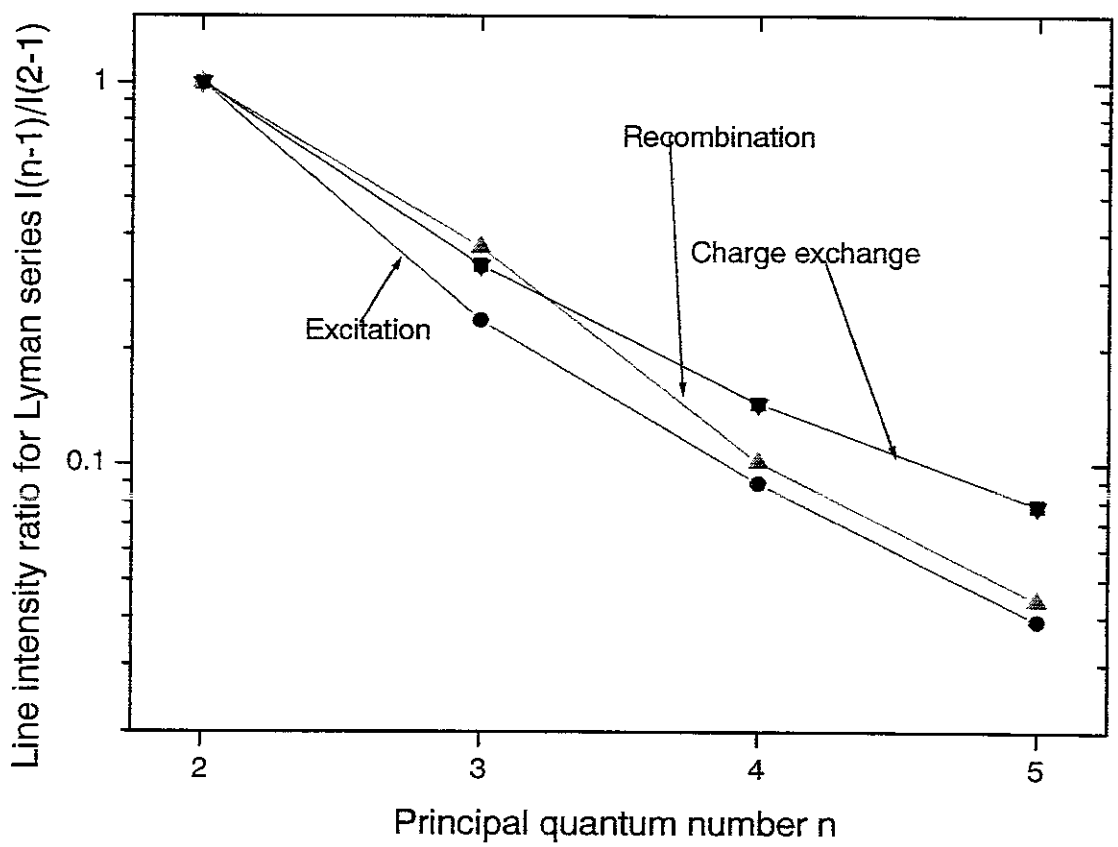
Line intensity ratio for Lyman series I(n-1)/I(2-1)
1
0.1
Recombination
Charge exchange
Excitation
2
3
4
5
Principal quantum number n

Fig. 16

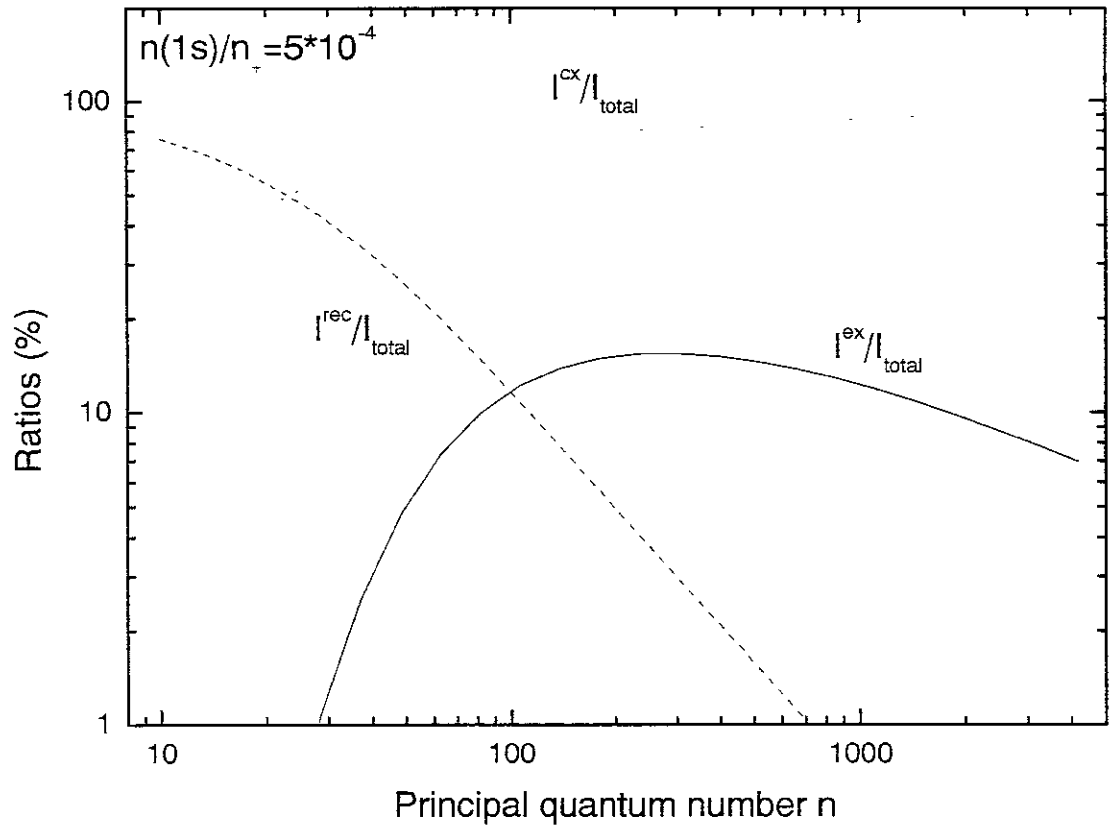
n(1s)/n =5*10^-4
I^cx/I_total
I^rec/I_total
I^ex/I_total
Ratios (%)
100
10
1
10
100
1000
Principal quantum number n

Fig. 17

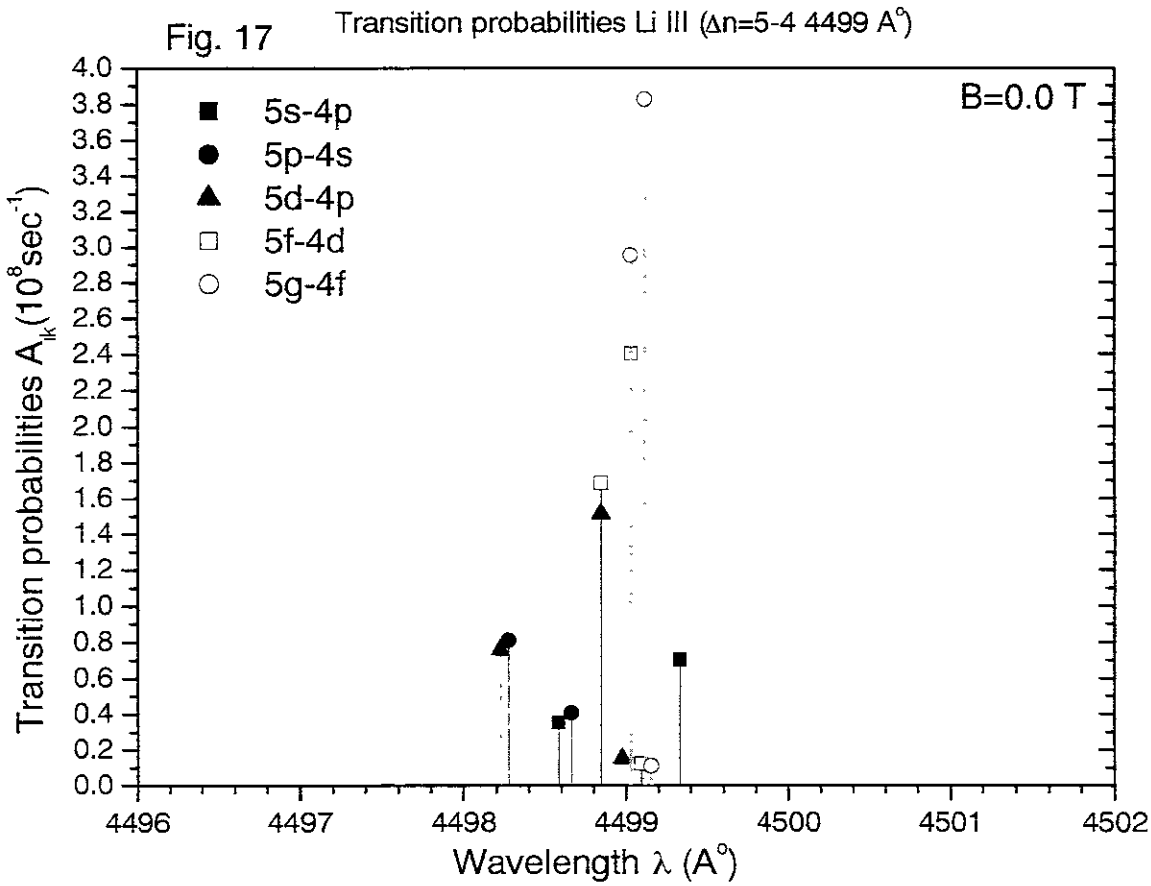
Transition probabilities Li III (Δn=5-4 4499 A°)
B=0.0 T
5s-4p
5p-4s
5d-4p
5f-4d
5g-4f
Transition probabilities A_ik(10^8sec^-1)
4.0
3.8
3.6
3.4
3.2
3.0
2.8
2.6
2.4
2.2
2.0
1.8
1.6
1.4
1.2
1.0
0.8
0.6
0.4
0.2
0.0
4496
4497
4498
4499
4500
4501
4502
Wavelength λ (A°)

Fig. 18(a) Tansition probabilities Li III (5s-4p)

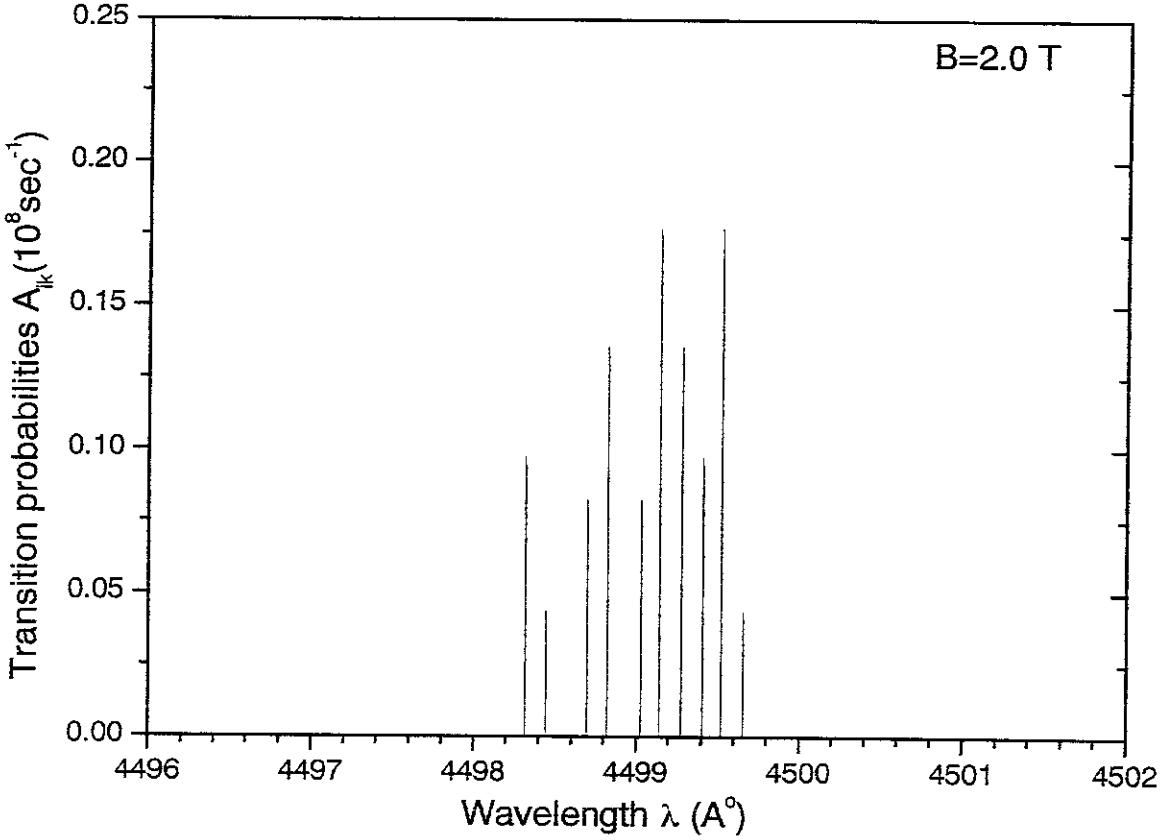

Fig. 18(b) Tansition probabilities Li III (5p-4s)

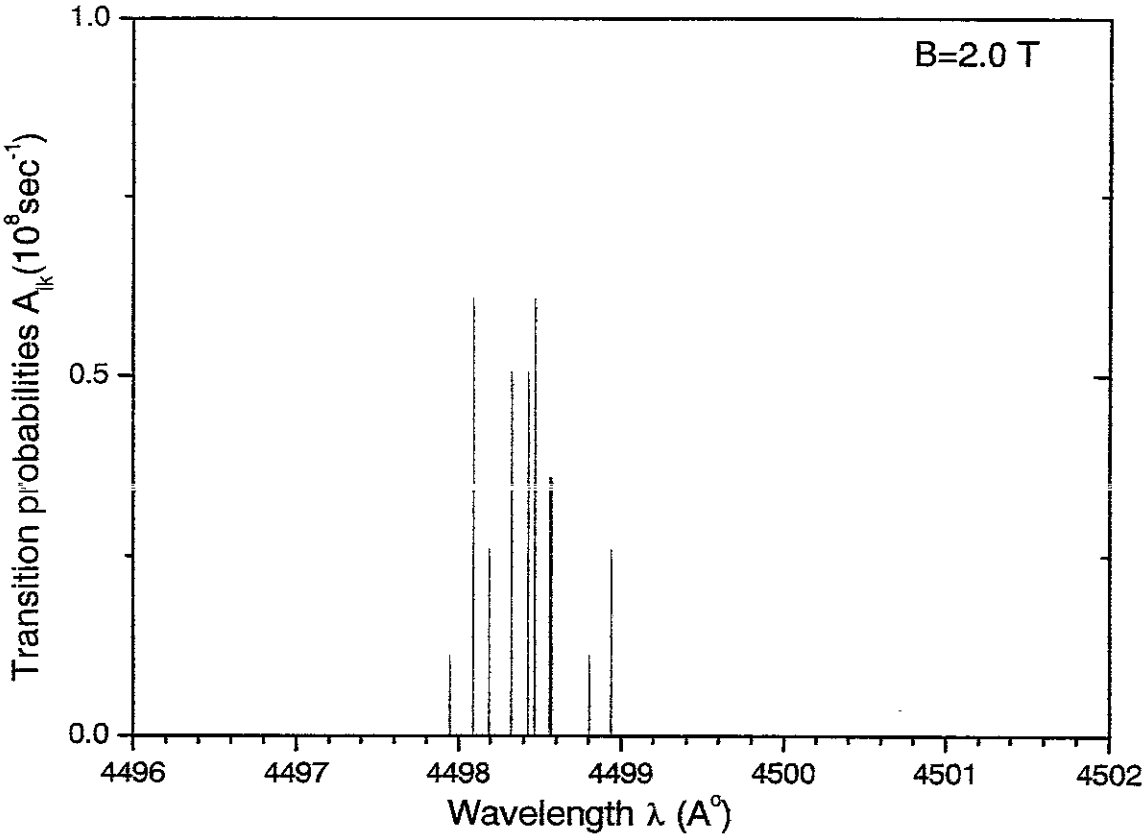

Fig. 18(c) Tansition probabilities Li III (5d-4p)

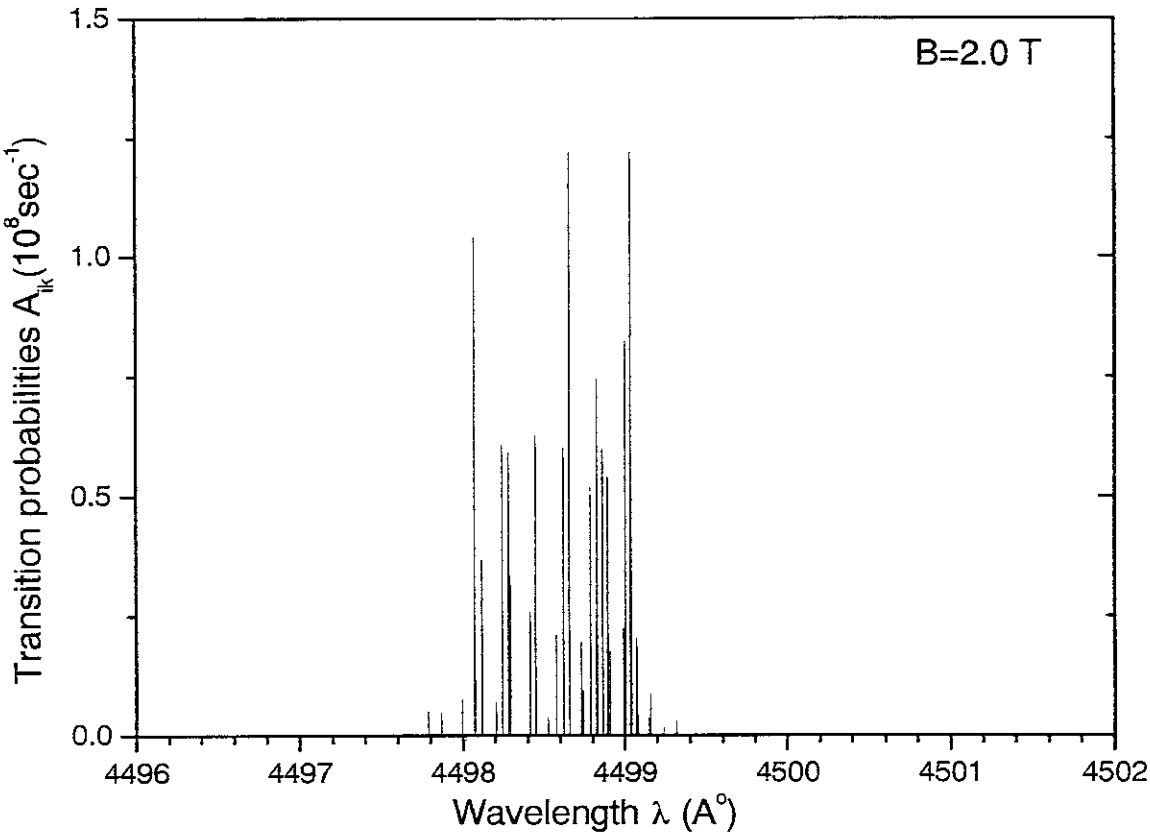

Fig. 18(d) Tansition probabilities Li III (5d-4f)

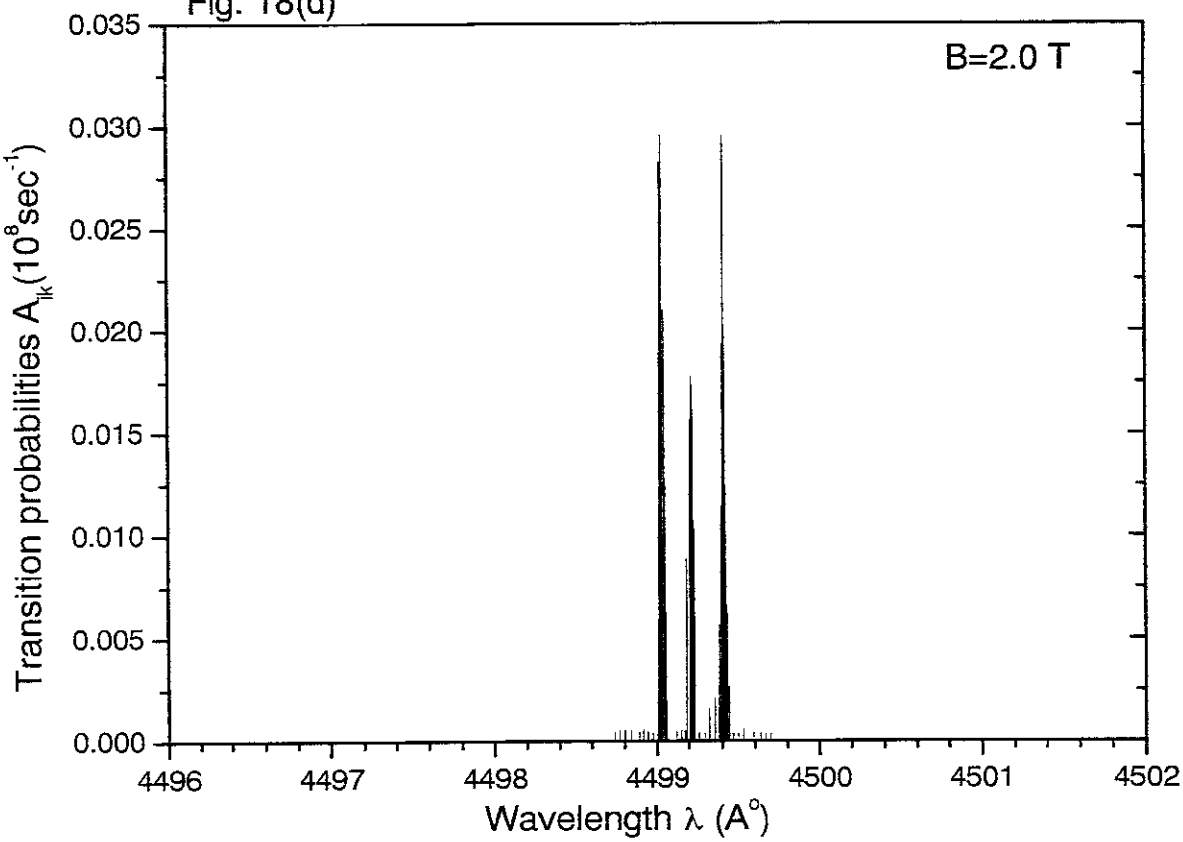

Fig. 18(e) Tansition probabilities Li III (5f-4d)

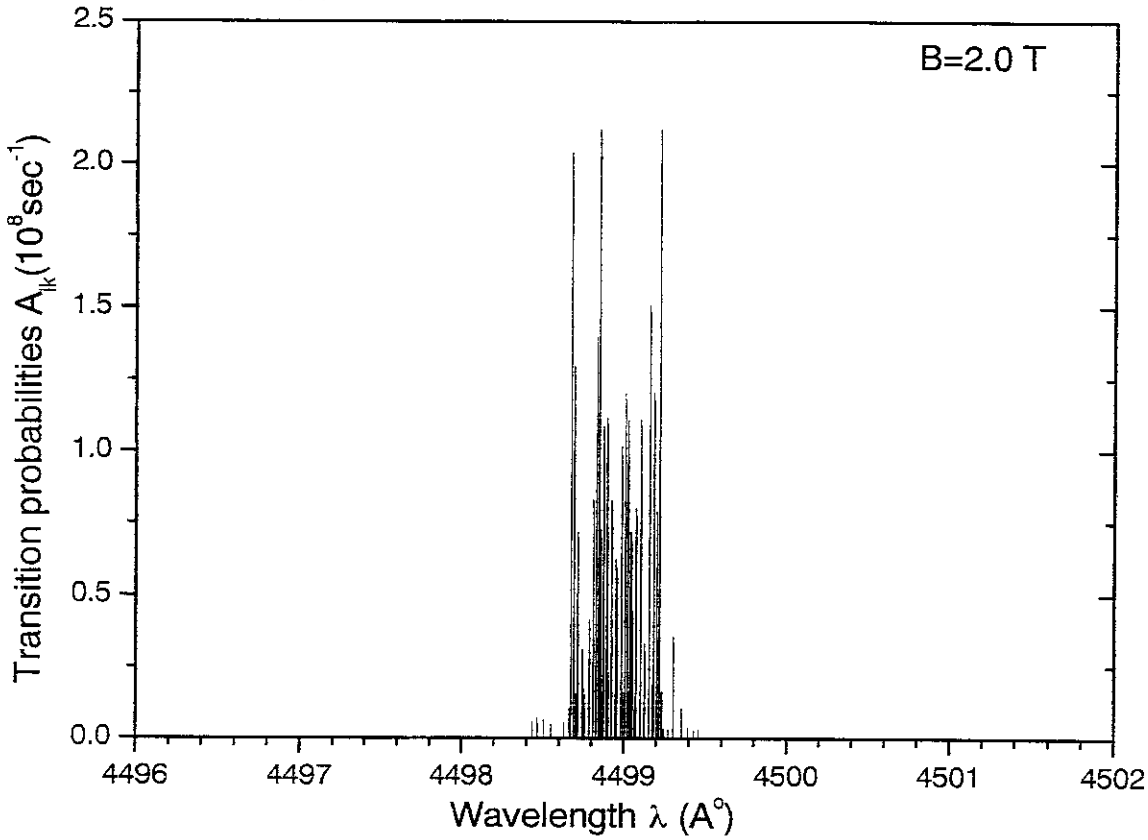

Fig. 18(f) Tansition probabilities Li III (5g-4f)

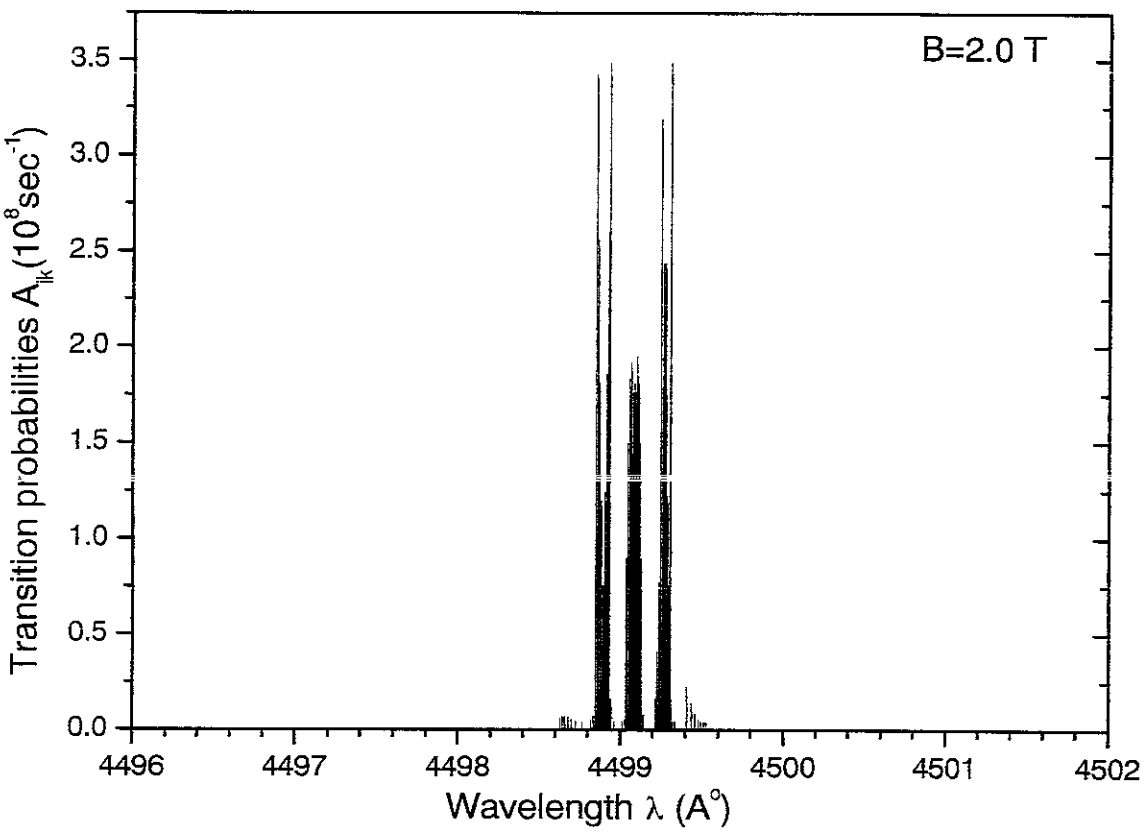

Fig. 18(g)

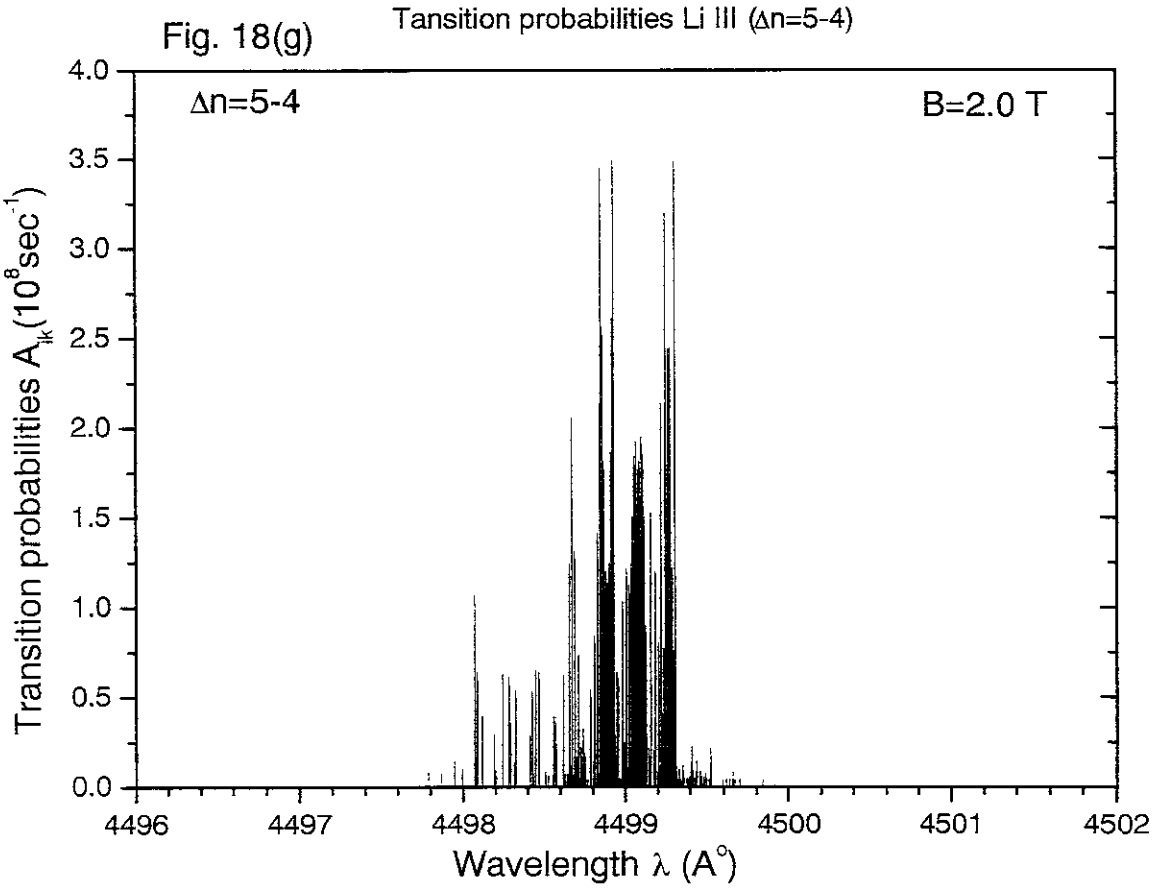

Fig. 19

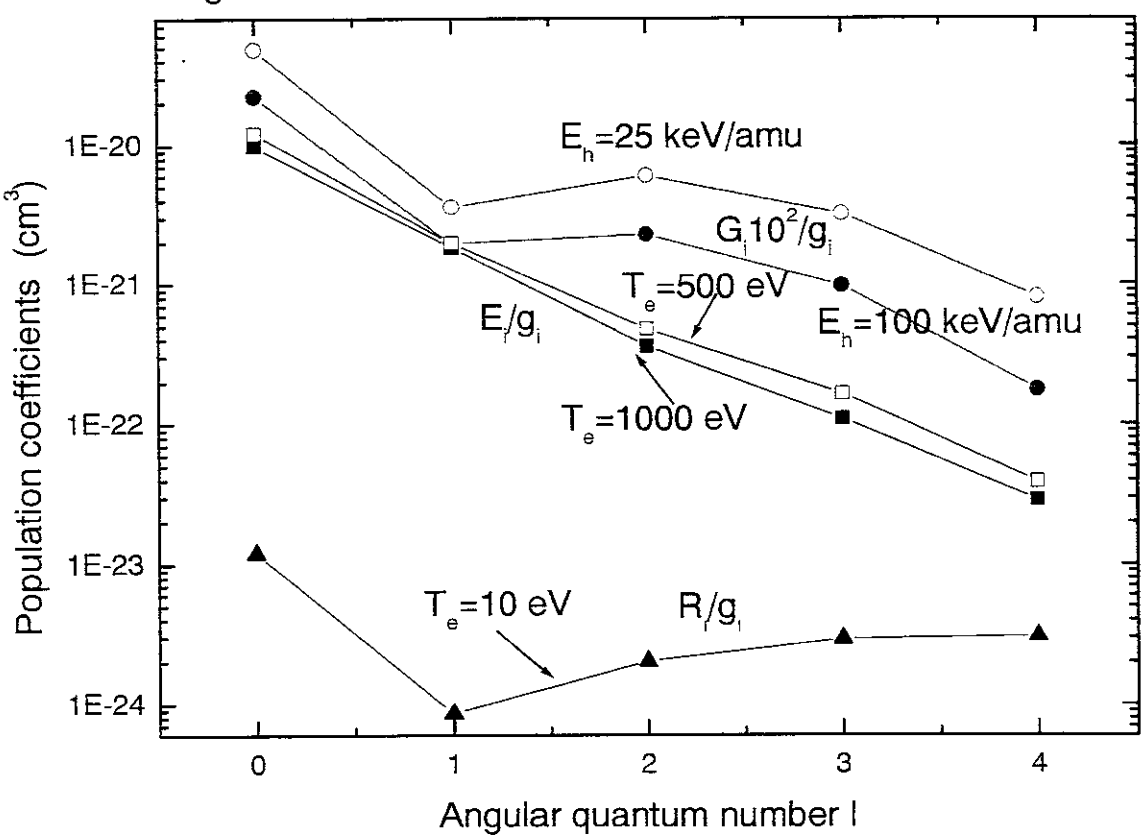

Fig. 20(a) Excitation spectral profiles Li III 4499 A°(Δn=5-4)

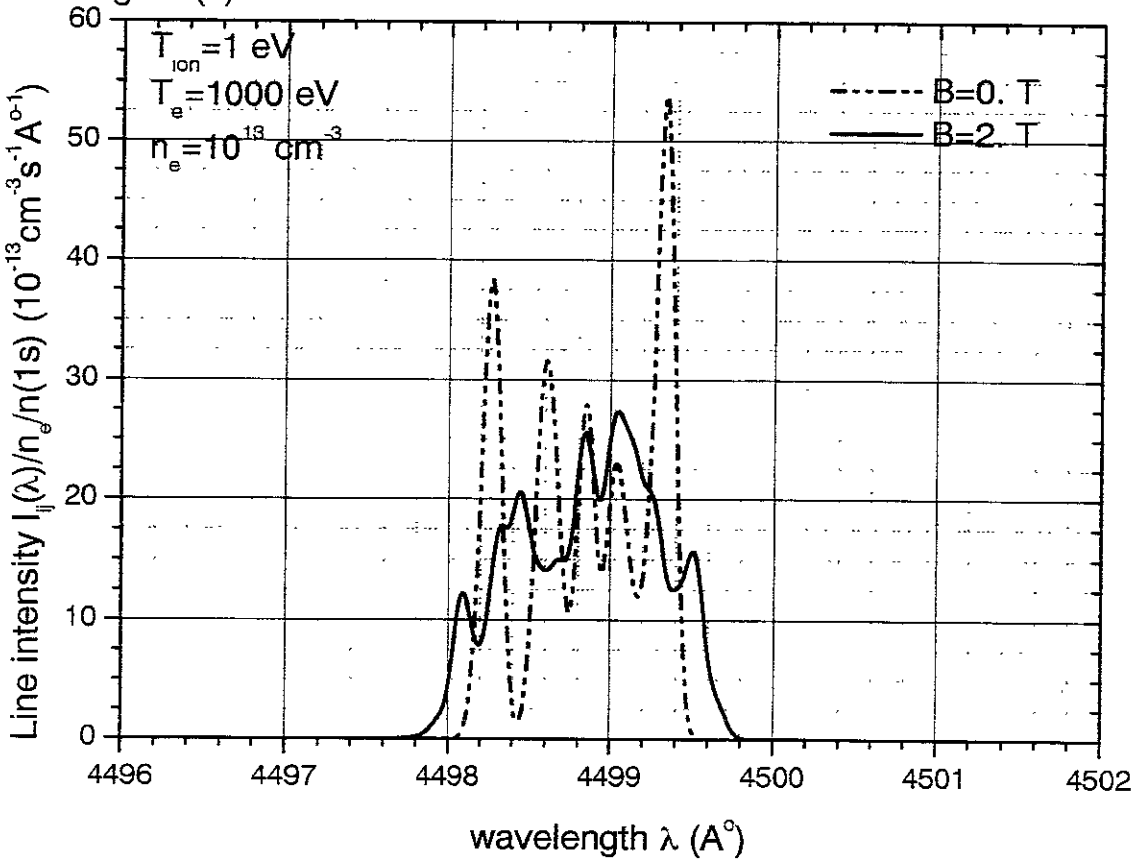

Fig. 20(b) Excitation spectral profiles Li III 4499 A°(Δn=5-4)

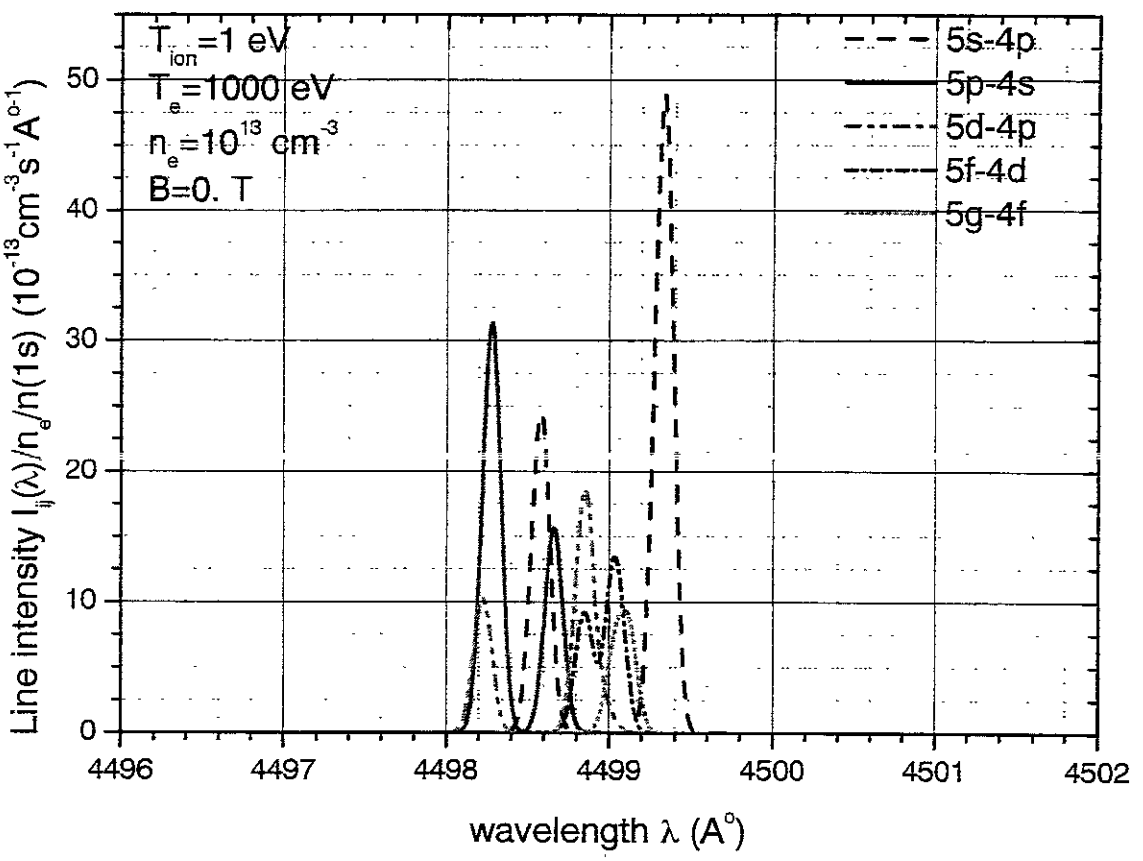

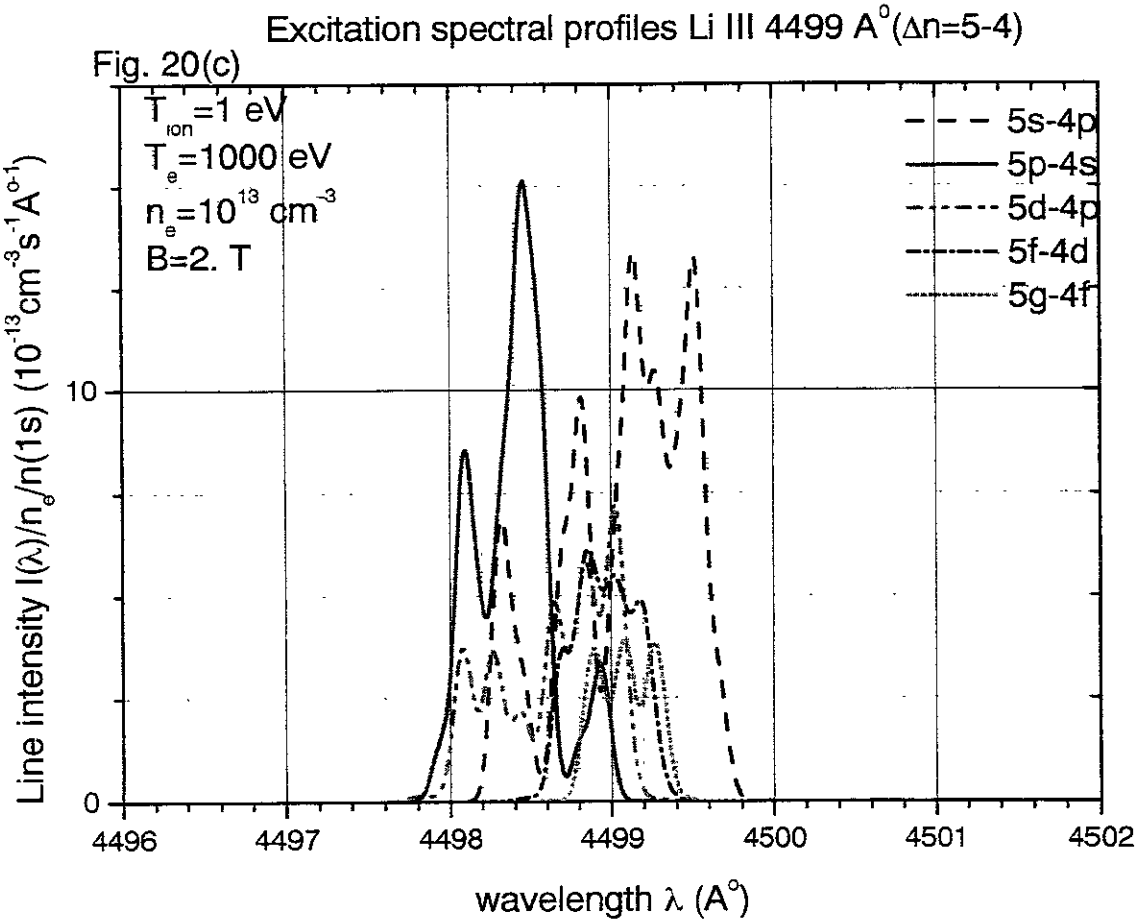
Excitation spectral profiles Li III 4499 A°(Δn=5-4)
Fig. 20(c)
T_ion=1 eV
T_e=1000 eV
n_e=10^13 cm^-3
B=2. T
5s-4p
5p-4s
5d-4p
5f-4d
5g-4f
Line intensity I(λ)/n_e/n(1s) (10^-13cm^-3s^-1A°^-1)
wavelength λ (A°)
0
10
4496
4497
4498
4499
4500
4501
4502

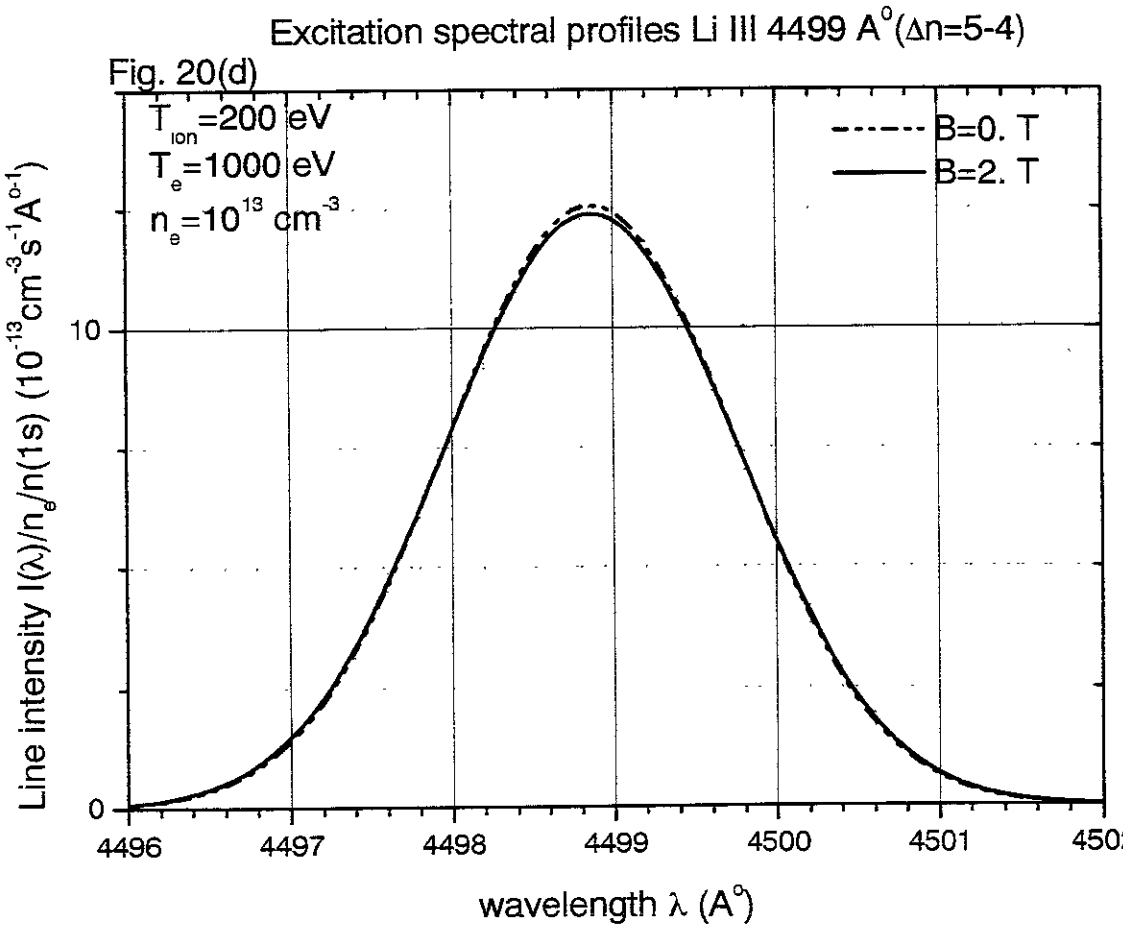
Excitation spectral profiles Li III 4499 A°(Δn=5-4)
Fig. 20(d)
T_ion=200 eV
T_e=1000 eV
n_e=10^13 cm^-3
B=0. T
B=2. T
Line intensity I(λ)/n_e/n(1s) (10^-13cm^-3s^-1A°^-1)
wavelength λ (A°)
0
10
4496
4497
4498
4499
4500
4501
4502

Charge exchange spectral profiles Li III 4499 A°(Δn=5-4)

Fig. 21(a)

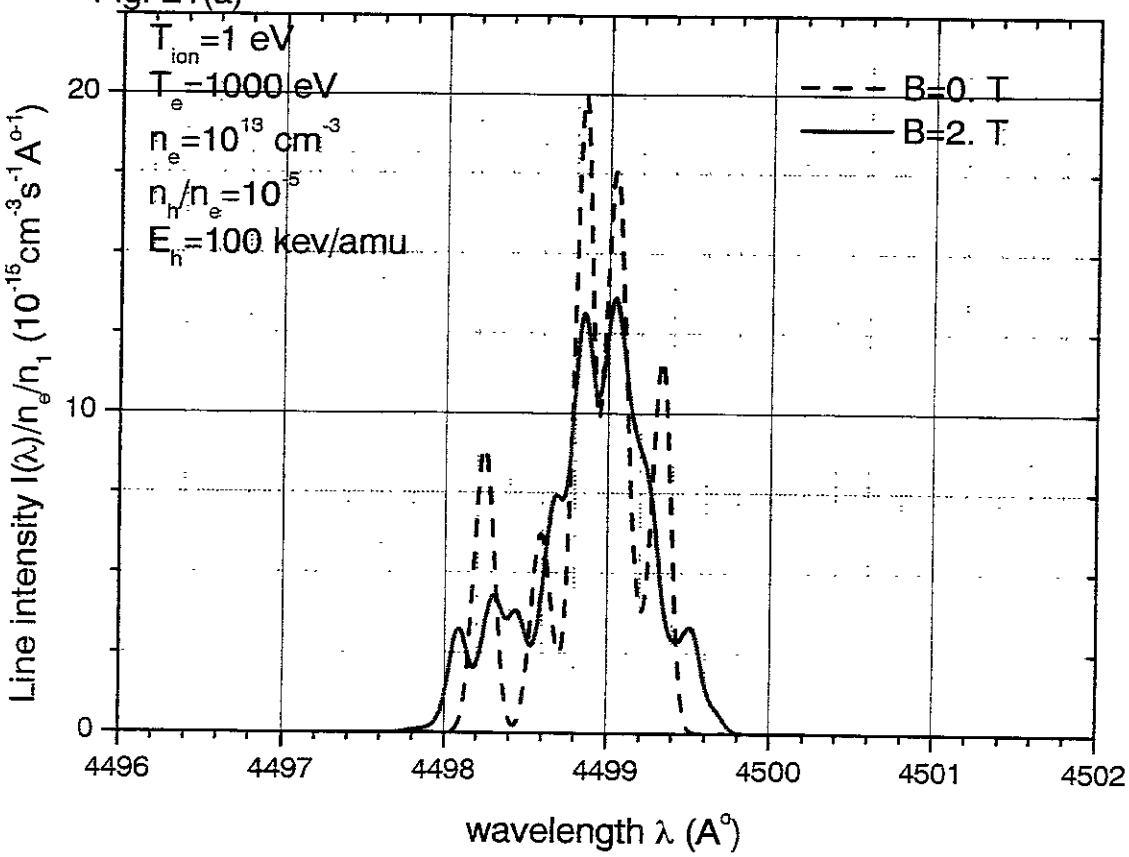

Charge exchange spectral profiles Li III 4499 A°(Δn=5-4)

Fig. 21(b)

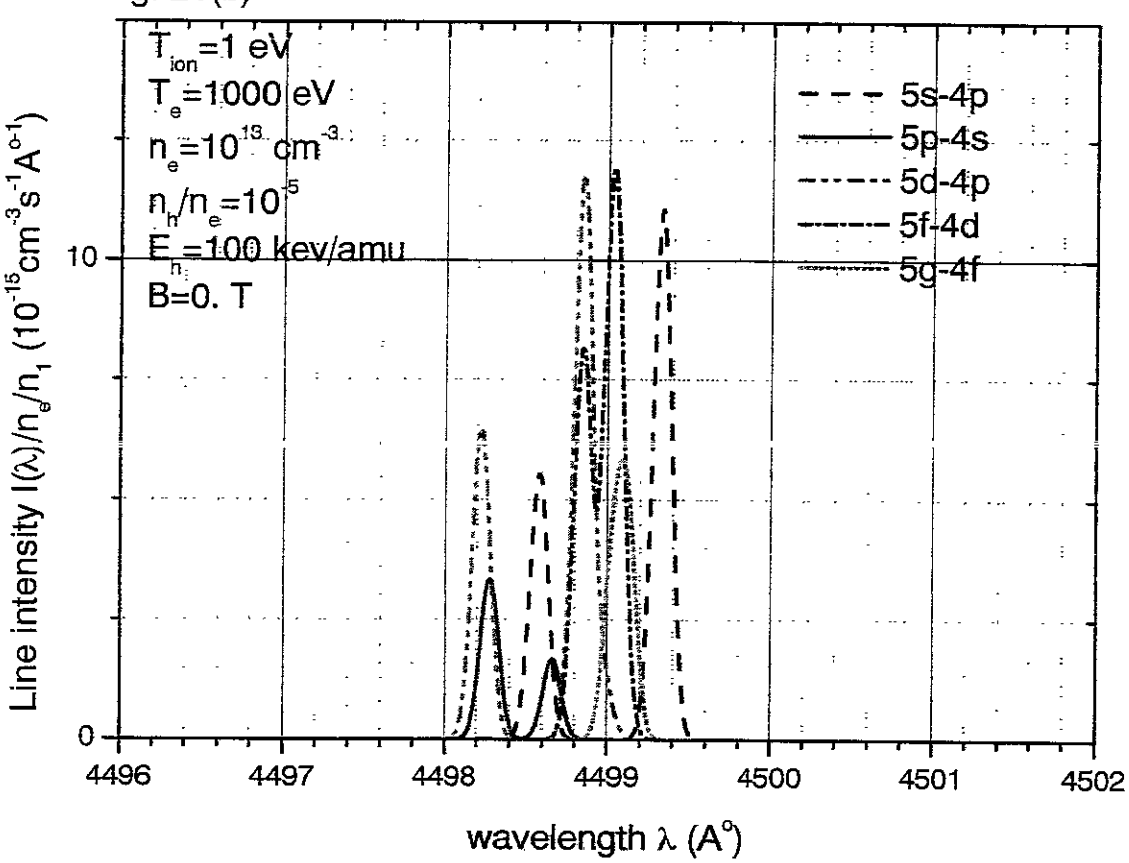

Charge exchange spectral profiles Li III 4499 A°(Δn=5-4)

Fig. 21(c)

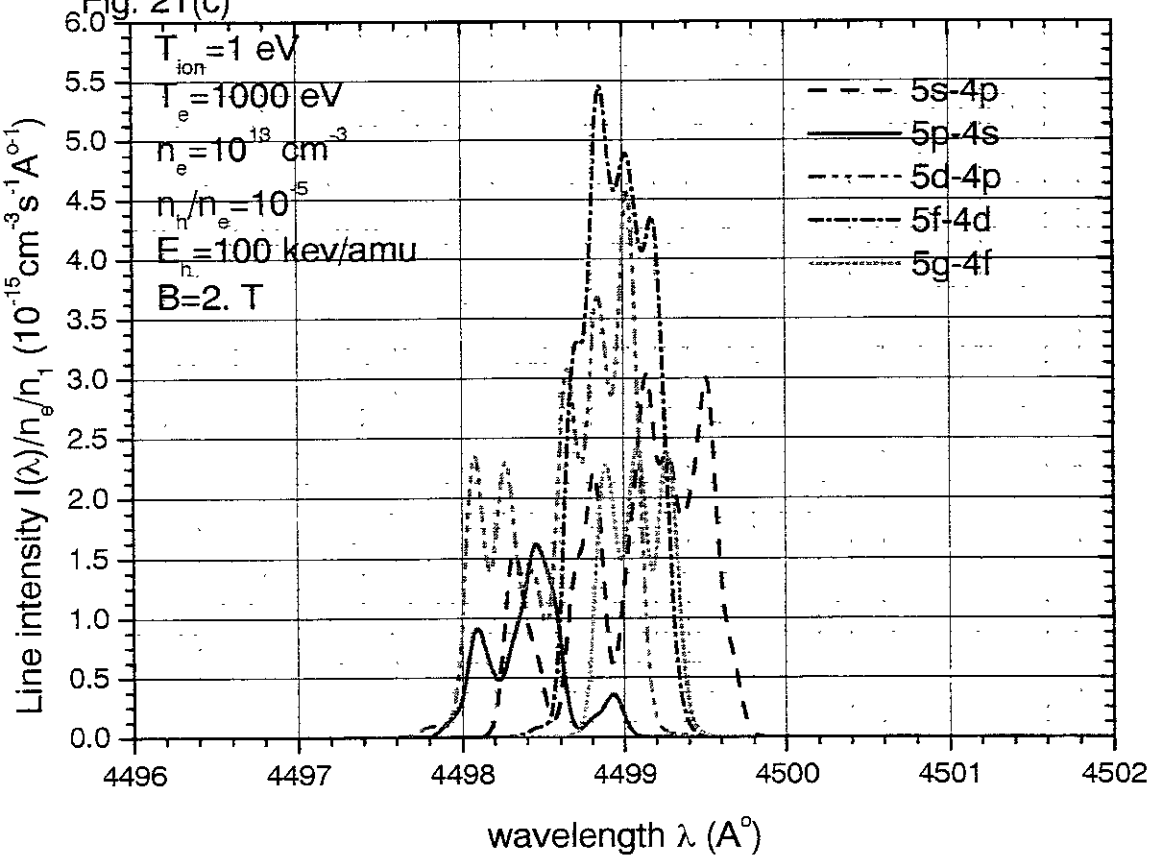

Charge exchange spectral profiles Li III 4499 A°(Δn=5-4)

Fig. 21(d)

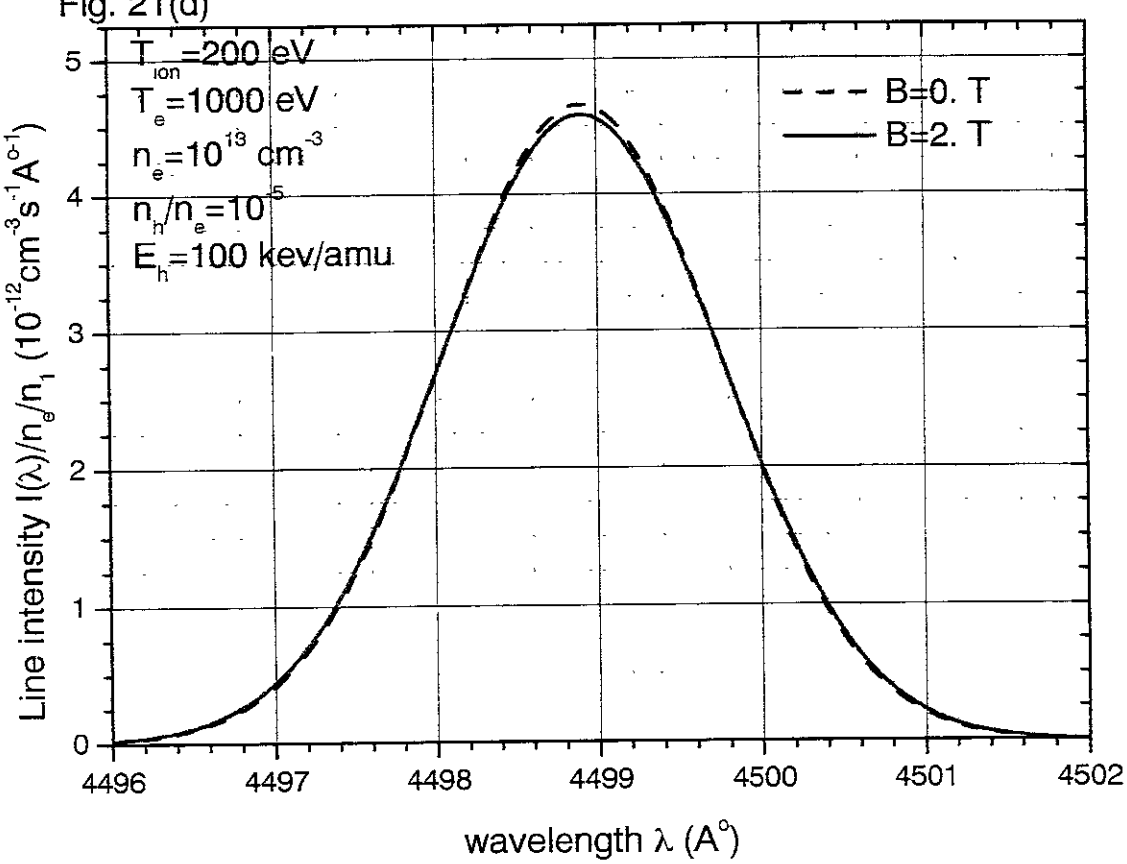

Charge exchange spectral profiles Li III 4499 A°(Δn=5-4)

Fig. 22(a)

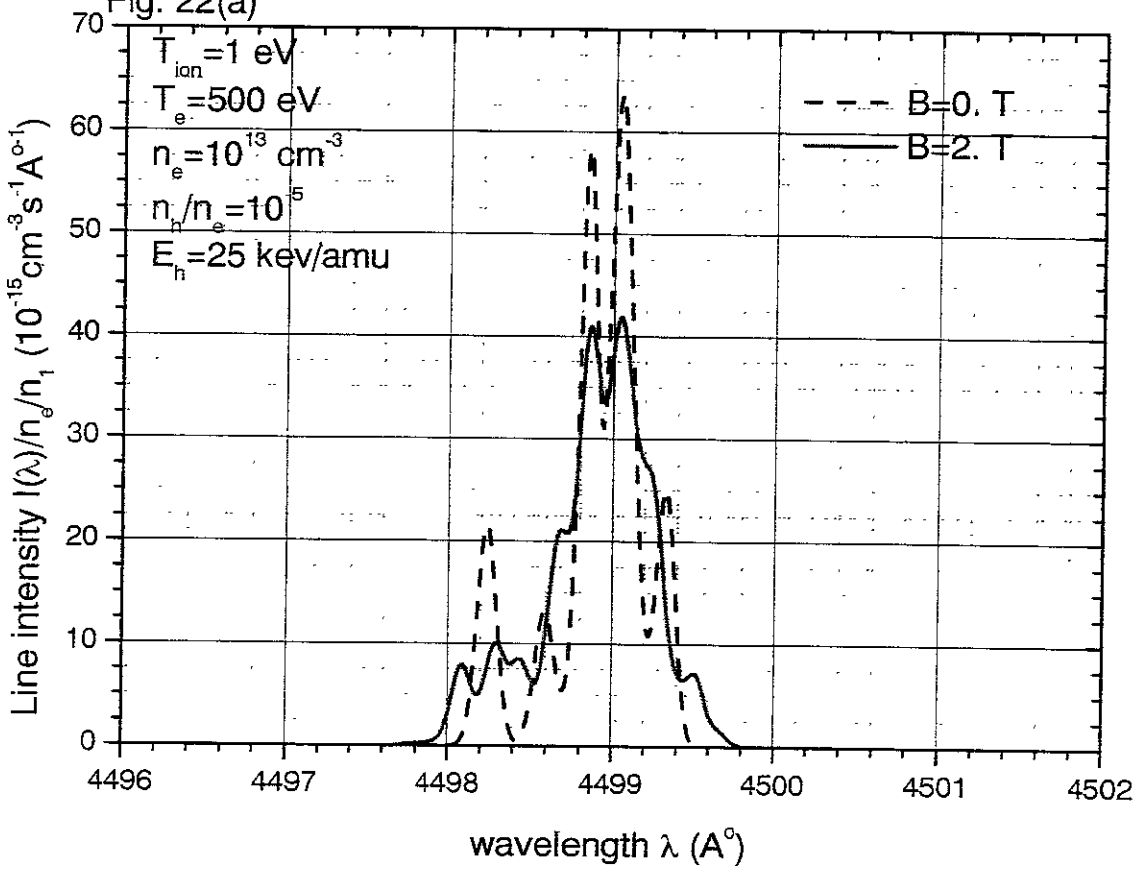

Charge exchange spectral profiles Li III 4499 A°(Δn=5-4)

Fig. 22(b)

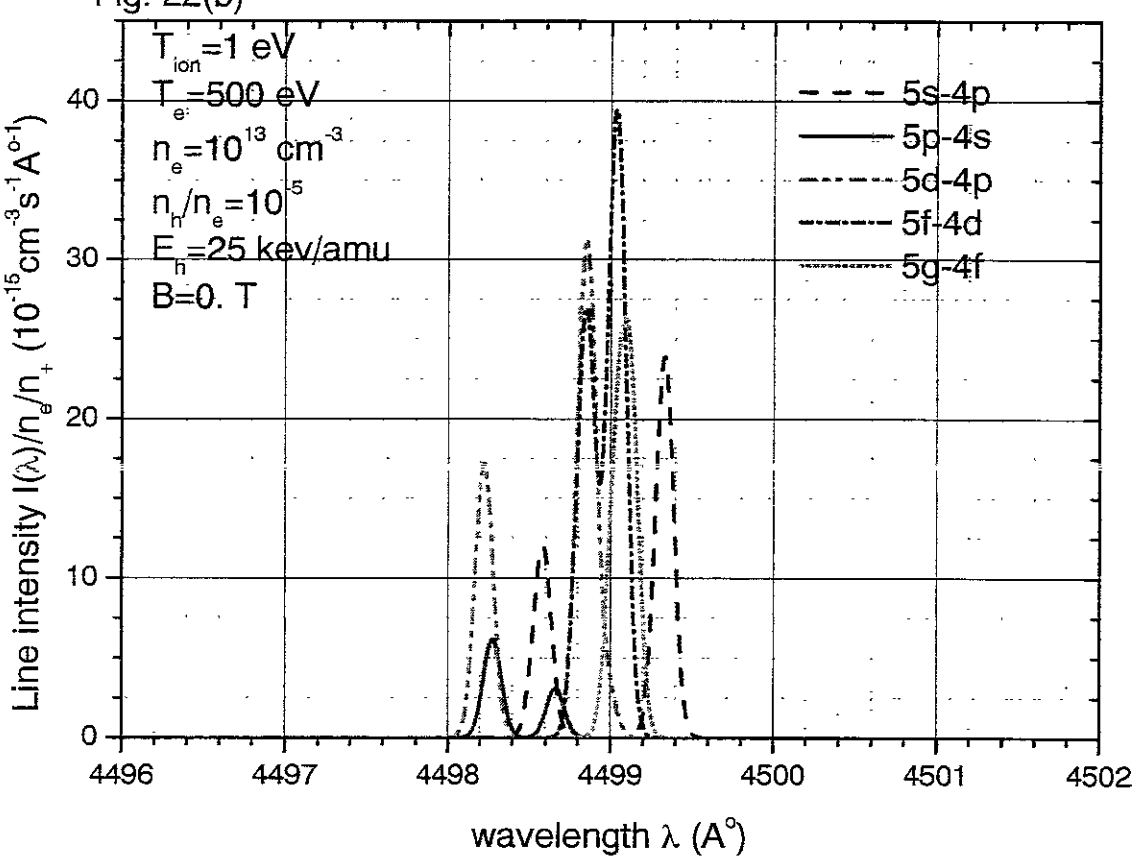

Charge exchange spectral profiles Li III 4499 A°(Δn=5-4)

Fig. 22(c)

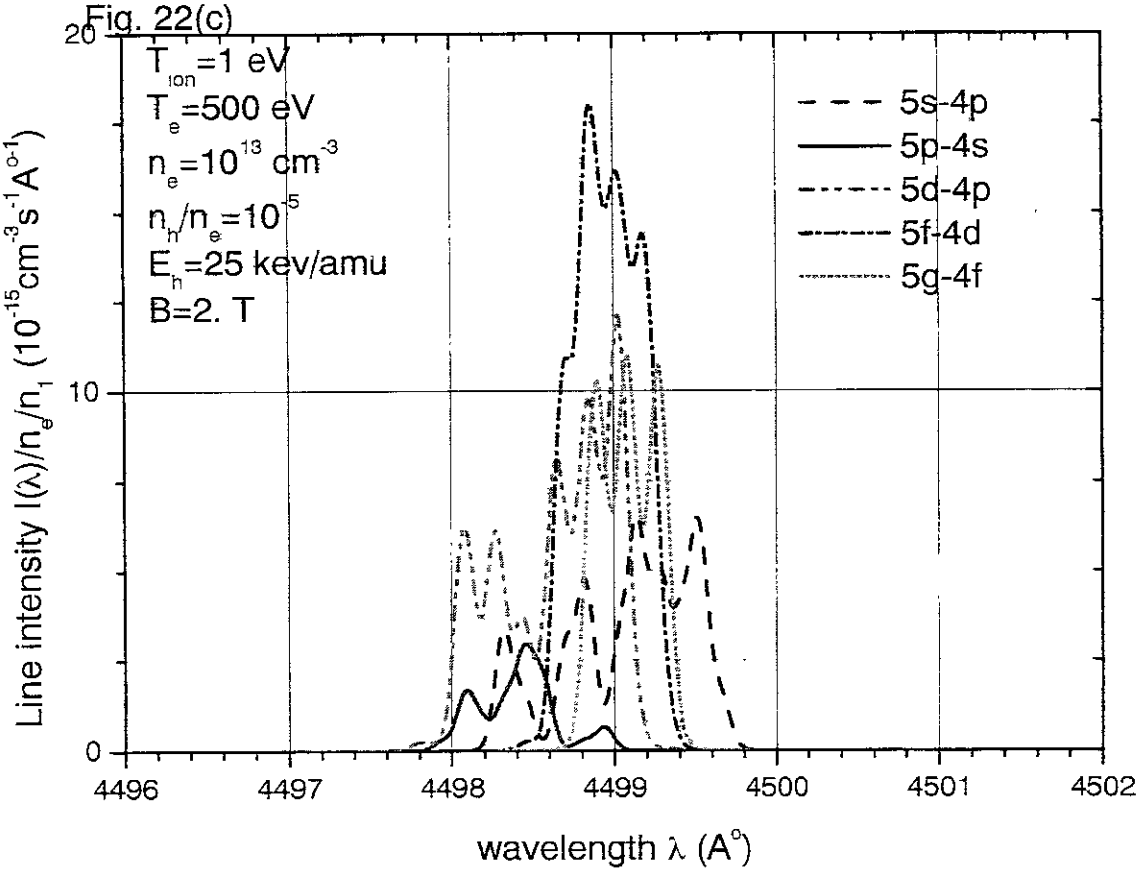

Charge exchange spectral profiles Li III 4499 A°(Δn=5-4)

Fig. 22(d)

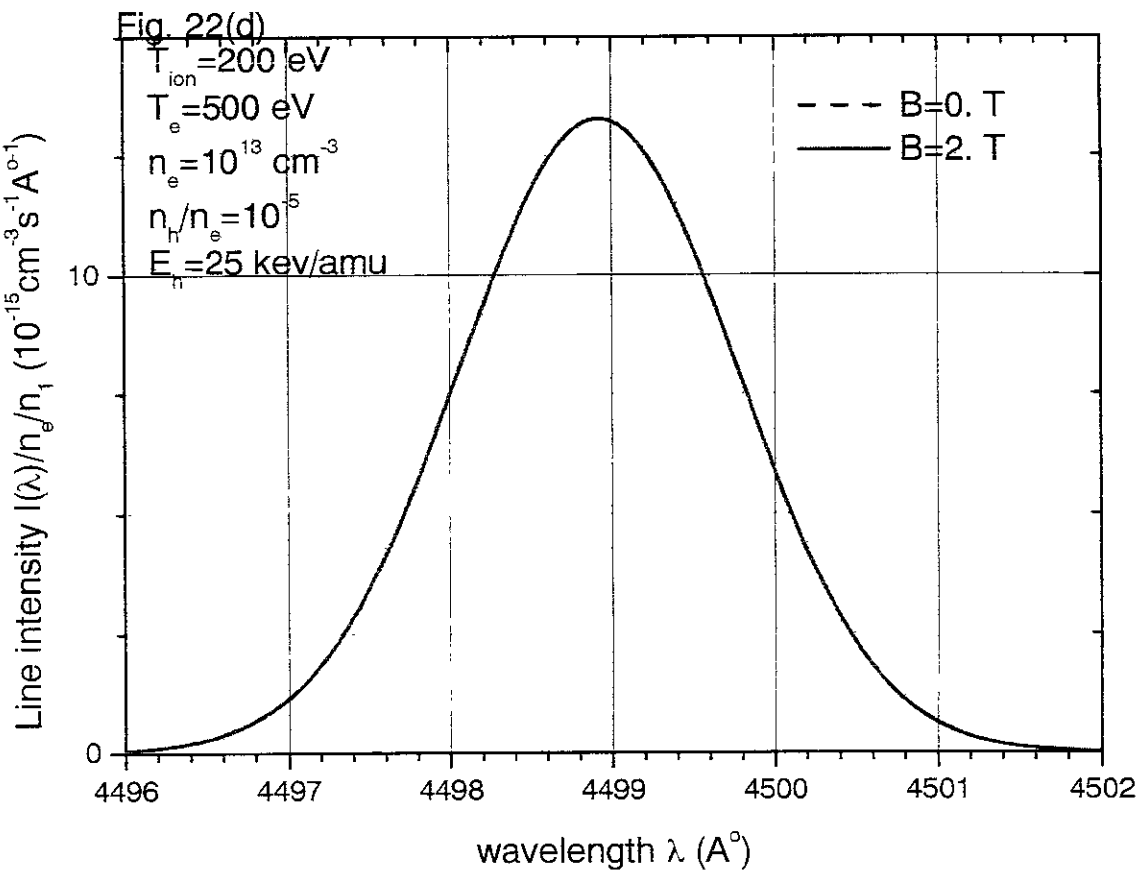

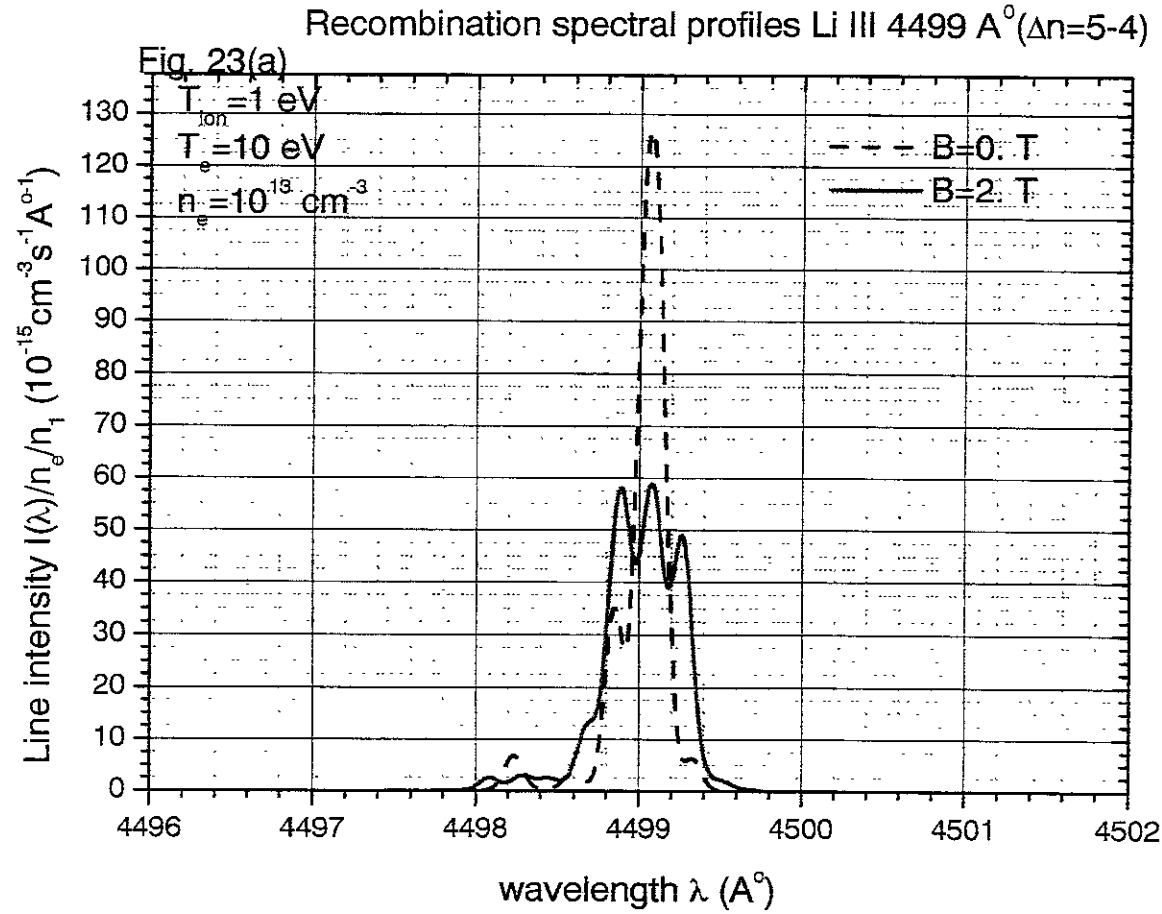
Recombination spectral profiles Li III 4499 A°(Δn=5-4)
Fig. 23(a)
T_ion=1 eV
T_e=10 eV
n_e=10^13 cm^-3
B=0. T
B=2. T
Line intensity I(λ)/n_e/n_1 (10^-15 cm^-3 s^-1 A°^-1)
wavelength λ (A°)

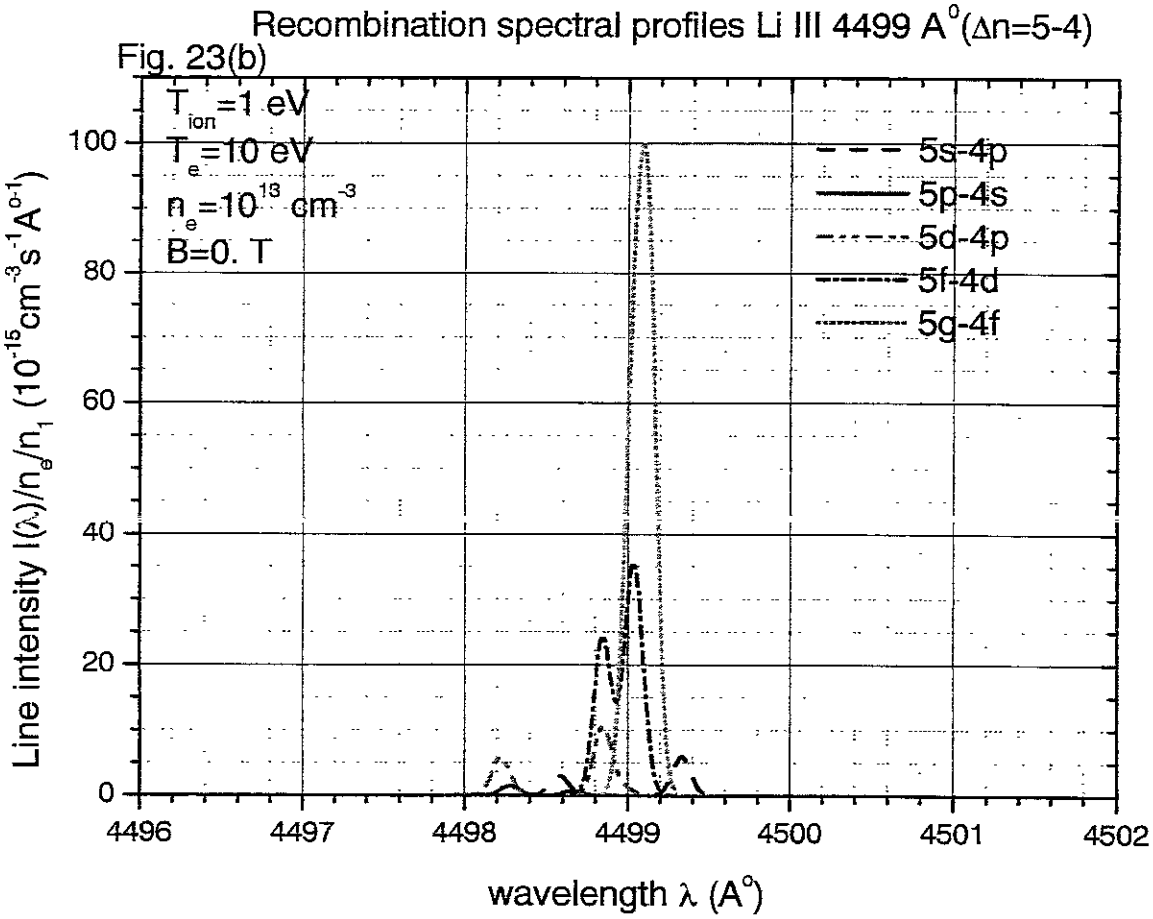
Recombination spectral profiles Li III 4499 A°(Δn=5-4)
Fig. 23(b)
T_ion=1 eV
T_e=10 eV
n_e=10^13 cm^-3
B=0. T
5s-4p
5p-4s
5d-4p
5f-4d
5g-4f
Line intensity I(λ)/n_e/n_1 (10^-15 cm^-3 s^-1 A°^-1)
wavelength λ (A°)

Recpmbination spectral profiles Li III 4499 A°(Δn=5-4)

Fig. 23(c)

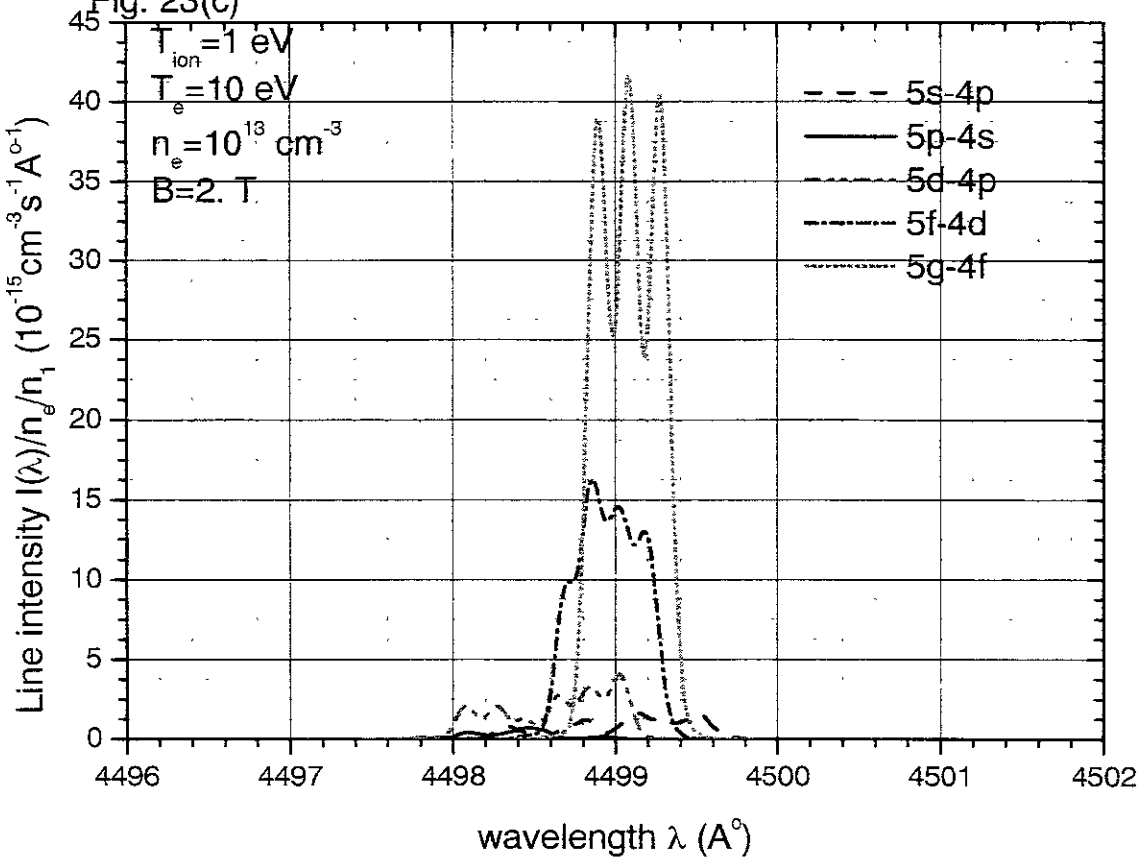

Recombination spectral profiles Li III 4499 A°(Δn=5-4)

Fig. 23(d)

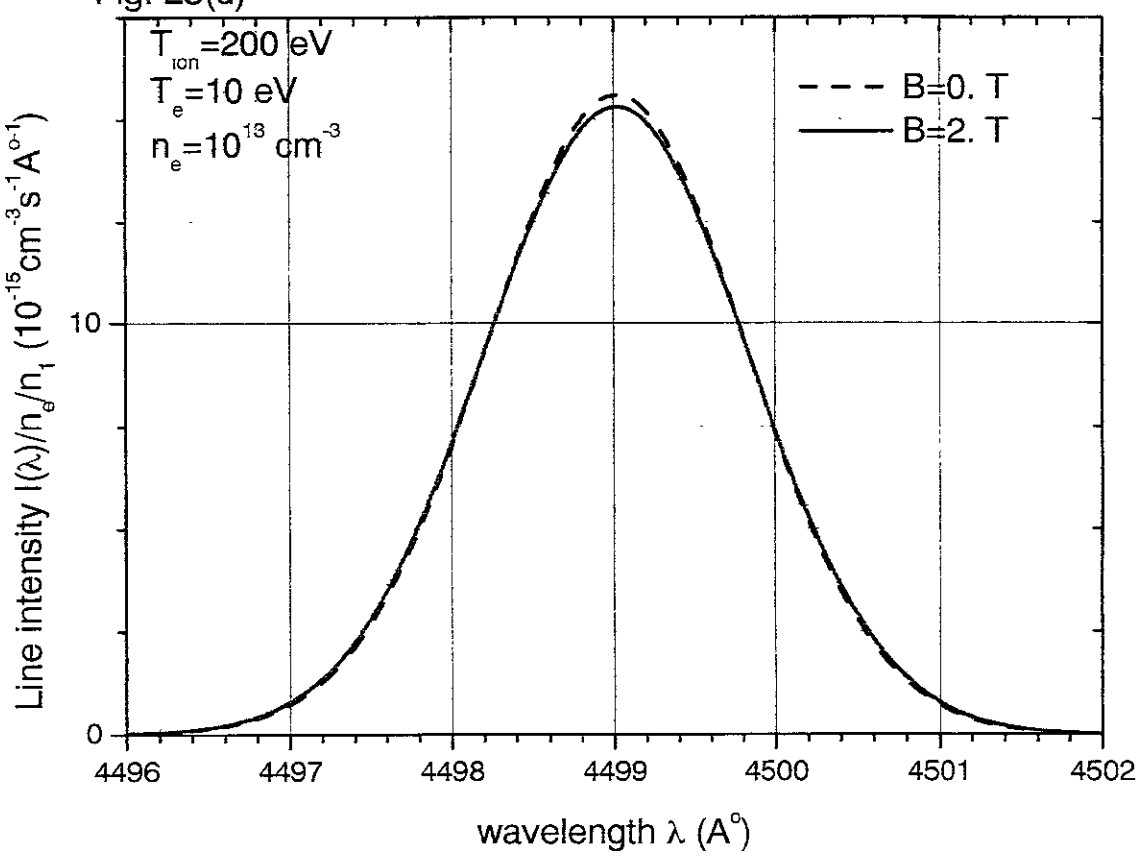

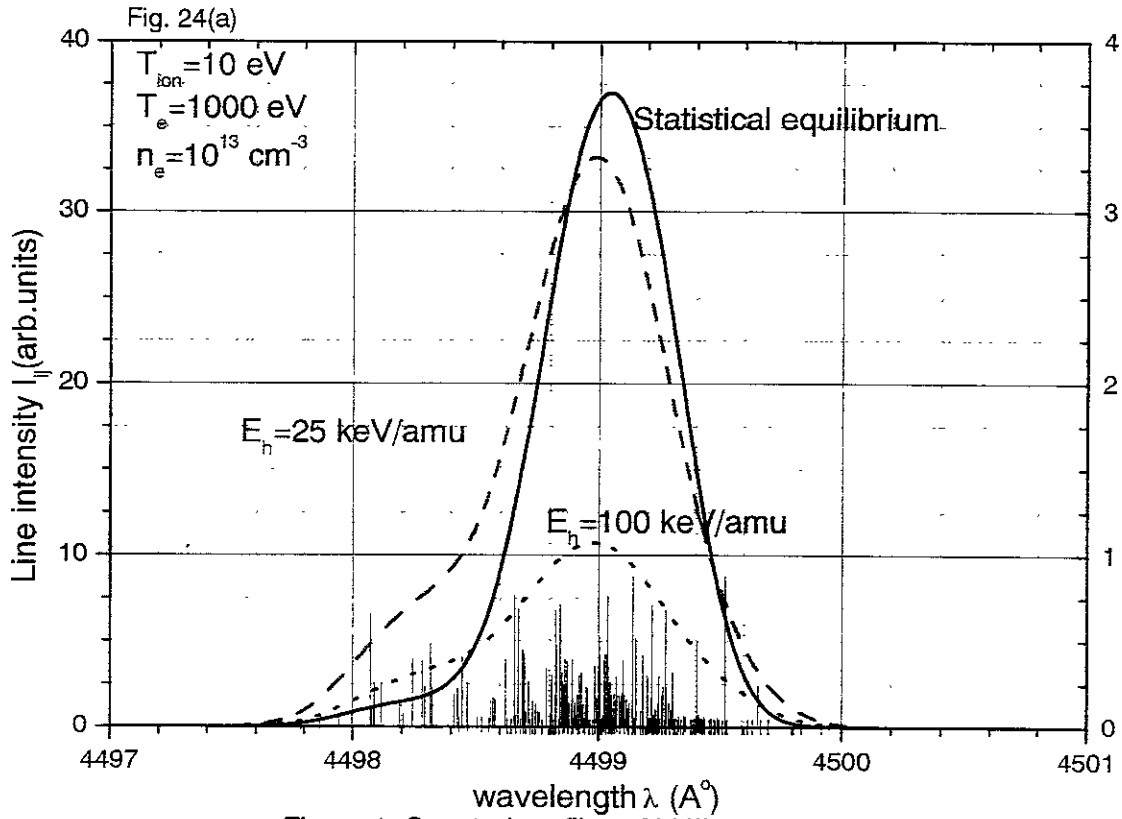

Figure 1. Spectral profiles of Li III Δn=5-4 produced by charge exchange with magnetic field B=2T.

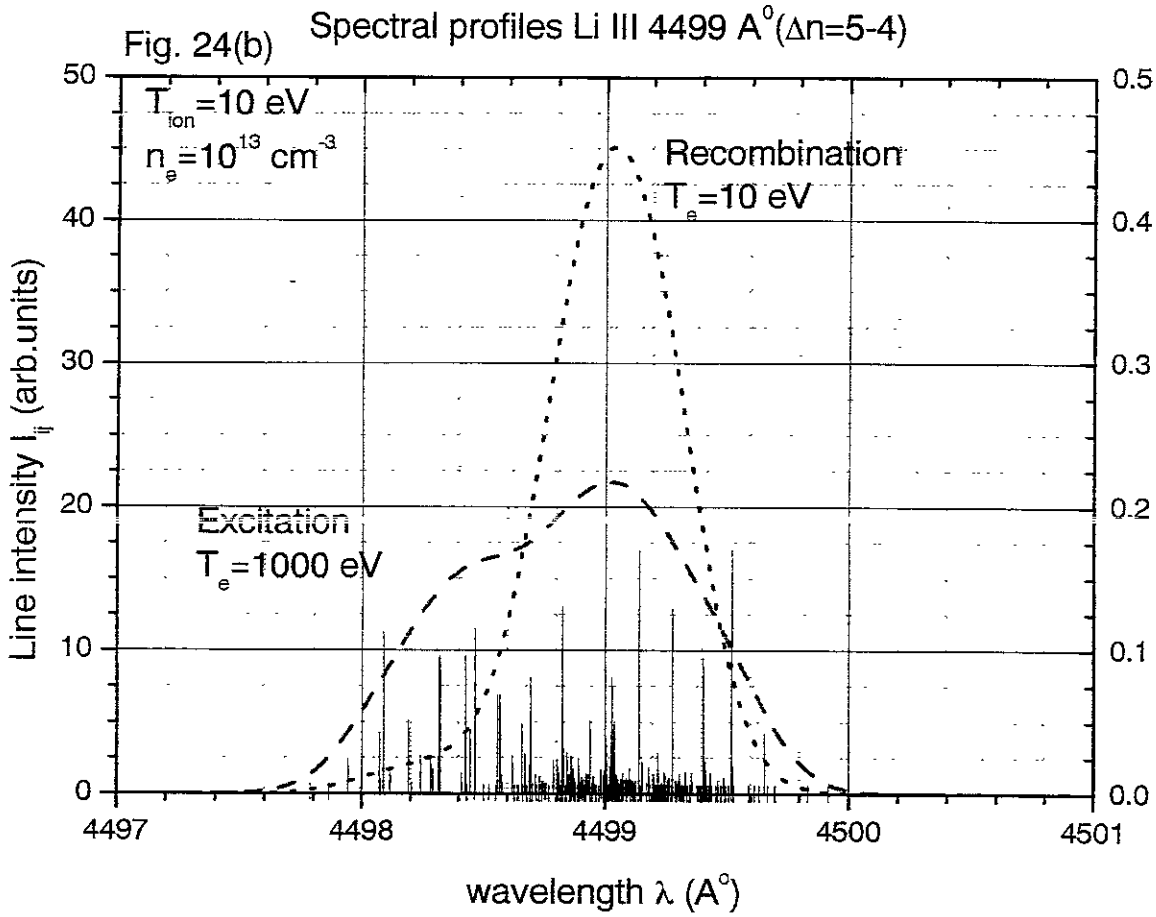

Statistical equilibrium spectra Li III 4499 A°(Δn=5-4)

Fig. 25

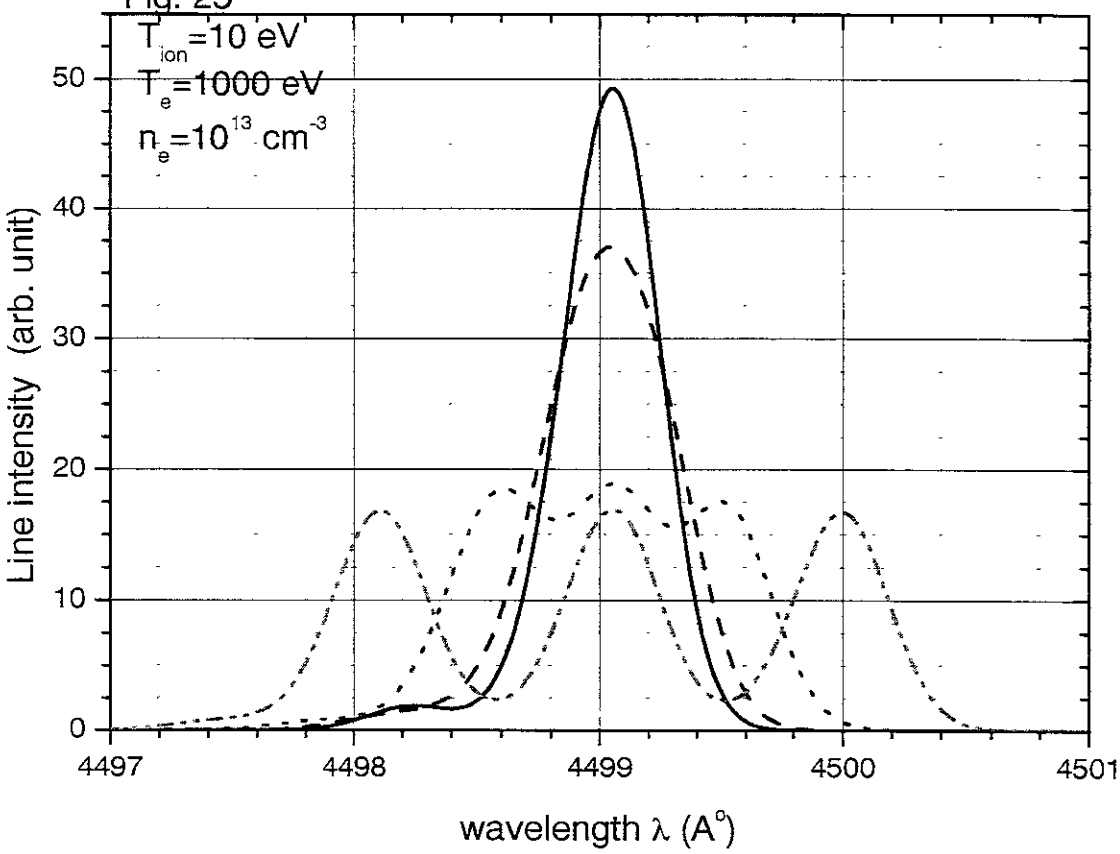

Recent Issues of NIFS-DATA Series

NIFS-DATA-47 I Murakami, K Moribayashi and T. Kato,
Effect of Recombination Processes on FeXXIII Line Intensities May 1998

NIFS-DATA-48 Zhijie Li, T Kenmotsu, T. Kawamura, T Ono and Y Yamamura,
Sputtering Yield Calculations Using an Interatomic Potential with the Shell Effect and a New Local Model Oct 1998

NIFS-DATA-49 S. Sasaki, M Goto, T Kato and S. Takamura,
Line Intensity Ratios of Helium Atom in an Ionizing Plasma Oct 1998

NIFS-DATA-50 I. Murakami, T. Kato and U Safronova,
Spectral Line Intensities of NeVII for Non-equilibrium Ionization Plasma Including Dielectronic Recombination Processses Jan 1999

NIFS-DATA-51 Hiro Tawara and Masa Kato,
Electron Impact Ionization Data for Atoms and Ions -up-dated in 1998-: Feb. 1999

NIFS-DATA-52 J.G. Wang, T. Kato and I. Murakami,
Validity of n^{-3} Scaling Law in Dielectronic Recombination Processes Apr 1999

NIFS-DATA-53 J G Wang, T. Kato and I Murakami,
Dielectronic Recombination Rate Coefficients to Excited States of He from He^{+} Apr 1999

NIFS-DATA-54 T. Kato and E. Asano,
Comparison of Recombination Rate Coefficients Given by Empirical Formulas for Ions from Hydrogen through Nickel June 1999

NIFS-DATA-55 H.P. Summers, H. Anderson, T. Kato and S. Murakami,
Hydrogen Beam Stopping and Beam Emission Data for LHD: Nov. 1999

NIFS-DATA-56 S Born, N Matsunami and H Tawara,
A Simple Theoretical Approach to Determine Relative Ion Yield (RIY) in Glow Discharge Mass Spectrometry (GDMS): Jan 2000

NIFS-DATA-57 T Ono, T. Kawamura, T Kenmotsu, Y Yamamura,
Simulation Study on Retention and Reflection from Tungsten Carbide under High Fluence of Helium Ions: Aug. 2000

NIFS-DATA-58 J.G. Wang, M. Kato and T. Kato,
Spectra of Neutral Carbon for Plasma Diagnostics: Oct. 2000

NIFS-DATA-59 Yu. V. Ralchenko, R. K Janev, T. Kato, D V Fursa, I Bray and F.J de Heer
Cross Section Database for Collision Processes of Helium Atom with Charged Particles
I. Electron Impact Processes Oct 2000

NIFS-DATA-60 U I Safronova, C Namba, W R. Johnson, M.S Safronova,
Relativistic Many-Body Calculations of Energies for n = 3 States in Aluminiumlike Ions. Jan 2001

NIFS-DATA-61 U I Safronova, C Namba, I Murakami, W.R Johnson and M S Safronova,
E1,E2, M1, and M2 Transitions in the Neon Isoelectronic Sequence. Jan. 2001

NIFS-DATA-62 R K Janev, Yu.V. Ralchenko, T. Kenmotsu,
Unified Analytic Formula for Physical Sputtering Yield at Normal Ion Incidence. Apr 2001

NIFS-DATA-63 Y. Itikawa,
Bibliography on Electron Collisions with Molecules· Rotational and Vibrational Excitations, 1980-2000 Apr 2001

NIFS-DATA-64 R K Janev, J G. Wang and TKato,
Cross Sections and Rate Coefficients for Charge Exchange Reactions of Protons with Hydrocarbon Molecules: May 2001

NIFS-DATA-65 T. Kenmotsu, Y. Yamamura, T. Ono and T. Kawamura,
A New Formula of the Energy Spectrum of Sputtered Atoms from a Target Material Bombarded with Light Ions at Normal Incidence· May 2001

NIFS-DATA-66 I Murakami, U. I. Safronova and T. Kato,
Dielectronic Recombination Rate Coefficients to Excited States of Be-like Oxygen· May 2001

NIFS-DATA-67 N Matsunami, E Hatanaka, J. Kondoh, H Hosaka, K Tsumori, H Sakaue and H Tawara,
Secondary Charged Particle Emission from Proton Conductive Oxides by Ion Impact; July 2001

NIFS-DATA-68 R.K. Janev, J.G. Wang, I Murakami and T. Kato,
Cross Sections and Rate Coefficients for Electron-Impact Ionization of Hydrocarbon Molecules Oct. 2001

NIFS-DATA-69 S Zou, T. Kato, I Murakami,
Charge Exchange Recombination Spectroscopy of Li III Ions for Fusion Plasma Diagnostics: Oct. 2001